

CERN-PH-EP-2014-201

Submitted to: Phys. Rev. C.

Measurement of long-range pseudorapidity correlations and azimuthal harmonics in $\sqrt{s_{NN}}=5.02$ TeV proton-lead collisions with the ATLAS detector

The ATLAS Collaboration

Abstract

Measurements of two-particle correlation functions and the first five azimuthal harmonics, v_1 to v_5 , are presented, using 28 nb^{-1} of $p+\text{Pb}$ collisions at a nucleon-nucleon center-of-mass energy of $\sqrt{s_{NN}} = 5.02$ TeV measured with the ATLAS detector at the LHC. Significant long-range “ridge-like” correlations are observed for pairs with small relative azimuthal angle ($|\Delta\phi| < \pi/3$) and back-to-back pairs ($|\Delta\phi| > 2\pi/3$) over the transverse momentum range $0.4 < p_T < 12$ GeV and in different intervals of event activity. The event activity is defined by either the number of reconstructed tracks or the total transverse energy on the Pb-fragmentation side. The azimuthal structure of such long-range correlations is Fourier decomposed to obtain the harmonics v_n as a function of p_T and event activity. The extracted v_n values for $n = 2$ to 5 decrease with n . The v_2 and v_3 values are found to be positive in the measured p_T range. The v_1 is also measured as a function of p_T and is observed to change sign around $p_T \approx 1.5\text{--}2.0$ GeV and then increase to about 0.1 for $p_T > 4$ GeV. The $v_2(p_T)$, $v_3(p_T)$ and $v_4(p_T)$ are compared to the v_n coefficients in Pb+Pb collisions at $\sqrt{s_{NN}} = 2.76$ TeV with similar event multiplicities. Reasonable agreement is observed after accounting for the difference in the average p_T of particles produced in the two collision systems.

Measurement of long-range pseudorapidity correlations and azimuthal harmonics in $\sqrt{s_{\text{NN}}}=5.02$ TeV proton-lead collisions with the ATLAS detector

The ATLAS Collaboration

Measurements of two-particle correlation functions and the first five azimuthal harmonics, v_1 to v_5 , are presented, using 28 nb^{-1} of $p+\text{Pb}$ collisions at a nucleon-nucleon center-of-mass energy of $\sqrt{s_{\text{NN}}} = 5.02$ TeV measured with the ATLAS detector at the LHC. Significant long-range “ridge-like” correlations are observed for pairs with small relative azimuthal angle ($|\Delta\phi| < \pi/3$) and back-to-back pairs ($|\Delta\phi| > 2\pi/3$) over the transverse momentum range $0.4 < p_{\text{T}} < 12$ GeV and in different intervals of event activity. The event activity is defined by either the number of reconstructed tracks or the total transverse energy on the Pb-fragmentation side. The azimuthal structure of such long-range correlations is Fourier decomposed to obtain the harmonics v_n as a function of p_{T} and event activity. The extracted v_n values for $n = 2$ to 5 decrease with n . The v_2 and v_3 values are found to be positive in the measured p_{T} range. The v_1 is also measured as a function of p_{T} and is observed to change sign around $p_{\text{T}} \approx 1.5\text{--}2.0$ GeV and then increase to about 0.1 for $p_{\text{T}} > 4$ GeV. The $v_2(p_{\text{T}})$, $v_3(p_{\text{T}})$ and $v_4(p_{\text{T}})$ are compared to the v_n coefficients in Pb+Pb collisions at $\sqrt{s_{\text{NN}}} = 2.76$ TeV with similar event multiplicities. Reasonable agreement is observed after accounting for the difference in the average p_{T} of particles produced in the two collision systems.

PACS numbers: 25.75.Dw

I. INTRODUCTION

One striking observation in high-energy nucleus-nucleus (A+A) collisions is the large anisotropy of particle production in the azimuthal angle ϕ [1, 2]. This anisotropy is often studied via a two-particle correlation of particle pairs in relative pseudorapidity ($\Delta\eta$) and azimuthal angle ($\Delta\phi$) [3, 4]. The anisotropy manifests itself as a strong excess of pairs at $\Delta\phi \sim 0$ and π , and the magnitude of the excess is relatively constant out to large $|\Delta\eta|$ [5–9]. The azimuthal structure of this “ridge-like” correlation is commonly characterized by its Fourier harmonics, $dN_{\text{pairs}}/d\Delta\phi \sim 1 + 2 \sum_n v_n^2 \cos n\Delta\phi$. While the elliptic flow, v_2 , and triangular flow, v_3 , are the dominant harmonics in A+A collisions, significant v_1 , v_4 , v_5 and v_6 harmonics have also been measured [8–13]. These v_n values are commonly interpreted as the collective hydrodynamic response of the created matter to the collision geometry and its fluctuations in the initial state [14]. The success of hydrodynamic models in describing the anisotropy of particle production in heavy-ion collisions at RHIC and the LHC places important constraints on the transport properties of the produced matter [15–20].

For a small collision system, such as proton-proton ($p+p$) or proton-nucleus ($p+\text{A}$) collisions, it was assumed that the transverse size of the produced system is too small for the hydrodynamic flow description to be applicable. Thus, it came as a surprise that ridge-like structures were also observed in two-particle correlations in high-multiplicity $p+p$ [21] and proton-lead ($p+\text{Pb}$) [22–24] collisions at the LHC and later in deuteron-gold collisions [25] at RHIC. A Fourier decomposition technique has been employed to study the azimuthal distribution of the ridge in $p+\text{Pb}$ collisions. The transverse momentum (p_{T}) dependence of the extracted v_2 and v_3 [23, 24], and the particle-mass dependence of v_2 [26] are found to be similar to those measured in A+A collisions. Large v_2 coefficients are also measured via the four-particle cumulant method [27, 28], suggesting that the ridge reflects genuine multi-particle correlations.

The interpretation of the long-range correlations in high-multiplicity $p+p$ and $p+\text{Pb}$ collisions is currently a subject of intense study. References [29–32] argue that the produced matter in these collisions is sufficiently voluminous and dense such that the hydrodynamic model framework may still apply. On the other hand, models based on gluon saturation and color connections suggest that the long-range correlations are an initial-state effect, intrinsic to QCD at high gluon density [33–37]. Recently a hybrid model that takes into account both the initial- and final-state effects has been proposed [38]. All these approaches can describe, qualitatively and even quantitatively, the v_2 and v_3 data in the $p+\text{Pb}$ collisions.

In order to provide more insights into the nature of the ridge correlation and to discriminate between different theoretical interpretations, this paper provides a detailed measurement of the two-particle correlation and v_n coefficients in $p+\text{Pb}$ collisions at a nucleon-nucleon center-of-mass energy of $\sqrt{s_{\text{NN}}} = 5.02$ TeV. The data correspond to an integrated luminosity of approximately 28 nb^{-1} , recorded in 2013 by the ATLAS experiment at the LHC. This measurement benefits from a dedicated high-multiplicity trigger (see Sec. II B) that provides a large sample of high-multiplicity events, not only extending the previous v_2 and v_3 results to higher p_{T} , but also enabling the first measurement of v_1 , v_4 and v_5 . The results are extracted independently for two different event-activity definitions:

the total transverse energy in the forward calorimeter on the Pb-fragmentation side¹ ($-4.9 < \eta < -3.2$), E_T^{Pb} , or the number of reconstructed tracks in $|\eta| < 2.5$, $N_{\text{ch}}^{\text{rec}}$. The results are also compared to the Pb+Pb data with similar multiplicity. The analysis technique follows closely the previous ATLAS study of v_2 and v_3 based on a much smaller dataset from a short p +Pb run in 2012 [24].

II. EXPERIMENTAL SETUP

A. Detector and dataset

The ATLAS detector [39] provides nearly full solid-angle coverage of the collision point with tracking detectors, calorimeters and muon chambers. The measurements presented in this paper are performed using the ATLAS inner detector (ID), forward calorimeters (FCal), minimum-bias trigger scintillators (MBTS), zero-degree calorimeter (ZDC) and the trigger and data acquisition systems. The ID measures charged particles within the pseudorapidity region $|\eta| < 2.5$ using a combination of silicon pixel detector, silicon microstrip detector (SCT), and a straw-tube transition radiation tracker, all immersed in a 2 T axial magnetic field. The MBTS detects charged particles over $2.1 < |\eta| < 3.9$ using two hodoscopes of 16 counters positioned at $z = \pm 3.6$ m. The FCal consists of two sections that cover $3.2 < |\eta| < 4.9$. The FCal modules are composed of tungsten and copper absorbers with liquid argon as the active medium, which provide 10 interaction lengths of material. The ZDC, situated at ≈ 140 m from the collision vertex, detects neutral particles, mostly neutrons and photons, with $|\eta| > 8.3$.

This analysis uses approximately 28 nb^{-1} of p +Pb data recorded by the ATLAS experiment at the LHC in 2013. The LHC was configured with a 4 TeV proton beam and a 1.57 TeV per-nucleon Pb beam that together produced collisions at $\sqrt{s_{\text{NN}}} = 5.02$ TeV. The beam directions were reversed approximately half-way through the running period. The higher energy of the proton beam results in a net rapidity shift of the nucleon–nucleon center-of-mass frame relative to the ATLAS rest frame. This rapidity shift is 0.47 towards the proton beam direction.

B. Trigger

The minimum-bias (MB) Level-1 (L1) trigger [40] used for this analysis requires a signal in at least one MBTS counter on each side, or a signal in the ZDC on the Pb-fragmentation side with the trigger threshold set just below the peak corresponding to a single neutron. A timing requirement based on signals from each side of the MBTS is imposed to suppress beam backgrounds. Due to the high event rate during the run, only a small fraction of the MB events ($\sim 1/1000$) were recorded. In order to enhance the number of events with high multiplicity, a dedicated high-multiplicity trigger (HMT) was implemented, which uses the ATLAS L1 and high-level trigger (HLT) systems [41]. At L1, the total transverse energy E_T^{L1} in the FCal rapidity interval is required to be above a certain threshold. In the HLT, the charged-particle tracks are reconstructed by requiring at least two hits in the pixel detector and three hits in the SCT. For each event, the collision vertex reconstructed with the highest number of online tracks is selected, and the number of tracks ($N_{\text{trk}}^{\text{HLT}}$) associated with this vertex with $p_T > 0.4$ GeV and a distance of closest approach of less than 4 mm is calculated.

The HMT triggers are implemented by requiring different thresholds on the values of E_T^{L1} and $N_{\text{trk}}^{\text{HLT}}$ with prescale factors adjusted to the instantaneous luminosity provided by the LHC [41]. This analysis uses the six pairs of thresholds on E_T^{L1} and $N_{\text{trk}}^{\text{HLT}}$ listed in Table I. The $N_{\text{trk}}^{\text{HLT}} \geq 225$ trigger was not prescaled throughout the entire running period.

$N_{\text{trk}}^{\text{HLT}}$	≥ 100	≥ 130	≥ 150	≥ 180	≥ 200	≥ 225
E_T^{L1} [GeV]	≥ 10	≥ 10	≥ 50	≥ 50	≥ 65	≥ 65

TABLE I: A list of thresholds in E_T^{L1} and $N_{\text{trk}}^{\text{HLT}}$ for the high-multiplicity triggers used in this analysis.

¹ ATLAS uses a right-handed coordinate system with its origin at the nominal interaction point (IP) in the center of the detector and the z -axis along the beam pipe. The x -axis points from the IP towards the center of the LHC ring, and the y -axis completes the right-handed system. Cylindrical coordinates (r, ϕ) are used in the transverse plane, ϕ being the azimuthal angle around the beam pipe. The pseudorapidity is defined in terms of the polar angle θ as $\eta = -\ln \tan(\theta/2)$. During 2013 p +Pb data taking, the beam directions were reversed approximately half-way through the running period, but in presenting results the direction of the proton beam is always chosen to point to positive η .

III. DATA ANALYSIS

A. Event and track selections

In the offline analysis, p +Pb events are required to have a reconstructed vertex containing at least two associated offline tracks, with its z position satisfying $|z_{\text{vtx}}| < 150$ mm. Non-collision backgrounds and photonuclear interactions are suppressed by requiring at least one hit in a MBTS counter on each side of the interaction point, and the difference between times measured on the two sides to be less than 10 ns. In the 2013 p +Pb run, the luminosity conditions provided by the LHC result in an average probability of 3% that an event contains two or more p +Pb collisions (pileup). The pileup events are suppressed by rejecting events containing more than one good reconstructed vertex. The remaining pileup events are further suppressed based on the signal in the ZDC on the Pb-fragmentation side. This signal is calibrated to the number of detected neutrons (N_n) based on the location of the peak corresponding to a single neutron. The distribution of N_n in events with pileup is broader than that for the events without pileup. Hence a simple cut on the high tail-end of the ZDC signal distribution further suppresses the pileup, while retaining more than 98% of the events without pileup. After this pileup rejection procedure, the residual pileup fraction is estimated to be $\lesssim 10^{-2}$ in the event class with the highest track multiplicity studied in this analysis. About 57 million MB-selected events and 15 million HMT-selected events are included in this analysis.

Charged-particle tracks are reconstructed in the ID using an algorithm optimized for p + p minimum-bias measurements [42]: the tracks are required to have $p_T > 0.3$ GeV and $|\eta| < 2.5$, at least seven hits in the pixel detector and the SCT, and a hit in the first pixel layer when one is expected. In addition, the transverse (d_0) and longitudinal ($z_0 \sin \theta$) impact parameters of the track relative to the vertex are required to be less than 1.5 mm. They are also required to satisfy $|d_0/\sigma_{d_0}| < 3$ and $|z_0 \sin \theta/\sigma_z| < 3$, respectively, where σ_{d_0} and σ_z are uncertainties on d_0 and $z_0 \sin \theta$ obtained from the track-fit covariance matrix.

The efficiency, $\epsilon(p_T, \eta)$, for track reconstruction and track selection cuts is obtained using p +Pb Monte Carlo events produced with version 1.38b of the HIJING event generator [43] with a center-of-mass boost matching the beam conditions. The response of the detector is simulated using GEANT4 [44, 45] and the resulting events are reconstructed with the same algorithms as applied to the data. The efficiency increases with p_T by 6% between 0.3 and 0.5 GeV, and varies only weakly for $p_T > 0.5$ GeV, where it ranges from 82% at $\eta = 0$ to 70% at $|\eta| = 2$ and 60% at $|\eta| > 2.4$. The efficiency is also found to vary by less than 2% over the multiplicity range used in the analysis. The extracted efficiency function $\epsilon(p_T, \eta)$ is used in the correlation analysis, as well as to estimate the average efficiency-corrected charged-particle multiplicity in the collisions.

B. Characterization of the event activity

The two-particle correlation (2PC) analyses are performed in event classes with different overall activity. The event activity is characterized by either E_T^{Pb} , the sum of transverse energy measured on the Pb-fragmentation side of the FCal with $-4.9 < \eta < -3.2$, or $N_{\text{ch}}^{\text{rec}}$, the offline-reconstructed track multiplicity in the ID with $|\eta| < 2.5$ and $p_T > 0.4$ GeV. These event-activity definitions have been used in previous p +Pb analyses [21, 22, 24, 27, 28]. Events with larger activity have on average a larger number of participating nucleons in the Pb nucleus and a smaller impact parameter. Hence the term ‘‘centrality’’, familiar in A+A collisions, is used to refer to the event activity. The terms ‘‘central’’ and ‘‘peripheral’’ are used to refer to events with large activity and small activity, respectively.

Due to the wide range of trigger thresholds and the prescale values required by the HMT triggers, the E_T^{Pb} and $N_{\text{ch}}^{\text{rec}}$ distributions are very different for the HMT events and the MB events. In order to properly include the HMT events in the event-activity classification, an event-by-event weight, $w = 1/P$, is utilized. The combined probability, P , for a given event to be accepted by the MB trigger or any of the HMT triggers is calculated via the inclusion-exclusion principle as

$$P = \sum_{1 \leq i \leq N} p_i - \sum_{1 \leq i < j \leq N} p_i p_j + \sum_{1 \leq i < j < k \leq N} p_i p_j p_k - \dots, \quad (1)$$

where N is the total number of triggers, and p_i is the probability for the i^{th} -trigger to accept the event, defined as zero if the event does not fire the trigger and otherwise as the inverse of the prescale factor of the trigger. The higher-order terms in Eq. (1) account for the probability of more than one trigger being fired. The weight factor, w , is calculated and applied event by event. The distribution for all events after re-weighting has the same shape as the distribution for MB events, as should be the case if the re-weighting is done correctly.

Figure 1 shows the distribution of $N_{\text{ch}}^{\text{rec}}$ (left panels) and E_T^{Pb} (right panels) for the MB and MB+HMT events

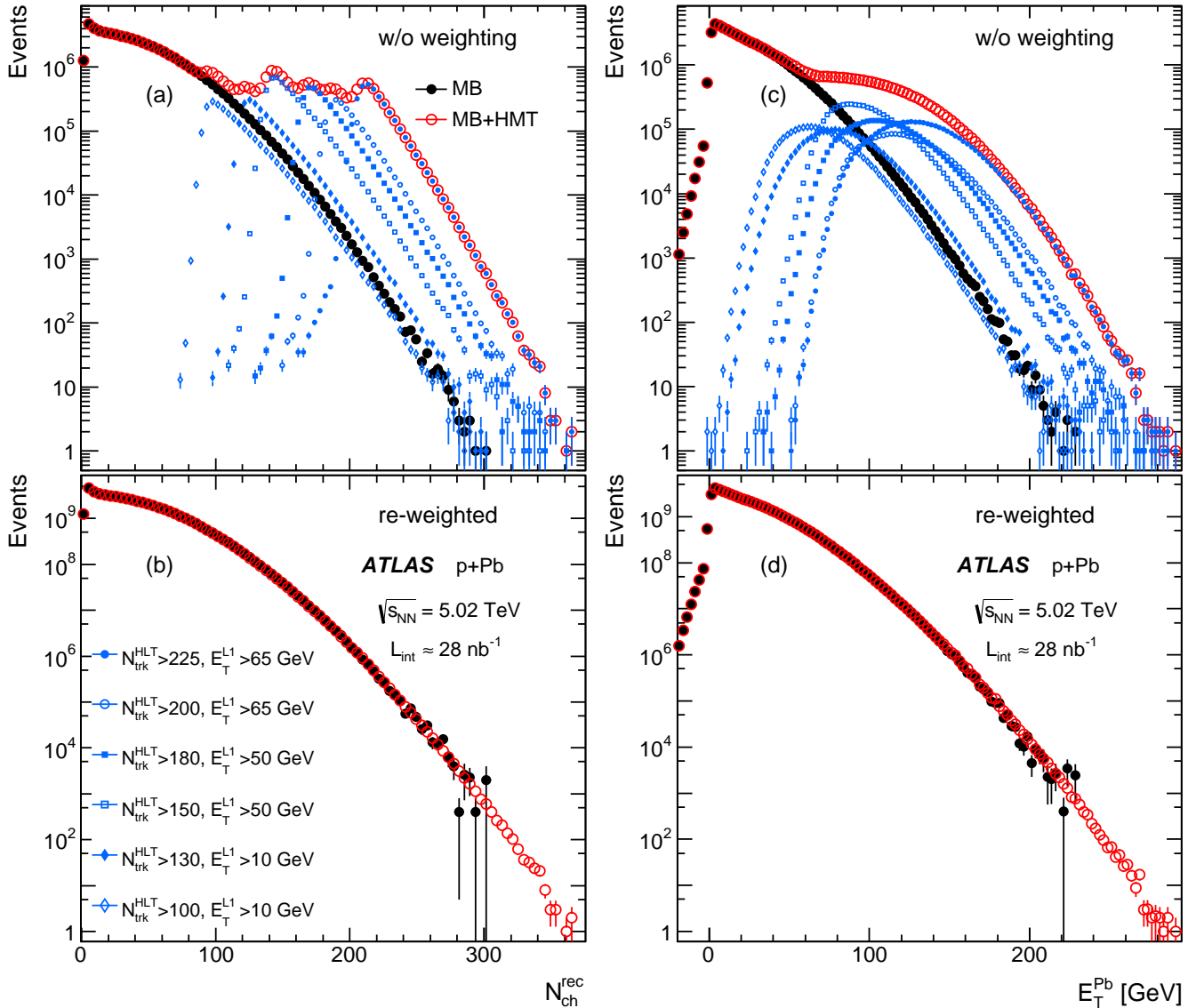


FIG. 1: The distributions of $N_{\text{ch}}^{\text{rec}}$ (left panels) and E_{T}^{Pb} (right panels) for MB and MB+HMT events before (top panels) and after (bottom panels) applying an event-by-event weight (see text). The smaller symbols in the top panels represent the distributions from the six HMT triggers listed in Table I.

before (top panels) and after (bottom panels) the re-weighting procedure. For MB-selected events, the re-weighted distribution differs from the original distribution by a constant factor, reflecting the average prescale. The multiple steps in the $N_{\text{ch}}^{\text{rec}}$ distribution (top-left panel) reflect the rapid turn-on behavior of individual HMT triggers in $N_{\text{ch}}^{\text{rec}}$. The broad shoulder in the E_{T}^{Pb} distribution (top-right panel) is due to the finite width of the $N_{\text{ch}}^{\text{rec}}$ vs. E_{T}^{Pb} correlation, which smears the contributions from different HMT triggers in E_{T}^{Pb} . All these structures disappear after the re-weighting procedure. The results of this analysis are obtained using the MB+HMT combined dataset, with event re-weighting.

Due to the relatively slow turn-on of the HMT triggers as a function of E_{T}^{Pb} (Fig. 1(c)), the events selected in a given E_{T}^{Pb} range typically receive contributions from several HMT triggers with very different weights. Hence the effective increase in the number of events from the HMT triggers in the large E_{T}^{Pb} region is much smaller than the increase in the large $N_{\text{ch}}^{\text{rec}}$ region.

Figure 2(a) shows the correlation between E_{T}^{Pb} and $N_{\text{ch}}^{\text{rec}}$ from MB+HMT p+Pb events. This distribution is similar to that obtained for the MB events, except that the HMT triggers greatly extend the reach in both quantities. The E_{T}^{Pb} value grows with increasing $N_{\text{ch}}^{\text{rec}}$, suggesting that, on average, E_{T}^{Pb} in the nucleus direction correlates well with

the particle production at mid-rapidity. On the other hand, the broad distribution of E_T^{Pb} at fixed $N_{\text{ch}}^{\text{rec}}$ also implies significant fluctuations. To study the relation between E_T^{Pb} and $N_{\text{ch}}^{\text{rec}}$, events are divided into narrow bins in $N_{\text{ch}}^{\text{rec}}$, and the mean and root-mean-square values of the E_T^{Pb} distribution are calculated for each bin. The results are shown in Fig. 2(b). A nearly linear relation between $\langle E_T^{\text{Pb}} \rangle$ and $N_{\text{ch}}^{\text{rec}}$ is observed. This relationship is used to match a given $N_{\text{ch}}^{\text{rec}}$ event class to the corresponding E_T^{Pb} event class. This approximately linear relation can also be parameterized (indicated by the solid line in Fig. 2(b)) as

$$\langle E_T^{\text{Pb}} \rangle / \text{GeV} \approx 0.60 N_{\text{ch}}^{\text{rec}}. \quad (2)$$

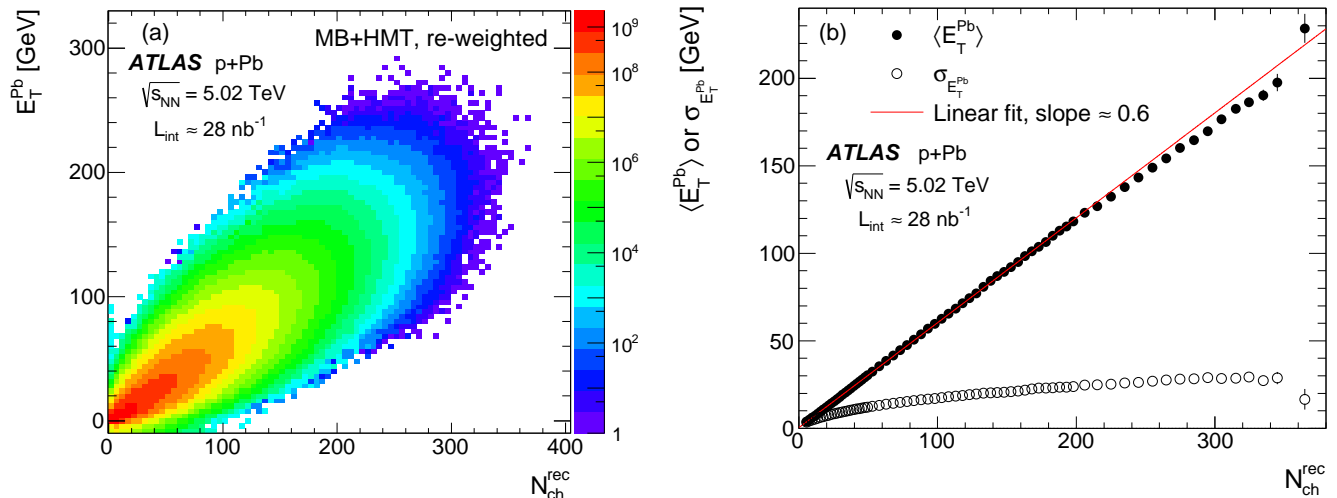


FIG. 2: (a) Correlation between E_T^{Pb} and $N_{\text{ch}}^{\text{rec}}$ in MB+HMT events. (b) The mean $\langle E_T^{\text{Pb}} \rangle$ and root-mean-square $\sigma_{E_T^{\text{Pb}}}$ of the E_T^{Pb} distributions for slices of $N_{\text{ch}}^{\text{rec}}$. The line is a linear fit to all points.

The 2PC analysis is performed in different intervals of the event activity defined by either E_T^{Pb} or $N_{\text{ch}}^{\text{rec}}$. Table II gives a list of representative event-activity classes, together with the fraction of MB+HMT events (after re-weighting as shown in Fig. 2(a)) contained in each event class. The table also provides the average $N_{\text{ch}}^{\text{rec}}$ and E_T^{Pb} values for each event-activity class, as well as the efficiency-corrected number of charged particles within $|\eta| < 2.5$ and $p_T > 0.4$ GeV, $\langle N_{\text{ch}} \rangle$. The event classes defined in narrow E_T^{Pb} or $N_{\text{ch}}^{\text{rec}}$ ranges are used for detailed studies of the centrality dependence of the 2PC, while the event classes in broad E_T^{Pb} or $N_{\text{ch}}^{\text{rec}}$ ranges are optimized for the studies of the p_T dependence. As the number of events at large E_T^{Pb} is smaller than at large $N_{\text{ch}}^{\text{rec}}$, the main results in this paper are presented for event classes defined in $N_{\text{ch}}^{\text{rec}}$.

C. Two-particle correlation

For a given event class, the two-particle correlations are measured as a function of relative azimuthal angle, $\Delta\phi = \phi_a - \phi_b$, and relative pseudorapidity, $\Delta\eta = \eta_a - \eta_b$, with $|\Delta\eta| \leq \eta_{\Delta}^{\text{max}} = 5$. The labels a and b denote the two particles in the pair, which may be selected from different p_T intervals. The particles a and b are conventionally referred to as the “trigger” and “associated” particles, respectively. The correlation strength, expressed in terms of the number of pairs per trigger particle, is defined as [4–6]

$$Y(\Delta\phi, \Delta\eta) = \frac{\int B(\Delta\phi, \Delta\eta) d\Delta\phi d\Delta\eta}{\pi \eta_{\Delta}^{\text{max}}} \left(\frac{S(\Delta\phi, \Delta\eta)}{B(\Delta\phi, \Delta\eta)} \right), \quad Y(\Delta\phi) = \frac{\int B(\Delta\phi) d\Delta\phi}{\pi} \left(\frac{S(\Delta\phi)}{B(\Delta\phi)} \right), \quad (3)$$

where S and B represent pair distributions constructed from the same event and from “mixed events” [4], respectively, which are then normalized by the number of trigger particles in the event. These distributions are also referred to as per-trigger yield distributions. The mixed-event distribution, $B(\Delta\phi, \Delta\eta)$, measures the distribution of uncorrelated pairs. The $B(\Delta\phi, \Delta\eta)$ distribution is constructed by choosing the two particles in the pair from different events of similar $N_{\text{ch}}^{\text{rec}}$ (match to $|\Delta N_{\text{ch}}^{\text{rec}}| < 10$ tracks), E_T^{Pb} (match to $|\Delta E_T^{\text{Pb}}| < 10$ GeV), and z_{vtx} (match to $|\Delta z_{\text{vtx}}| < 10$ mm), so that $B(\Delta\phi, \Delta\eta)$ properly reflects the known detector effects in $S(\Delta\phi, \Delta\eta)$. The one-dimensional (1-D) distributions

Event-activity classes based on $N_{\text{ch}}^{\text{rec}}$					Event-activity classes based on E_{T}^{Pb}				
$N_{\text{ch}}^{\text{rec}}$ range	Fraction	$\langle E_{\text{T}}^{\text{Pb}} \rangle$ [GeV]	$\langle N_{\text{ch}}^{\text{rec}} \rangle$	$\langle N_{\text{ch}} \rangle$	E_{T}^{Pb} range	Fraction	$\langle E_{\text{T}}^{\text{Pb}} \rangle$ [GeV]	$\langle N_{\text{ch}}^{\text{rec}} \rangle$	$\langle N_{\text{ch}} \rangle$
< 20	0.31	7.3	10.3	12.6 ± 0.6	< 10	0.28	4.8	12.4	15.4 ± 0.7
[20, 40)	0.27	18.6	29.1	37.9 ± 1.7	[10, 23)	0.26	16.1	29.2	38.1 ± 1.7
[40, 60)	0.19	30.8	48.8	64.3 ± 2.9	[23, 37)	0.19	29.5	47.3	62.3 ± 2.8
[60, 80)	0.12	42.8	68.6	90.7 ± 4.1	[37, 52)	0.12	43.8	64.0	84.7 ± 3.8
[80, 100)	0.064	54.9	88.3	117 ± 5	[52, 68)	0.067	58.8	80.4	107 ± 5
[100, 120)	0.029	66.4	108	144 ± 7	[68, 83)	0.028	74.2	96.1	128 ± 6
[120, 140)	0.011	78.4	128	170 ± 8	[83, 99)	0.012	89.7	111	147 ± 7
[140, 160)	0.0040	90.3	148	196 ± 9	[99, 116)	0.0043	106	126	168 ± 8
[160, 180)	0.0013	102	168	223 ± 10	[116, 132)	0.0012	122	141	187 ± 8
[180, 200)	3.6×10^{-4}	113	187	249 ± 11	[132, 148)	3.6×10^{-4}	138	155	206 ± 9
[200, 220)	9.4×10^{-5}	125	207	276 ± 12	[148, 165)	1.0×10^{-4}	155	169	225 ± 10
[220, 240)	2.1×10^{-5}	134	227	303 ± 14	[165, 182)	2.2×10^{-5}	171	184	244 ± 11
[240, 260)	4.6×10^{-6}	145	247	329 ± 15	[182, 198)	4.6×10^{-6}	188	196	261 ± 12
[260, 290)	1.1×10^{-6}	157	269	358 ± 16	[198, 223)	1.1×10^{-6}	206	211	281 ± 13
[290, 370)	8.9×10^{-8}	174	301	393 ± 18	[223, 300)	9.6×10^{-8}	232	230	306 ± 14
< 40	0.58	12.5	19.0	24.4 ± 1.1	< 25	0.59	10.2	21.7	28.0 ± 1.3
[40, 80)	0.32	35.3	56.4	74.4 ± 3.3	[25, 50)	0.27	35.1	54.7	72.2 ± 3.3
[80, 110)	0.081	56.8	91.7	122 ± 6	[50, 75)	0.096	61.5	81.4	108 ± 5
[110, 140)	0.023	74.2	121	161 ± 7	[75, 100)	0.025	84.5	106	141 ± 6
[140, 180)	0.0053	93.0	153	203 ± 9	[100, 130)	0.0051	110	130	173 ± 8
[180, 220)	4.6×10^{-4}	116	192	255 ± 12	[130, 165)	5.6×10^{-4}	141	156	208 ± 9
[220, 260)	2.6×10^{-5}	136	231	307 ± 14	[165, 200)	2.7×10^{-5}	174	186	248 ± 11
[260, 370)	1.2×10^{-6}	158	271	361 ± 16	[200, 300)	1.0×10^{-6}	208	214	284 ± 13

TABLE II: A list of event-activity classes defined in $N_{\text{ch}}^{\text{rec}}$ (left) and E_{T}^{Pb} (right) ranges, where the notation $[a, b)$ implies $a \leq N_{\text{ch}}^{\text{rec}}$ or $E_{\text{T}}^{\text{Pb}} < b$. For each event class, the fraction of MB+HMT events after trigger re-weighting (Fig. 2(a)), the average values of $\langle E_{\text{T}}^{\text{Pb}} \rangle$ and $\langle N_{\text{ch}}^{\text{rec}} \rangle$, and the efficiency-corrected average number of charged particles with $p_{\text{T}} > 0.4$ GeV and $|\eta| < 2.5$, $\langle N_{\text{ch}} \rangle$, are also listed.

$S(\Delta\phi)$ and $B(\Delta\phi)$ are obtained by integrating $S(\Delta\phi, \Delta\eta)$ and $B(\Delta\phi, \Delta\eta)$, respectively, over a $\Delta\eta$ range. The region $|\Delta\eta| < 1$ is chosen to focus on the short-range features of the correlation functions, while the region $|\Delta\eta| > 2$ is chosen to focus on the long-range features of the correlation functions. These two regions are hence referred to as the “short-range region” and “long-range region”, respectively. The normalization factors in front of the S/B ratio are chosen such that the $(\Delta\phi, \Delta\eta)$ -averaged value of $B(\Delta\phi, \Delta\eta)$ and $\Delta\phi$ -averaged value of $B(\Delta\phi)$ are both unity. When measuring S and B , pairs are filled in one quadrant of the $(\Delta\phi, \Delta\eta)$ space and then reflected to the other quadrants [24]. To correct $S(\Delta\phi, \Delta\eta)$ and $B(\Delta\phi, \Delta\eta)$ for the individual inefficiencies of particles a and b , the pairs are weighted by the inverse product of their tracking efficiencies $1/(\epsilon_a \epsilon_b)$. Remaining detector distortions not accounted for in the efficiency largely cancel in the S/B ratio.

Examples of two-dimensional (2-D) correlation functions are shown in Fig. 3 for charged particles with $1 < p_{\text{T}}^{\text{a,b}} < 3$ GeV in low-activity events, $E_{\text{T}}^{\text{Pb}} < 10$ GeV or $N_{\text{ch}}^{\text{rec}} < 20$ in the top panels, and high-activity events, $E_{\text{T}}^{\text{Pb}} > 100$ GeV or $N_{\text{ch}}^{\text{rec}} > 220$ in the bottom panels. The correlation for low-activity events shows a sharp peak centered at $(\Delta\phi, \Delta\eta) = (0, 0)$ due to short-range correlations for pairs resulting from jets, high- p_{T} resonance decays, and Bose-Einstein correlations. The correlation function also shows a broad structure at $\Delta\phi \sim \pi$ from low- p_{T} resonances, dijets, and momentum conservation that is collectively referred to as “recoil” [24] in the remainder of this paper. In the high-activity events, the correlation reveals a flat ridge-like structure at $\Delta\phi \sim 0$ (the “near-side”) that extends over the full measured $\Delta\eta$ range. This $\Delta\eta$ independence is quantified by integrating the 2-D correlation functions over $|\Delta\phi| < 1$ to obtain $Y(\Delta\eta) = \int_{|\Delta\phi| < 1} Y(\Delta\phi, \Delta\eta) \Delta\phi$. The yield associated with the near-side short-range correlation peak centered at $(\Delta\phi, \Delta\eta) = (0, 0)$ can then be estimated as

$$Y^{\text{N-Peak}} = \int_{|\Delta\eta| < 1} Y(\Delta\eta) d\Delta\eta - \frac{1}{5 - \eta_{\Delta}^{\text{min}}} \int_{\eta_{\Delta}^{\text{min}} < |\Delta\eta| < 5} Y(\Delta\eta) d\Delta\eta, \quad (4)$$

where the second term accounts for the contribution of uncorrelated pairs and the ridge component under the near-side peak. The default value of $Y^{N-\text{Peak}}$ is obtained with a lower-end of the integration range of $\eta_{\Delta}^{\text{min}} = 2$, but the value of $\eta_{\Delta}^{\text{min}}$ is varied from 2 to 4 to check the stability of $Y^{N-\text{Peak}}$. The distribution at $\Delta\phi \sim \pi$ (the ‘‘away-side’’) is also broadened in high-activity events, consistent with the presence of a long-range component in addition to the recoil component [24]. This recoil component can be estimated from the low-activity events and subtracted from the high-activity events using the procedure detailed in the next section.

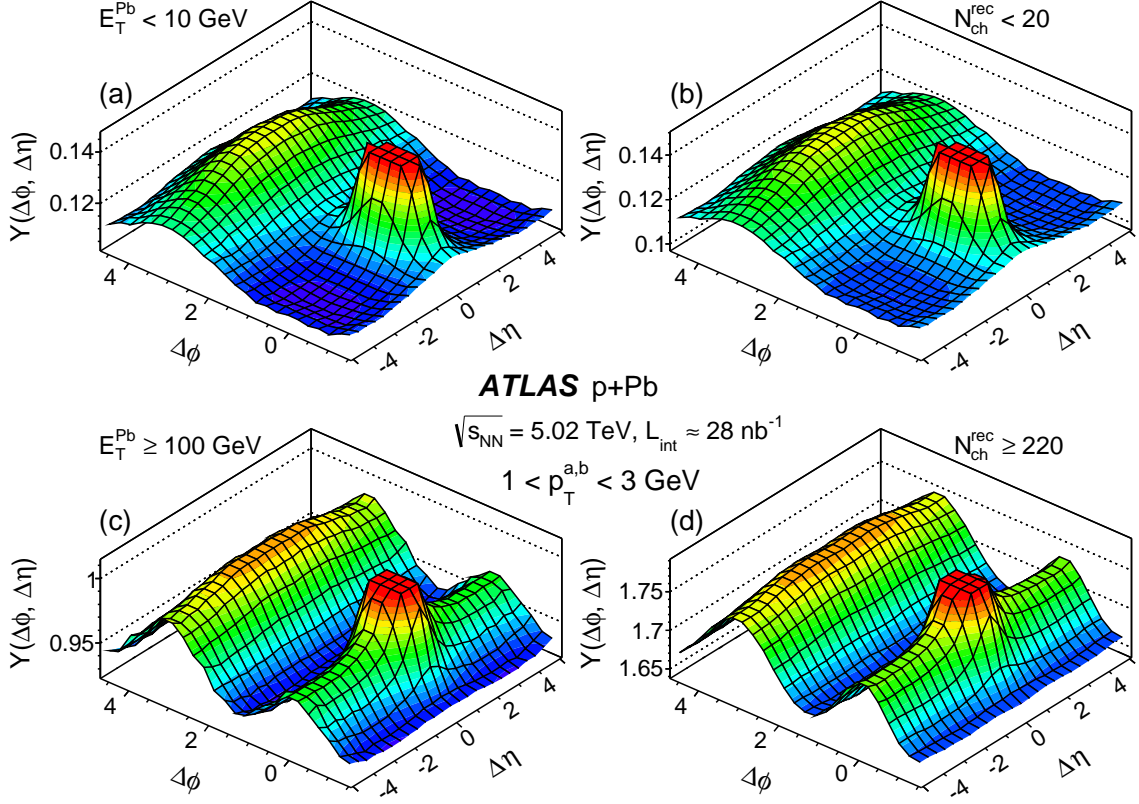


FIG. 3: The 2-D correlation function in $\Delta\phi$ and $\Delta\eta$ for the peripheral event class selected by either (a) $E_{\text{T}}^{\text{Pb}} < 10 \text{ GeV}$ or (b) $N_{\text{ch}}^{\text{rec}} < 20$ and the central event class selected by either (c) $E_{\text{T}}^{\text{Pb}} \geq 100 \text{ GeV}$ or (d) $N_{\text{ch}}^{\text{rec}} \geq 220$.

D. Recoil subtraction

The correlated structure above a flat pedestal in the correlation functions is calculated using a zero-yield-at-minimum (ZYAM) method [4, 46] following previous measurements [22–24],

$$Y^{\text{corr}}(\Delta\phi, \Delta\eta) = \frac{\int B(\Delta\phi, \Delta\eta) d\Delta\phi d\Delta\eta}{\pi \eta_{\Delta}^{\text{max}}} \left(\frac{S(\Delta\phi, \Delta\eta)}{B(\Delta\phi, \Delta\eta)} - b_{\text{ZYAM}} \right), \quad Y^{\text{corr}}(\Delta\phi) = \frac{\int B(\Delta\phi) d\Delta\phi}{\pi} \left(\frac{S(\Delta\phi)}{B(\Delta\phi)} - b_{\text{ZYAM}} \right), \quad (5)$$

where the parameter b_{ZYAM} represents the pedestal formed by uncorrelated pairs. A second-order polynomial fit to the 1-D $Y(\Delta\phi)$ distribution in the long-range region is used to find the location of the minimum point, $\Delta\phi_{\text{ZYAM}}$, and from this the value of b_{ZYAM} is determined and subtracted from the 2-D correlation function. The $Y^{\text{corr}}(\Delta\phi, \Delta\eta)$ functions differ, therefore, by a constant from the $Y(\Delta\phi, \Delta\eta)$ functions, such as those in Fig. 3.

In low-activity events, $Y^{\text{corr}}(\Delta\phi, \Delta\eta)$ contains mainly the short-range correlation component and the recoil component. In high-activity events, the contribution from the long-range ‘‘ridge’’ correlation also becomes important. This long-range component of the correlation function in a given event class is obtained by estimating the short-range

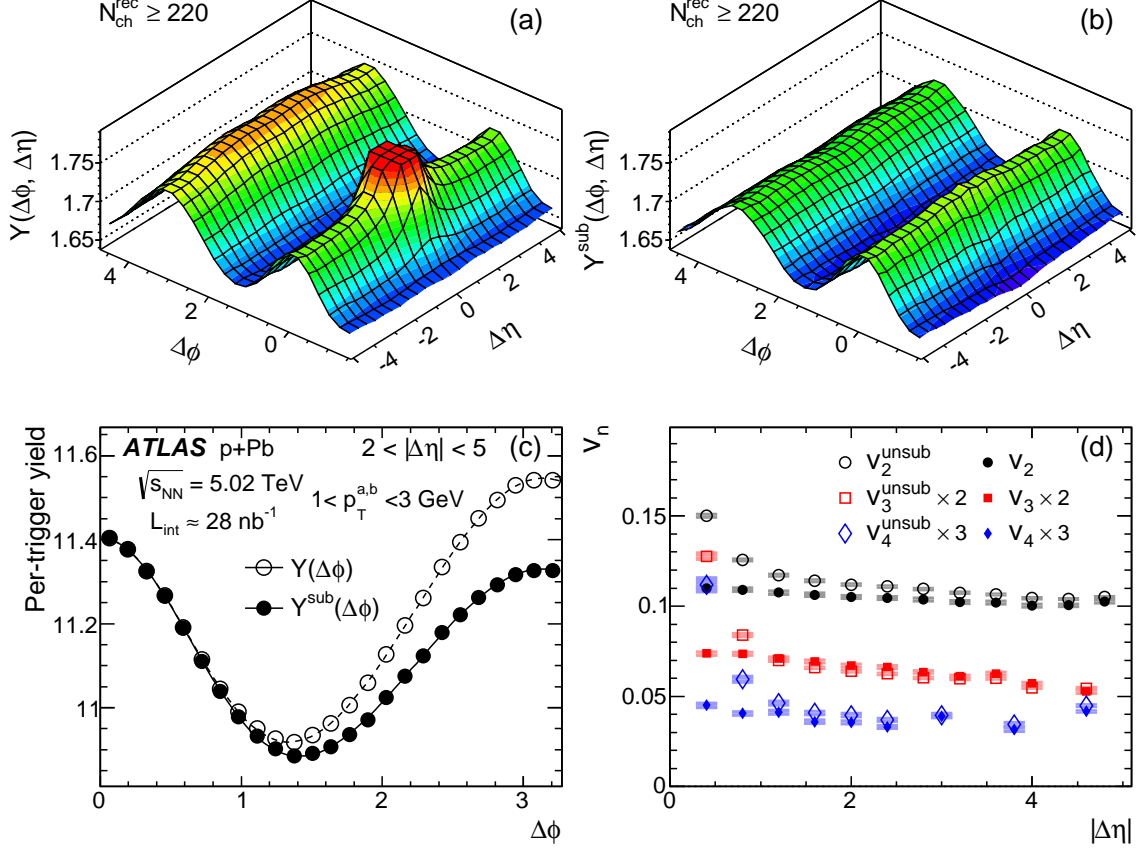


FIG. 4: The 2-D correlation function in $\Delta\phi$ and $\Delta\eta$ for events with $N_{\text{ch}}^{\text{rec}} \geq 220$ (a) before and (b) after subtraction of the peripheral yield. Panel (c) shows the corresponding 1-D correlation functions in $\Delta\phi$ for pairs integrated over $2 < |\Delta\eta| < 5$ from panels (a) and (b), together with Fourier fits including the first five harmonics. Panel (d) shows the 2nd, 3rd, and 4th-order Fourier coefficients as a function of $|\Delta\eta|$ calculated from the 2-D distributions in panel (a) or panel (b), represented by the open or filled symbols, respectively. The error bars and shaded boxes are statistical and systematic uncertainties, respectively.

correlation component using the peripheral events and is then subtracted,

$$Y^{\text{sub}}(\Delta\phi, \Delta\eta) = Y(\Delta\phi, \Delta\eta) - \alpha Y_{\text{peri}}^{\text{corr}}(\Delta\phi, \Delta\eta), \quad Y^{\text{sub}}(\Delta\phi) = Y(\Delta\phi) - \alpha Y_{\text{peri}}^{\text{corr}}(\Delta\phi), \quad (6)$$

where the Y^{corr} in a low-activity or peripheral event class, denoted by $Y_{\text{peri}}^{\text{corr}}$, is used to estimate and subtract (hence the superscript “sub” in Eq. (6)) the short-range correlation at the near-side and the recoil at the away-side. The parameter α is chosen to adjust the near-side short-range correlation yield in the peripheral events to match that in the given event class for each p_{T}^{a} and p_{T}^{b} combination, $\alpha = Y^{\text{N-Peak}}/Y_{\text{peri}}^{\text{N-Peak}}$. This scaling procedure is necessary to account for enhanced short-range correlations and away-side recoil in higher-activity events, under the assumption that the relative contribution of the near-side short-range correlation and away-side recoil is independent of the event activity. A similar rescaling procedure has also been used by the CMS Collaboration [28]. The default peripheral event class is chosen to be $E_{\text{T}}^{\text{Pb}} < E_{\text{T}}^0 = 10$ GeV. However, the results have also been checked with other E_{T}^0 values, as well as with a peripheral event class defined by $N_{\text{ch}}^{\text{rec}} < 20$. In the events with the highest multiplicity, the value of α determined with the default peripheral event class varies from ~ 2 at $p_{\text{T}} \approx 0.5$ GeV to ~ 1 for $p_{\text{T}} > 3$ GeV, with a p_{T} -dependent uncertainty of 3–5%.

The uncertainty on b_{ZYAM} only affects the recoil-subtracted correlation functions through the $Y_{\text{peri}}^{\text{corr}}$ term in Eq. (6). This uncertainty is usually very small in high-activity p +Pb collisions, due to their much larger pedestal level than for the peripheral event class.

Figures 4(a) and (b) show, respectively, the 2-D correlation functions before and after the subtraction procedure given by Eq. (6). Most of the short-range peak and away-side recoil structures are removed by the subtraction, and the remaining distributions exhibit a $\Delta\phi$ -symmetric double-ridge that is almost independent of $\Delta\eta$. Figure 4(c) shows the corresponding 1-D correlation functions before and after recoil subtraction in the long-range region of $|\Delta\eta| > 2$.

The distribution at the near-side is not affected since the near-side short-range peak is narrow in η (Fig. 4(a)), while the away-side distribution is reduced due to the removal of the recoil component.

E. Extraction of the azimuthal harmonics associated with long-range correlation

The azimuthal structure of the long-range correlation is studied via a Fourier decomposition similar to the approach used in the analysis of Pb+Pb collisions [7, 9],

$$Y^{\text{sub}}(\Delta\phi) = \frac{\int Y^{\text{sub}}(\Delta\phi)d\Delta\phi}{\pi} \left(1 + \sum_n 2v_{n,n} \cos(n\Delta\phi) \right), \quad (7)$$

where $v_{n,n}$ are the Fourier coefficients calculated via a discrete Fourier transformation,

$$v_{n,n} = \frac{\sum_{m=1}^N \cos(n\Delta\phi_m) Y^{\text{sub}}(\Delta\phi_m)}{\sum_{m=1}^N Y^{\text{sub}}(\Delta\phi_m)}, \quad (8)$$

where $N = 24$ is the number of $\Delta\phi$ bins from 0 to π . The first five Fourier coefficients are calculated as a function of p_{T}^{a} and p_{T}^{b} for each event-activity class.

The azimuthal anisotropy coefficients for single particles, v_n , can be obtained via the factorization relation commonly used for heavy-ion collisions [7, 9, 47],

$$v_{n,n}(p_{\text{T}}^{\text{a}}, p_{\text{T}}^{\text{b}}) = v_n(p_{\text{T}}^{\text{a}})v_n(p_{\text{T}}^{\text{b}}). \quad (9)$$

From this the p_{T} dependence of v_n for $n = 2-5$ are calculated as

$$v_n(p_{\text{T}}^{\text{a}}) = v_{n,n}(p_{\text{T}}^{\text{a}}, p_{\text{T}}^{\text{b}}) / \sqrt{v_{n,n}(p_{\text{T}}^{\text{b}}, p_{\text{T}}^{\text{b}})}, \quad (10)$$

where the default transverse momentum range for the associated particle (b) is chosen to be $1 < p_{\text{T}}^{\text{b}} < 3$ GeV, and the Fourier coefficient as a function of the transverse momentum of the trigger particle is denoted by $v_n(p_{\text{T}}^{\text{a}})$, or simply $v_n(p_{\text{T}})$ where appropriate. The extraction of v_1 requires a slight modification and is discussed separately in Sec. IV C. The factorization behavior is checked by comparing the $v_n(p_{\text{T}}^{\text{a}})$ obtained for different p_{T}^{b} ranges, as discussed in Sec. IV B.

A similar Fourier decomposition procedure is also carried out for correlation functions without peripheral subtraction, i.e. $Y(\Delta\phi)$. The harmonics obtained in this way are denoted by $v_{n,n}^{\text{unsub}}$ and v_n^{unsub} , respectively.

Figure 4(d) shows the azimuthal harmonics obtained by Fourier decomposition of the $Y(\Delta\phi, \Delta\eta)$ and $Y^{\text{sub}}(\Delta\phi, \Delta\eta)$ distributions in Figs. 4(a) and (b) for different, narrow slices of $\Delta\eta$. The resulting $v_{n,n}^{\text{unsub}}$ and v_n values are plotted as a function of $\Delta\eta$ for $n = 2, 3$ and 4. The v_n values are much smaller than v_n^{unsub} for $|\Delta\eta| < 1$, reflecting the removal of the short-range correlations at the near-side. The v_2 values are also systematically smaller than v_2^{unsub} for $|\Delta\eta| > 1$, reflecting the removal of the away-side recoil contribution.

F. Systematic uncertainties

The systematic uncertainties in this analysis arise from pair acceptance, the ZYAM procedure, tracking efficiency, Monte Carlo consistency, residual pileup, and the recoil subtraction. Each source is discussed separately below.

The correlation functions rely on the pair acceptance functions, $B(\Delta\phi, \Delta\eta)$ and $B(\Delta\phi)$ in Eq. (3), to reproduce detector acceptance effects in the signal distribution. A natural way of quantifying the influence of detector effects on $v_{n,n}$ and v_n is to express the single-particle and pair acceptance functions as Fourier series, similar to Eq. (7). The resulting coefficients for pair acceptance $v_{n,n}^{\text{det}}$ are the product of those for the two single-particle acceptances $v_n^{\text{det,a}}$ and $v_n^{\text{det,b}}$. In general, the pair acceptance function in $\Delta\phi$ is quite flat: the maximum fractional variation from its average value is observed to be less than 0.001 for pairs integrated in $2 < |\Delta\eta| < 5$, and the corresponding $|v_{n,n}^{\text{det}}|$ values are found to be less than 2×10^{-4} . These $v_{n,n}^{\text{det}}$ values are expected to mostly cancel in the correlation function, and only a small fraction contributes to the uncertainties in the pair acceptance function. Possible residual effects on the pair acceptance are evaluated following Ref. [9], by varying the criteria for matching in $N_{\text{ch}}^{\text{rec}}$, E_{T}^{pb} , and z_{vtx} . In each case, the residual $v_{n,n}^{\text{det}}$ values are evaluated by a Fourier expansion of the ratio of the pair acceptances before and

after the variation. This uncertainty varies in the range of $(5-8) \times 10^{-6}$. It is negligible for v_2 and v_3 , but become sizable for higher-order harmonics, particularly at low p_T , where the v_n values are small.

As discussed in Sec. III D, the value of b_{ZYAM} is determined by a second-order polynomial fit of the $Y(\Delta\phi)$ distribution. The stability of the fit is studied by varying the $\Delta\phi$ range in the fit. The uncertainty in b_{ZYAM} depends on the local curvature around $\Delta\phi_{ZYAM}$, and is estimated to be 0.0003–0.001 of the minimum value of $Y(\Delta\phi)$. This uncertainty contributes directly to $Y^{corr}(\Delta\phi)$, but contributes to $Y^{sub}(\Delta\phi)$ and v_n indirectly through the peripheral subtraction (see Eq. (6)). The resulting uncertainty on v_n is found to be less than 2%, for all n .

The values of per-trigger yields, $Y(\Delta\phi)$, $Y^{corr}(\Delta\phi)$, and $Y^{sub}(\Delta\phi)$, are sensitive to the uncertainty on the tracking efficiency correction for the associated particles. This uncertainty is estimated by varying the track quality cuts and the detector material in the simulation, re-analyzing the data using corresponding Monte Carlo efficiencies and evaluating the change in the extracted yields. The resulting uncertainty is estimated to be 2.5% due to the track selection and 2–3% related to our limited knowledge of the detector material. The $v_{n,n}$ and v_n values depend only on the shape of the $Y^{sub}(\Delta\phi)$ distribution and hence are not sensitive to the tracking efficiency.

The analysis procedure is also validated by measuring v_n values in fully simulated HIJING events [44, 45] and comparing them to those measured using the generated particles. A small but systematic difference between the two results are included in the systematic uncertainties.

Nearly all of the events containing pileup are removed by the procedure described in Sec. III A. The influence of the residual pileup is evaluated by relaxing the pileup rejection criteria and then calculating the change in the per-trigger yields and v_n values. The differences are taken as an estimate of the uncertainty, and are found to be negligible in low event-activity classes, and increase to 2% for events with $E_T^{pb} > 200$ GeV or $N_{ch}^{rec} > 300$.

According to Table II, the low-activity events used in the peripheral subtraction ($E_T^{pb} < E_T^0 = 10$ GeV) correspond to 28% of the MB-triggered events. The pair distributions for these events may contain a small genuine long-range component, leading to a reduction of the long-range correlation signal in a high-activity class via the peripheral subtraction procedure. The influence of this over-subtraction is evaluated by varying the definition of the low-activity events in the range of $E_T^0 = 5$ GeV to $E_T^0 = 20$ GeV. The $Y^{sub}(\Delta\phi)$ and v_n values are calculated for each variation. The v_n values are found to decrease approximately linearly with increasing E_T^0 . The amount of over-subtraction can be estimated by extrapolating E_T^0 to zero. The estimated changes of v_n and $Y^{sub}(\Delta\phi)$ vary from less than 1% for $E_T^{pb} > 100$ GeV or $N_{ch}^{rec} > 150$, and increase for lower event-activity classes approximately as $1.5/N_{ch}^{rec}$. The relative change of v_n is also found to be independent of p_T . As a cross-check, the analysis is repeated by defining peripheral events as $N_{ch}^{rec} < 20$. The variation of v_n values is found to be consistent with the variation from varying E_T^0 .

The stability of the scale factor, α , is evaluated by varying the $\Delta\eta$ window of the long-range region in Eq. (4). A 3–5% uncertainty is quoted for α from these variations. The resulting uncertainty on v_n for $n = 2-5$ is within 1% at low p_T (< 4 GeV), and increases to $\sim 10\%$ at the highest p_T . However, the v_1 extraction is directly affected by the subtraction of the recoil component, and hence the v_1 value is very sensitive to the uncertainty in α . The estimated uncertainty is 8–12% for $p_T < 1$ GeV and is about 20–30% for $p_T > 3$ GeV.

The different sources of the systematic uncertainties described above are added in quadrature to give the total systematic uncertainties for per-trigger yields and v_n , which are summarized in Tables III and IV, respectively. The systematic uncertainty quoted for each source usually covers the maximum uncertainty over the measured p_T range and event-activity range. However, since $v_1(p_T)$ changes sign within 1.5–2.0 GeV (see Fig. 15), the relative uncertainties are quoted for $p_T < 1$ GeV and $p_T > 3$ GeV. The uncertainty of pair acceptance, which is less than 8×10^{-6} for $v_{n,n}$, was converted to percent uncertainties. This uncertainty can be significant at high p_T .

Residual pair acceptance [%]	1–2
ZYAM procedure [%]	0.2–1.5
Tracking efficiency & material [%]	4.2
Residual pileup [%]	0–2

TABLE III: Summary of relative systematic uncertainties for $Y(\Delta\phi)$, $Y^{corr}(\Delta\phi)$ and $Y^{sub}(\Delta\phi)$.

IV. RESULTS

A. Correlation functions and integrated yields

Figure 5 shows the 1-D correlation functions after the ZYAM procedure, $Y^{corr}(\Delta\phi)$, in various ranges of p_T^a for a fixed p_T^b range of 1–3 GeV. The correlation functions are obtained in the long-range region ($|\Delta\eta| > 2$) and are shown

	$n = 1$	$n = 2$	$n = 3$	$n = 4$	$n = 5$
Residual pair acceptance [%]	1.0–5.0	<0.5	1.0–4.0	7.0–12	7.0–20
ZYAM procedure [%]	0.6	0.3	0.3	0.5	0.6
Tracking efficiency& material [%]	1.0	0.4	0.8	1.2	2.4
Monte Carlo consistency [%]	4.0	1.0	2.0	4.0	8.0
Residual pileup [%]	0–2.0	0–2.0	0–2.0	0–2.0	0–2.0
Uncertainty on scale factor α [%]	8.0–30	0.2–10	0.2–12	0.2–14	1.0–14
Choice of peripheral events for $N_{\text{ch}}^{\text{rec}} > 160$ or $E_{\text{T}}^{\text{Pb}} > 100$ GeV [%]	4.0	1.0	1.0	2.0	4.0

TABLE IV: Summary of relative systematic uncertainties on v_n , for $n = 1$ to 5.

for events selected by $N_{\text{ch}}^{\text{rec}} \geq 220$. This event class contains a small fraction (3×10^{-5}) of the minimum-bias p +Pb events with highest multiplicity. The correlation functions are compared to the distributions of the recoil component, $\alpha Y_{\text{peri}}^{\text{corr}}(\Delta\phi)$ in Eq. (6), estimated from the peripheral event class defined by $E_{\text{T}}^{\text{Pb}} < 10$ GeV. The scale factor α is chosen such that the near-side short-range yield matches between the two event classes (see Eq. (6) and discussion around it). Figure 5 shows a clear near-side excess in the full p_{T}^{a} range studied in this analysis. An excess above the estimated recoil contribution is also observed on the away-side over the same p_{T} range.

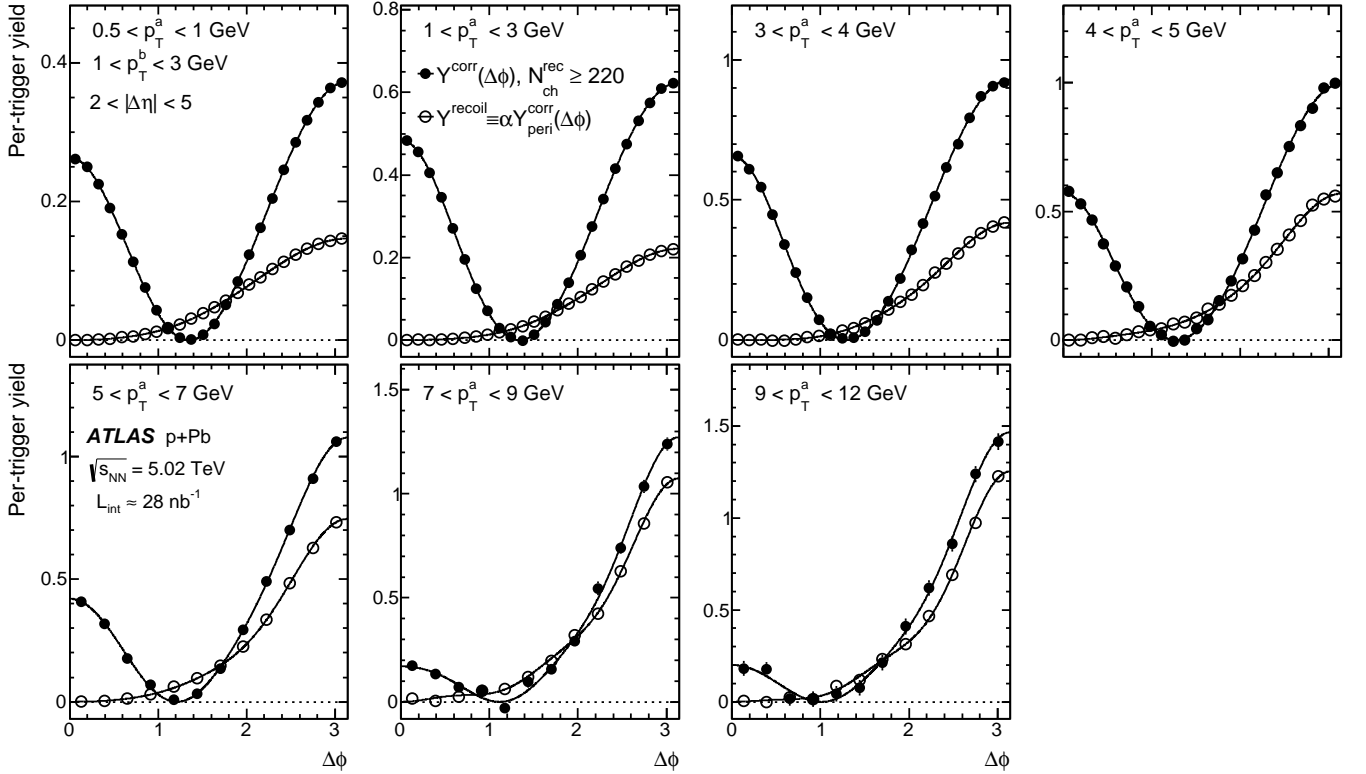


FIG. 5: The per-trigger yield distributions $Y^{\text{corr}}(\Delta\phi)$ and $Y^{\text{recoil}}(\Delta\phi)$ for events with $N_{\text{ch}}^{\text{rec}} \geq 220$ in the long-range region $|\Delta\eta| > 2$. The distributions are shown for $1 < p_{\text{T}}^{\text{b}} < 3$ GeV in various p_{T}^{a} ranges. They are compared to the recoil contribution estimated from a peripheral event class defined by $E_{\text{T}}^{\text{Pb}} < 10$ GeV using a rescaling procedure (see Eq. (6) and discussion around it). The curves are Fourier fits including the first five harmonics.

To further quantify the properties of the long-range components, the $Y^{\text{corr}}(\Delta\phi)$ distributions are integrated over $|\Delta\phi| < \pi/3$ and $|\Delta\phi| > 2\pi/3$, similar to the procedure used in previous analyses [23, 24]. The integrated yields, Y_{int} , are obtained in several event classes and are plotted as a function of p_{T}^{a} in Fig. 6. The near-side yields increase with trigger p_{T} , reach a maximum at $p_{\text{T}} \sim 3$ GeV, and then decrease to a value close to zero at $p_{\text{T}} > 10$ GeV. This trend is characteristic of the p_{T} dependence of the Fourier harmonics in A+A collisions. In contrast, the away-side yields show a continuous increase across the full p_{T} range, due to the contribution of the recoil component that mostly results

from dijets.

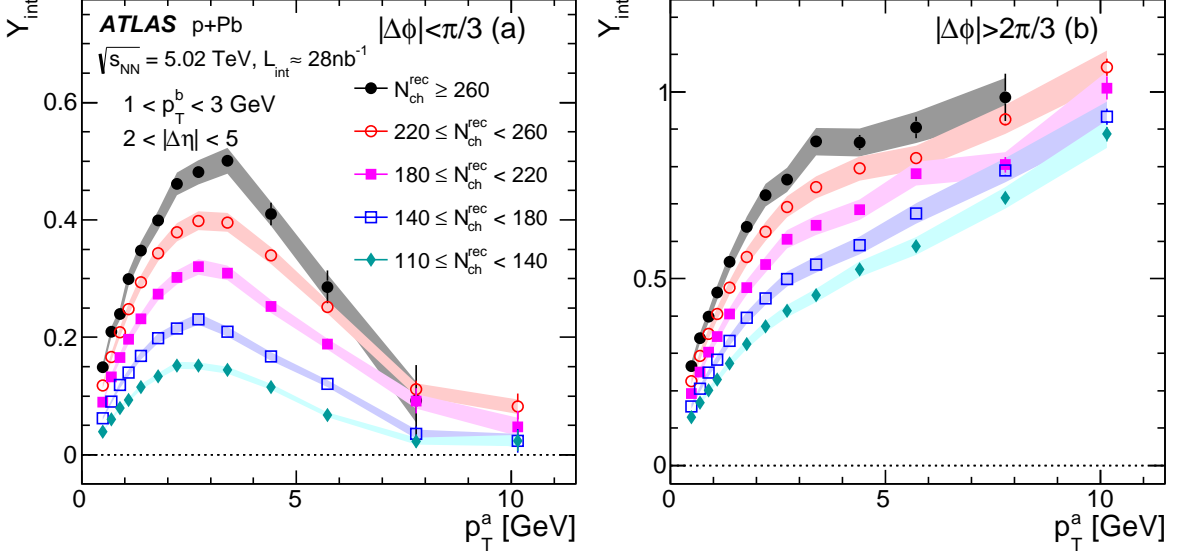


FIG. 6: Integrated per-trigger yields Y_{int} as a function of p_T^a for $1 < p_T^b < 3$ GeV, for events in various $N_{\text{ch}}^{\text{rec}}$ ranges on (a) the near-side and (b) the away-side. The errors bars and shaded bands represent the statistical and systematic uncertainties, respectively.

Figure 7 shows the centrality dependence of the long-range integrated yields for the event-activity based on $N_{\text{ch}}^{\text{rec}}$ (left) and E_T^{Pb} (right) for particles in $1 < p_T^{a,b} < 3$ GeV range. The near-side yield is close to zero in low-activity events and increases with E_T^{Pb} or $N_{\text{ch}}^{\text{rec}}$. The away-side yield shows a similar increase as a function of E_T^{Pb} or $N_{\text{ch}}^{\text{rec}}$, but it starts at a value significantly above zero. The yield difference between these two regions is found to vary slowly with E_T^{Pb} or $N_{\text{ch}}^{\text{rec}}$, indicating that the growth in the integrated yield with increasing event activity is similar on the near-side and the away-side. This behavior suggests the existence of an away-side long-range component that has a magnitude similar to the near-side long-range component.

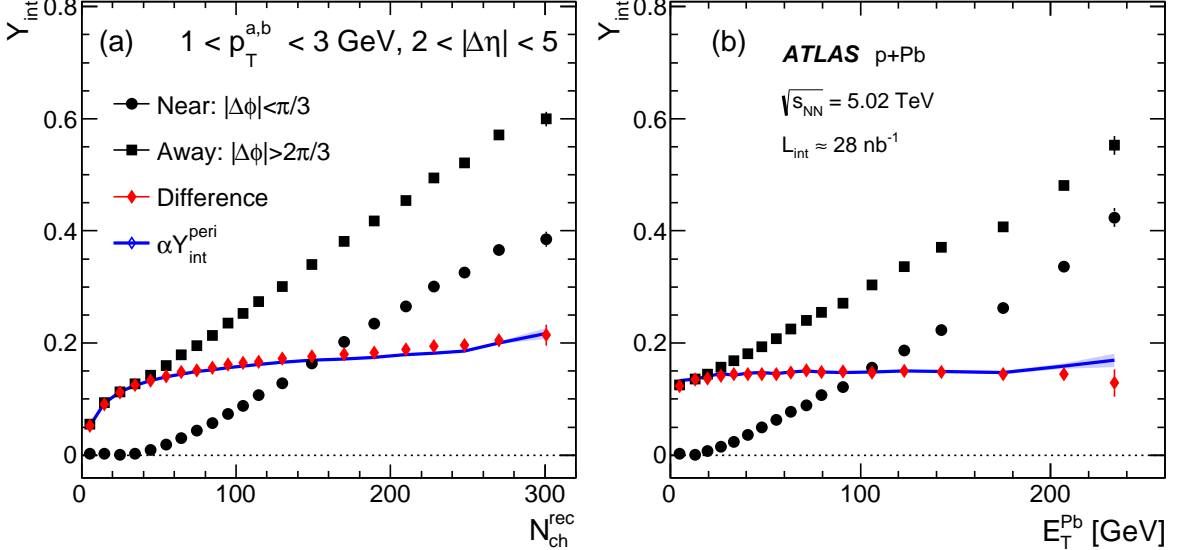


FIG. 7: The integrated per-trigger yield, Y_{int} , on the near-side (circles), the away-side (squares) and their difference (diamonds) as a function of (a) $N_{\text{ch}}^{\text{rec}}$ and (b) E_T^{Pb} for pairs in $2 < |\Delta\eta| < 5$ and $1 < p_T^{a,b} < 3$ GeV. The yield difference is compared to the estimated recoil contribution in the away-side (solid lines). The error bars or the shaded bands represent the combined statistical and systematic uncertainties.

Figure 7 also shows (solid lines) the recoil component estimated from the low event-activity class ($E_T^{\text{Pb}} < 10$ GeV) via the rescaling procedure discussed in Sec. III D. The yield difference between the away-side and the near-side in this p_T range is reproduced by this estimate of the recoil component. In other p_T ranges, a systematic difference between the recoil component and the yield difference is observed and is attributed to the contribution of a genuine dipolar flow, $v_{1,1}$, to the correlation function (see discussion in Sec. IV C).

To quantify the $\Delta\phi$ dependence of the measured long-range correlations, the first five harmonics of the correlation functions, v_1 to v_5 , are extracted via the procedure described in Sec. III E. The following section summarizes the results for v_2 – v_5 , and the results for v_1 are discussed in Sec. IV C.

B. Fourier coefficients v_2 – v_5

Figure 8 shows the v_2 , v_3 , and v_4 obtained using the 2PC method described in Sec. III E for $1 < p_T^b < 3$ GeV.

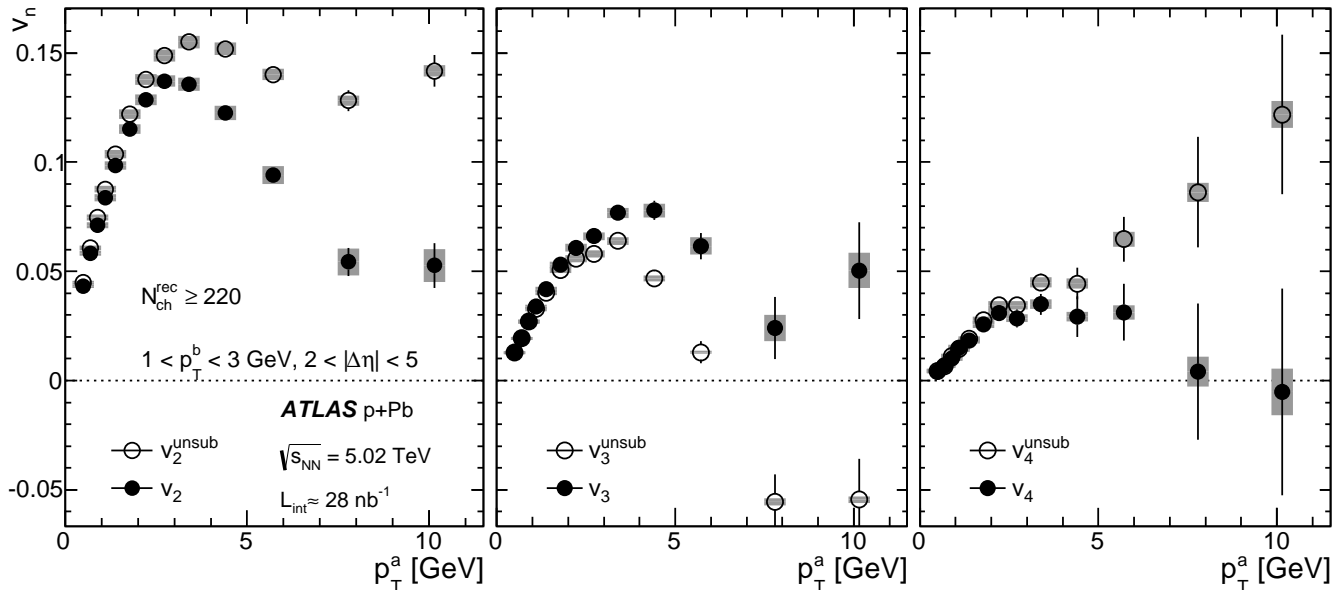


FIG. 8: The Fourier coefficients v_2 , v_3 , and v_4 as a function of p_T^a extracted from the correlation functions for events with $N_{\text{ch}}^{\text{rec}} \geq 220$, before (denoted by v_n^{unsub}) and after (denoted by v_n) the subtraction of the recoil component. Each panel shows the results for one harmonic. The pairs are formed from charged particles with $1 < p_T^b < 3$ GeV and $|\Delta\eta| > 2$. The error bars and shaded boxes represent the statistical and systematic uncertainties, respectively.

The results are shown both before (denoted by v_n^{unsub}) and after the subtraction of the recoil component (Eq. (6)). The recoil contribution affects slightly the v_n values for trigger $p_T < 3$ GeV, but becomes increasingly important for higher trigger p_T and higher-order harmonics. This behavior is expected as the dijet contributions, the dominant contribution to the recoil component, increase rapidly with p_T (for example see Fig. 5 or Ref. [9]). At high p_T , the contribution of dijets appears as a narrow peak at the away-side, leading to v_n^{unsub} coefficients with alternating sign: $(-1)^n$ [9]. In contrast, the v_n values after recoil subtraction are positive across the full measured p_T range. Hence, the recoil subtraction is necessary for the reliable extraction of the long-range correlations, especially at high p_T .

Figure 9 shows the trigger p_T dependence of the v_2 – v_5 in several $N_{\text{ch}}^{\text{rec}}$ event classes. The v_5 measurement is available only for three event-activity classes in a limited p_T range. All flow harmonics show similar trends, i.e. they increase with p_T up to 3–5 GeV and then decrease, but remain positive at higher p_T . For all event classes, the magnitude of the v_n is largest for $n = 2$, and decreases quickly with increasing n . The ATLAS data are compared to the measurement by the CMS experiment [28] for an event-activity class in which the number of offline reconstructed tracks, $N_{\text{trk}}^{\text{off}}$, within $|\eta| < 2.4$ and $p_T > 0.4$ GeV is $220 \leq N_{\text{trk}}^{\text{off}} < 260$. This is comparable to the $220 \leq N_{\text{ch}}^{\text{rec}} < 260$ event class used in the ATLAS analysis. A similar recoil removal procedure, with $N_{\text{trk}}^{\text{off}} < 20$ as the peripheral events, has been used for the CMS data. Excellent agreement is observed between the two results.

The extraction of the v_n from $v_{n,n}$ relies on the factorization relation in Eq. (9). This factorization is checked by calculating v_n using different ranges of p_T^b for events with $N_{\text{ch}}^{\text{rec}} \geq 220$ as shown in Fig. 10. The factorization behavior

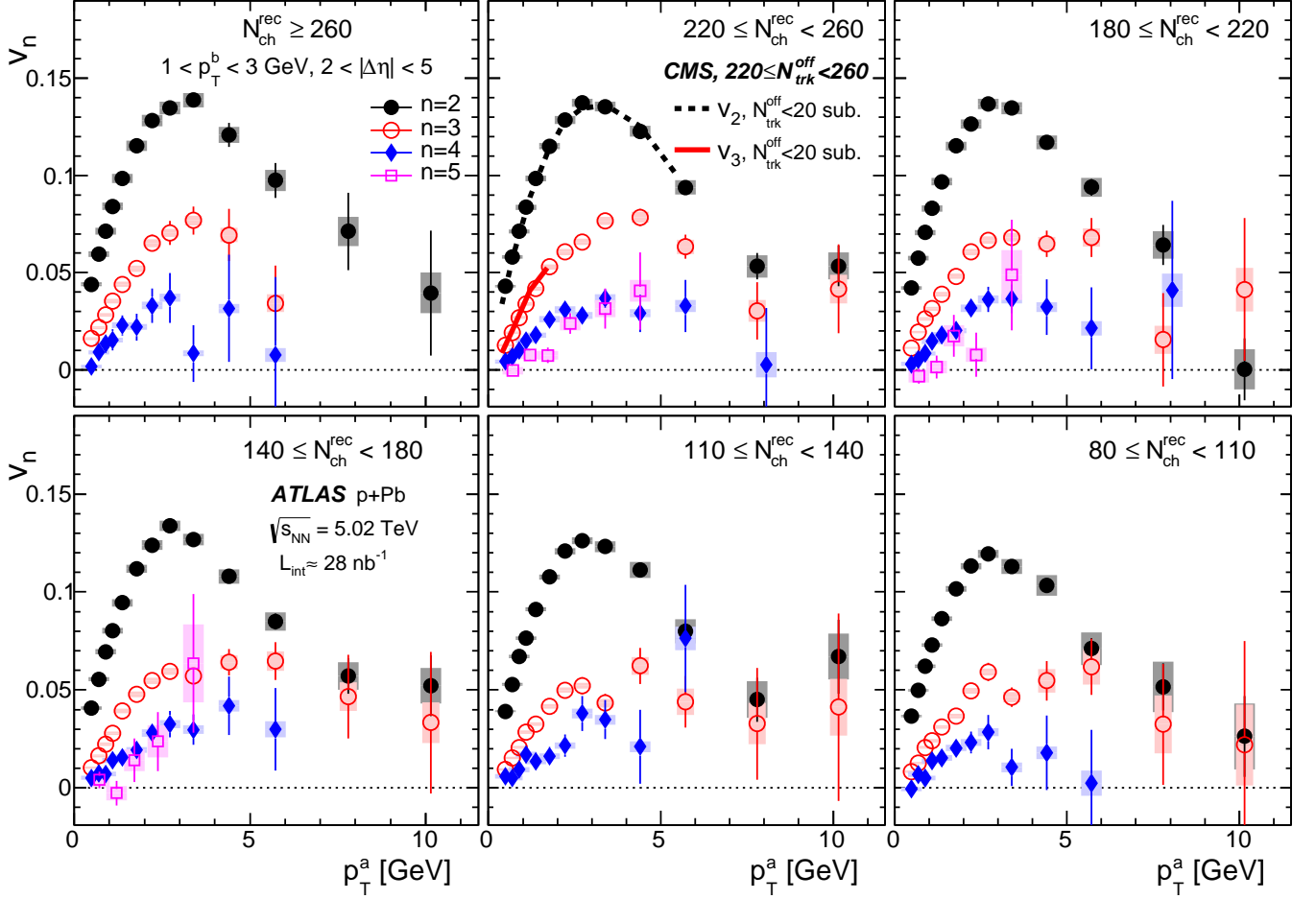


FIG. 9: The $v_n(p_T^a)$ with $n = 2$ to 5 for six $N_{\text{ch}}^{\text{rec}}$ event-activity classes obtained for $|\Delta\eta| > 2$ and the p_T^b range of 1–3 GeV. The error bars and shaded boxes represent the statistical and systematic uncertainties, respectively. Results in $220 \leq N_{\text{ch}}^{\text{rec}} < 260$ are compared to the CMS data [28] obtained by subtracting the peripheral events (the number of offline tracks $N_{\text{trk}}^{\text{off}} < 20$), shown by the solid and dashed lines.

can also be studied via the ratio [48, 49]

$$r_n(p_T^a, p_T^b) = \frac{v_{n,n}(p_T^a, p_T^b)}{\sqrt{v_{n,n}(p_T^a, p_T^a)v_{n,n}(p_T^b, p_T^b)}}, \quad (11)$$

with $r_n = 1$ for perfect factorization. The results with recoil subtraction (r_n) and without subtraction (r_n^{unsub}) are summarized in Fig. 11, and they are shown as a function of $p_T^b - p_T^a$, because by construction the ratios equal one for $p_T^b = p_T^a$. This second method is limited to $p_T^{a,b} \lesssim 4$ GeV, since requiring both particles to be at high p_T reduces the number of the available pairs for $v_{n,n}(p_T^a, p_T^a)$ or $v_{n,n}(p_T^b, p_T^b)$. In contrast, for the results shown in Fig. 10, using Eqs. (9) and (10), the restriction applies to only one of the particles, i.e. $p_T^b \lesssim 4$ GeV.

Results in Figs. 10 and 11 show that, in the region where the statistical uncertainty is small, the factorization holds to within a few percent for v_2 over $0.5 < p_T^{a,b} < 4$ GeV, within 10% for v_3 over $0.5 < p_T^{a,b} < 3$ GeV, and within 20–30% for v_4 over $0.5 < p_T^{a,b} < 4$ GeV (Fig. 10 only). Furthermore, in this p_T region, the differences between r_n and r_n^{unsub} are very small ($< 10\%$) as shown by Fig. 11, consistent with the observation in Fig. 8. This level of factorization is similar to what was observed in peripheral Pb+Pb collisions [9].

Figure 11 also compares the r_n data with a theoretical calculation from a viscous hydrodynamic model [50]. The model predicts at most a few percent deviation of r_n from one, which is attributed to p_T -dependent decorrelation effects associated with event-by-event flow fluctuations [48]. In most cases, the data are consistent with the prediction within uncertainties.

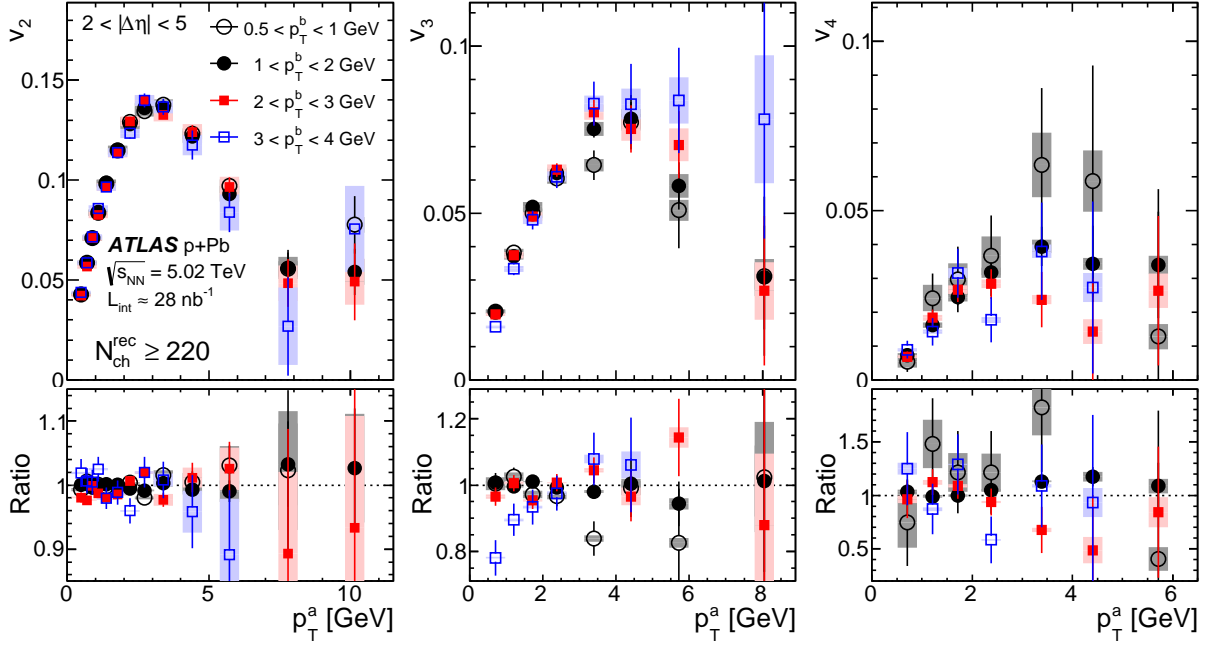


FIG. 10: The v_2 (left column), v_3 (middle column), and v_4 (right column) as a function of p_T^a extracted using four p_T^b bins in the long-range region $|\Delta\eta| > 2$ for events with $N_{ch}^{rec} \geq 220$. The ratio of the $v_n(p_T^a)$ in each p_T^b bin to those obtained with the default reference p_T^b bin of 1–3 GeV are shown in the bottom part of each column. The error bars and shaded bands represent the statistical and systematic uncertainties, respectively.

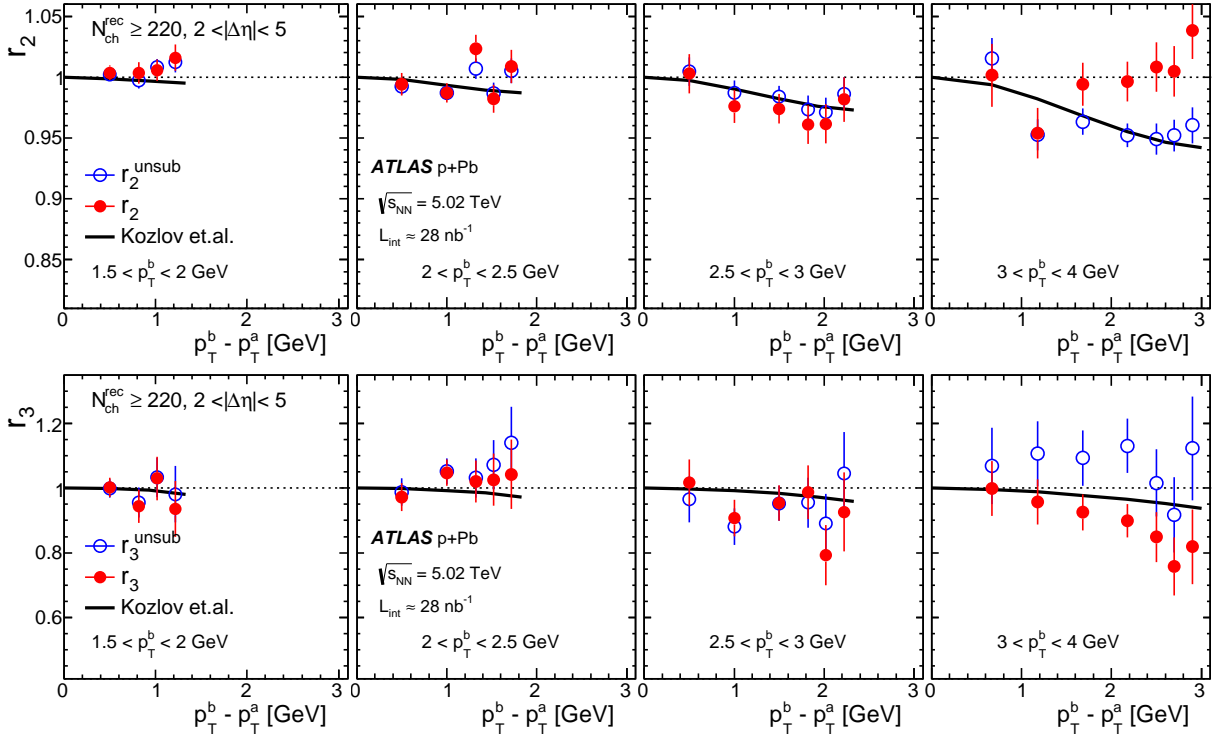


FIG. 11: The values of factorization variable defined by Eq. (11) before (denoted by r_n^{unsub}) and after (denoted by r_n) the subtraction of the recoil component. They are shown for $n = 2$ (top row) and $n = 3$ (bottom row) as a function of $p_T^b - p_T^a$ in various p_T^b ranges for events in $N_{ch}^{rec} \geq 220$. The solid lines represent a theoretical prediction from Ref. [50]. The error bars represent the total experimental uncertainties.

Figure 12 shows the centrality dependence of v_2 , v_3 , and v_4 as a function of $N_{\text{ch}}^{\text{rec}}$ and E_{T}^{Pb} . The results are obtained for $0.4 < p_{\text{T}}^{\text{a,b}} < 3$ GeV, both before and after subtraction of the recoil contribution. The difference between v_n^{unsub} and v_n is very small in central collisions, up to 3–4% for both event-activity definitions. For more peripheral collisions, the difference is larger and reaches 20–30% for $N_{\text{ch}}^{\text{rec}} \sim 40$ or $E_{\text{T}}^{\text{Pb}} \sim 30$ GeV. The sign of the difference also alternates in n (already seen in Fig. 8): i.e. $v_n^{\text{unsub}} > v_n$ for even n and $v_n^{\text{unsub}} < v_n$ for odd n . This behavior is characteristic of the influence of the away-side dijet contribution to v_n^{unsub} .

The v_n values in Fig. 12 exhibit modest centrality dependence. The change of v_2 is less than 8% over $140 < N_{\text{ch}}^{\text{rec}} < 300$ (top 0.5% of MB-triggered events) or $130 < E_{\text{T}}^{\text{Pb}} < 240$ GeV (top 0.05% of MB-triggered events), covering about half of the full dynamic range. The centrality dependence of v_3 is stronger and exhibits a nearly linear increase with $N_{\text{ch}}^{\text{rec}}$ and E_{T}^{Pb} .

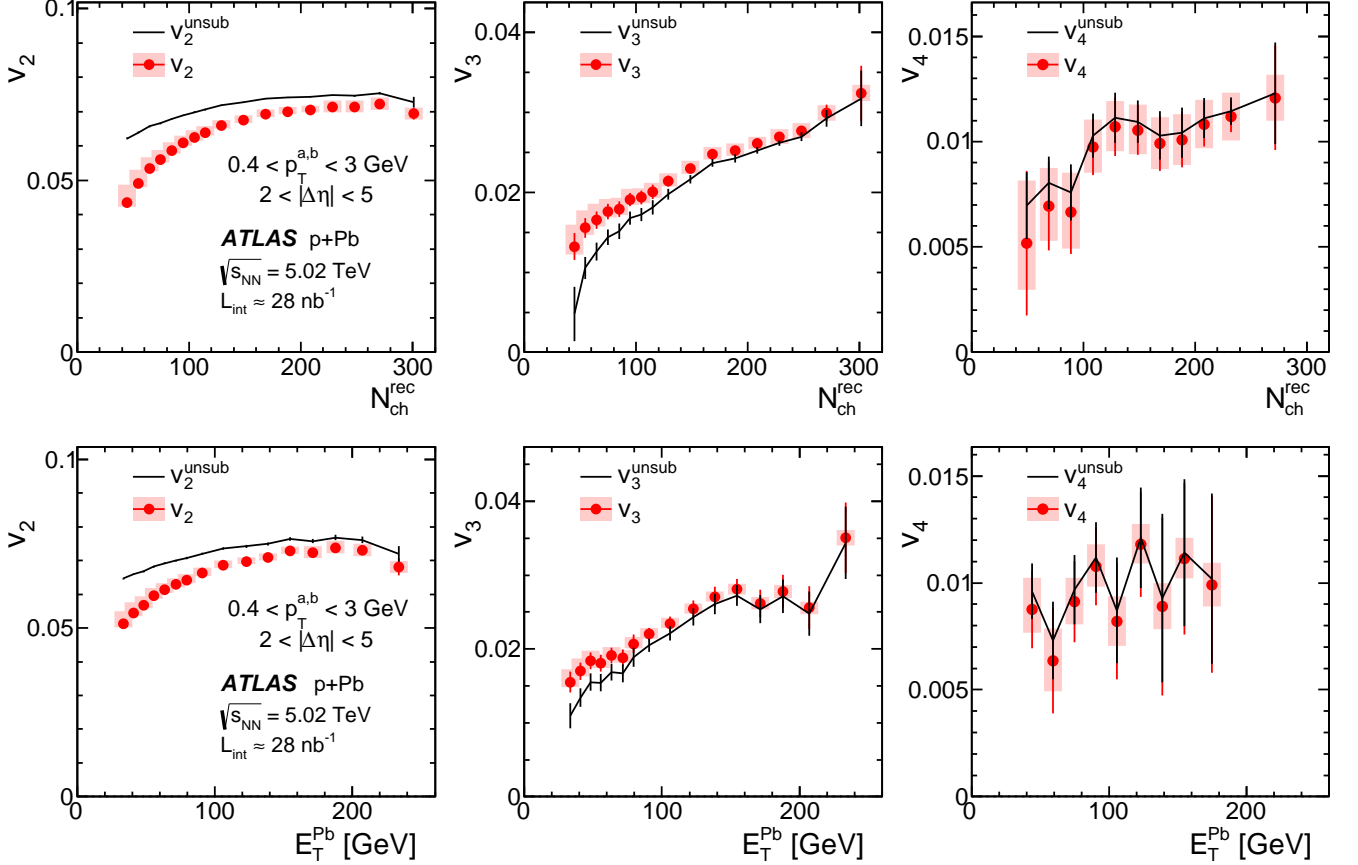


FIG. 12: The centrality dependence of v_2 , v_3 , and v_4 as a function of $N_{\text{ch}}^{\text{rec}}$ (top row) and E_{T}^{Pb} (bottom row) for pairs with $0.4 < p_{\text{T}}^{\text{a,b}} < 3$ GeV and $|\Delta\eta| > 2$. The results are obtained with (symbols) and without (lines) the subtraction of the recoil contribution. The error bars and shaded boxes on v_n data represent the statistical and systematic uncertainties, respectively, while the error bars on the v_n^{unsub} represent the combined statistical and systematic uncertainties.

Figure 12 shows that the overall centrality dependence is similar for $N_{\text{ch}}^{\text{rec}}$ and E_{T}^{Pb} . The correlation data (not the fit, Eq. (2)) in Fig. 2 are used to map the $N_{\text{ch}}^{\text{rec}}$ -dependence in the top row of Fig. 12 to a corresponding E_{T}^{Pb} -dependence. The E_{T}^{Pb} -dependence of v_n mapped from $N_{\text{ch}}^{\text{rec}}$ -dependence is then compared to the directly measured E_{T}^{Pb} -dependence in Fig. 13. Good agreement is seen for v_2 and v_3 .

C. First-order Fourier coefficient v_1

A similar analysis is performed to extract the dipolar flow v_1 . Figure 14 shows the $v_{1,1}$ values as a function of p_{T}^{a} in various ranges of p_{T}^{b} before and after the recoil subtraction. Before the recoil subtraction, $v_{1,1}^{\text{unsub}}$ values are always negative and decrease nearly linearly with p_{T}^{a} and p_{T}^{b} , except for the p_{T} region around 3–4 GeV where a shoulder-like structure is seen. This shoulder is very similar to that observed in A+A collisions, which is understood as a combined

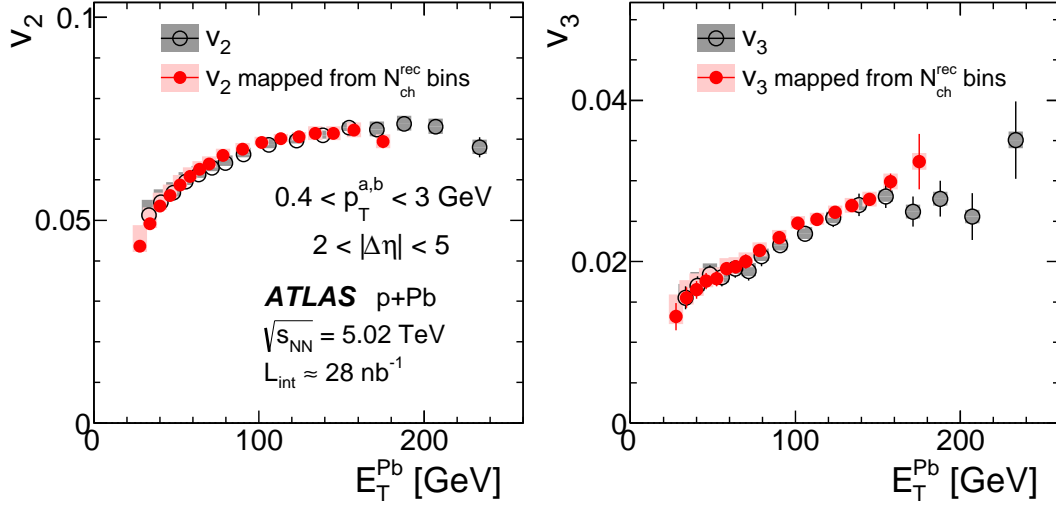


FIG. 13: The v_2 (left panel) and v_3 (right panel) as a function of E_T^{Pb} calculated directly for narrow ranges in E_T^{Pb} (open circles) or obtained indirectly by mapping from the $N_{\text{ch}}^{\text{rec}}$ -dependence of v_n using the correlation data shown in Fig. 2(b) (solid circles). The error bars and shaded boxes represent the statistical and systematic uncertainties, respectively.

contribution from the negative recoil and positive dipolar flow in this p_T range [9, 51] according to the following form [52, 53]:

$$v_{1,1}^{\text{unsub}}(p_T^{\text{a}}, p_T^{\text{b}}) \approx v_1(p_T^{\text{a}})v_1(p_T^{\text{b}}) - \frac{p_T^{\text{a}}p_T^{\text{b}}}{M\langle p_T^2 \rangle}, \quad (12)$$

where M and $\langle p_T^2 \rangle$ are the multiplicity and average squared transverse momentum of the particles in the whole event, respectively. The negative correction term reflects the global momentum conservation contribution, which is important in low-multiplicity events and at high p_T . The shoulder-like structure in Fig. 14 reflects the contribution of the dipolar flow term $v_1(p_T^{\text{a}})v_1(p_T^{\text{b}})$.

After the recoil subtraction, the magnitude of $v_{1,1}$ is greatly reduced, suggesting that most of the momentum conservation contribution has been removed. The resulting $v_{1,1}$ values cross each other at around $p_T^{\text{a}} \sim 1.5\text{--}2.0$ GeV. This behavior is consistent with the expectation that the $v_1(p_T)$ function crosses zero at $p_T \sim 1\text{--}2$ GeV, a feature that is also observed in A+A collisions [9, 51]. The trigger p_T dependence of v_1 is obtained via a factorization procedure very similar to that discussed in Sec. III E

$$v_1(p_T^{\text{a}}) \equiv \frac{v_{1,1}(p_T^{\text{a}}, p_T^{\text{b}})}{v_1(p_T^{\text{b}})}, \quad (13)$$

where the dipolar flow in the associated p_T bin, $v_1(p_T^{\text{b}})$, is defined as

$$v_1(p_T^{\text{b}}) = \text{sign}(p_T^{\text{b}} - p_T^0) \sqrt{|v_{1,1}(p_T^{\text{b}}, p_T^{\text{b}})|}, \quad (14)$$

where $\text{sign}(p_T^{\text{b}} - p_T^0)$ is the sign of the v_1 , defined to be negative for $p_T^{\text{b}} < p_T^0 = 1.5$ GeV and positive otherwise. This function is necessary in order to account for the sign change of v_1 at low p_T .

To obtain the $v_1(p_T^{\text{a}})$, three reference p_T^{b} ranges, 0.5–1 GeV, 3–4 GeV and 4–5 GeV, are used to first calculate $v_1(p_T^{\text{b}})$. These values are then inserted into Eq. (13) to obtain three $v_1(p_T^{\text{a}})$ functions. The uncertainties on the $v_1(p_T^{\text{a}})$ values are calculated via an error propagation through Eqs. (13) and (14). The calculation is not possible for p_T^{b} in the range of 1–3 GeV, where the $v_{1,1}$ values are close to zero and hence the resulting $v_1(p_T^{\text{b}})$ have large uncertainties.

The results for $v_1(p_T^{\text{a}})$ are shown in Fig. 15 for these three reference p_T^{b} bins. They are consistent with each other. The v_1 value is negative at low p_T , crosses zero at around $p_T \sim 1.5$ GeV, and increases to 0.1 at 4–6 GeV. This p_T -dependence is similar to the $v_1(p_T)$ measured by ATLAS experiment in Pb+Pb collisions at $\sqrt{s_{\text{NN}}} = 2.76$ TeV [9], except that the v_1 value in Pb+Pb collisions crosses zero at lower p_T (~ 1.1 GeV), which reflects the fact that the $\langle p_T \rangle$ in Pb+Pb at $\sqrt{s_{\text{NN}}} = 2.76$ TeV is smaller than that in p+Pb at $\sqrt{s_{\text{NN}}} = 5.02$ TeV.

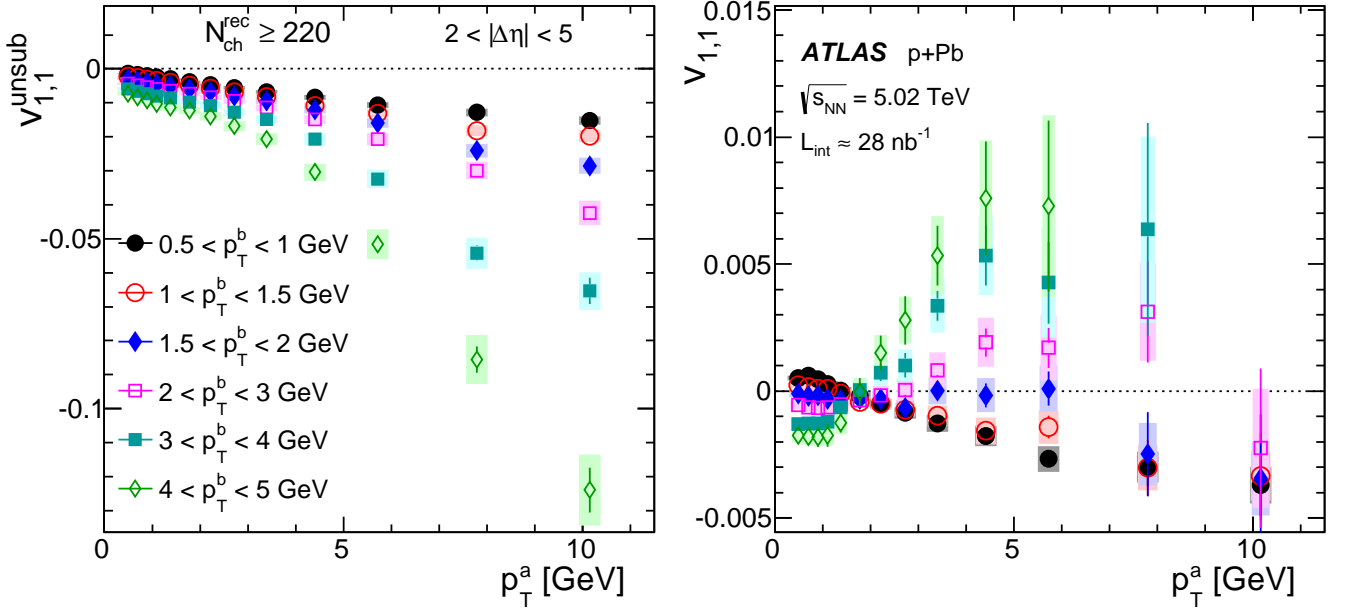


FIG. 14: The first-order harmonic of 2PC before recoil subtraction $v_{1,1}^{\text{unsub}}$ (left panel) and after recoil subtraction $v_{1,1}$ (right panel) as a function of p_T^a for different p_T^b ranges for events with $N_{\text{ch}}^{\text{rec}} \geq 220$. The error bars and shaded boxes represent the statistical and systematic uncertainties, respectively.

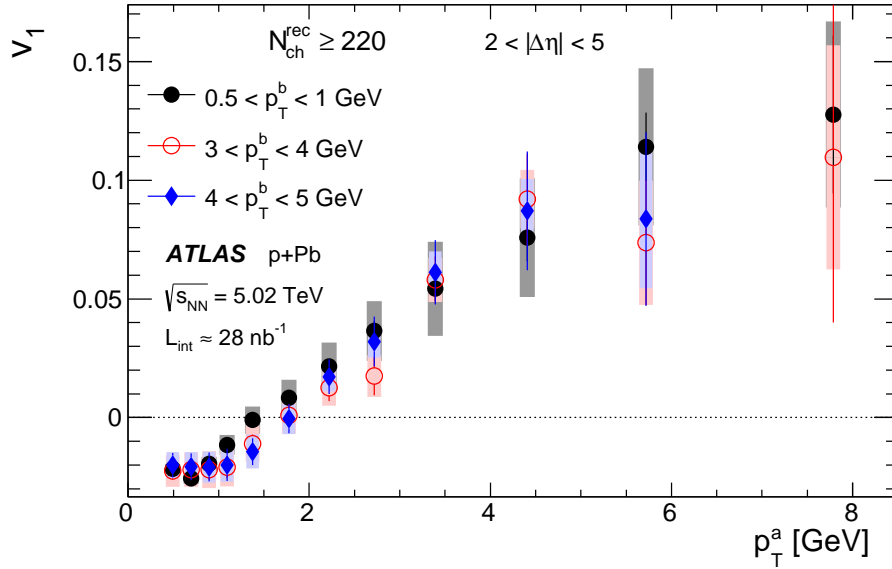


FIG. 15: The p_T^a dependence of v_1 extracted using the factorization relations Eqs. (13) and (14) in three reference p_T^b ranges for events with $N_{\text{ch}}^{\text{rec}} \geq 220$. The error bars and shaded boxes represent the statistical and systematic uncertainties, respectively.

D. Comparison of v_n results between high-multiplicity p+Pb and peripheral Pb+Pb collisions

In the highest multiplicity p+Pb collisions, the charged particle multiplicity, $N_{\text{ch}}^{\text{rec}}$, can reach more than 350 in $|\eta| < 2.5$ and E_T^{Pb} close to 300 GeV on the Pb-fragmentation side. This activity is comparable to Pb+Pb collisions at $\sqrt{s_{NN}} = 2.76$ TeV in the 45–50% centrality interval, where the long-range correlation is known to be dominated by collective flow. Hence a comparison of the v_n coefficients in similar event activity for the two collision systems can improve our current understanding of the origin of the long-range correlations.

The left column of Fig. 16 compares the v_n values from p+Pb collisions with $220 \leq N_{\text{ch}}^{\text{rec}} < 260$ to the v_n values for

Pb+Pb collisions in the 55–60% centrality interval from Ref. [9]. These two event classes are chosen to have similar efficiency-corrected multiplicity of charged particles with $p_T > 0.5$ GeV and $|\eta| < 2.5$, characterized by its average value ($\langle N_{\text{ch}} \rangle$) and its standard deviation (σ): $\langle N_{\text{ch}} \rangle \pm \sigma \approx 259 \pm 13$ for p +Pb collisions and $\langle N_{\text{ch}} \rangle \pm \sigma \approx 241 \pm 43$ for Pb+Pb collisions.

The Pb+Pb results on v_n [9] were obtained via an event-plane method by correlating tracks in $\eta > 0$ ($\eta < 0$) with the event plane determined in the FCal in the opposite hemisphere. The larger v_2 values in Pb+Pb collisions can be attributed to the elliptic collision geometry of the Pb+Pb system, while the larger v_4 values are due to the non-linear coupling between v_2 and v_4 in the collective expansion [54]. The v_3 data for Pb+Pb collisions are similar in magnitude to those in p +Pb collisions. However, the p_T dependence of v_n is different for the two systems. These observations are consistent with similar comparisons performed by the CMS experiment [28].

Recently, Basar and Teaney [55] have proposed a method to rescale the Pb+Pb data for a proper comparison to

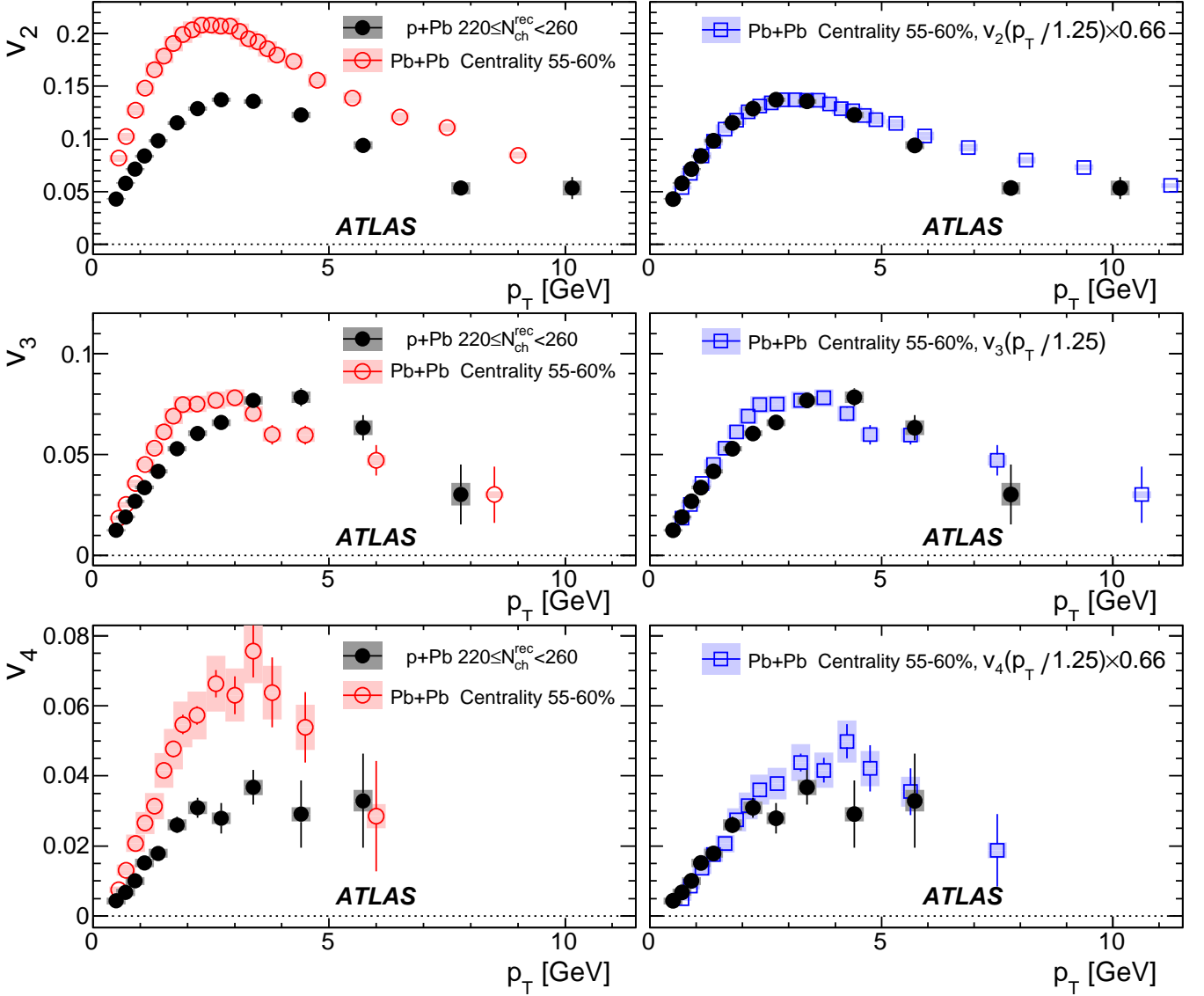


FIG. 16: The coefficients v_2 (top row), v_3 (middle row) and v_4 (bottom row) as a function of p_T compared between p +Pb collisions with $220 \leq N_{\text{ch}}^{\text{rec}} < 260$ in this analysis and Pb+Pb collisions in 55–60% centrality from Ref. [9]. The left column shows the original data with their statistical (error bars) and systematic uncertainties (shaded boxes). In the right column, the same Pb+Pb data are rescaled horizontally by a constant factor of 1.25, and the v_2 and v_4 are also down-scaled by an empirical factor of 0.66 to match the p +Pb data.

the p +Pb data. They argue that the $v_n(p_T)$ shape in the two collision systems are related to each other by a constant scale factor of $K = 1.25$ accounting for the difference in their $\langle p_T \rangle$, and that one should observe a similar $v_n(p_T)$

dependence shape after rescaling the p_T measured in Pb+Pb collisions to get $v_n(p_T/K)$. The difference in the overall magnitude of v_2 after the p_T -rescaling is entirely due to the elliptic geometry of Pb+Pb collisions.

In order to test this idea, the p_T for Pb+Pb collisions are rescaled by the constant factor of 1.25 and v_n values with rescaled p_T are displayed in the right column of Fig. 16. Furthermore, the magnitudes of v_2 and v_4 are also rescaled by a common empirical value of 0.66 to approximately match the magnitude of the corresponding p +Pb v_n data. The rescaled v_n results are shown in the right column and compared to the p +Pb v_n data. They agree well with each other, in particular in the low- p_T region ($p_T < 2$ –4 GeV) where the statistical uncertainties are small.

V. SUMMARY

This paper presents measurements of two-particle correlation (2PC) functions and the first five azimuthal harmonics v_1 – v_5 in $\sqrt{s_{NN}} = 5.02$ TeV p +Pb collisions with a total integrated luminosity of approximately 28 nb^{-1} recorded by the ATLAS detector at the LHC. The two-particle correlations and v_n coefficients are obtained as a function of p_T for pairs with $2 < |\Delta\eta| < 5$ in different intervals of event activity, defined by either $N_{\text{ch}}^{\text{rec}}$, the number of reconstructed tracks with $p_T > 0.4$ GeV and $|\eta| < 2.5$, or E_T^{Pb} , the total transverse energy over $-4.9 < \eta < -3.2$ on the Pb-fragmentation side.

Significant long-range correlations (extending to $|\Delta\eta| = 5$) are observed for pairs at the near-side ($|\Delta\phi| < \pi/3$) over a wide range of transverse momentum ($p_T < 12$ GeV) and broad ranges of $N_{\text{ch}}^{\text{rec}}$ and E_T^{Pb} . A similar long-range correlation is also observed on the away-side ($|\Delta\phi| > 2\pi/3$), after subtracting the recoil contribution estimated using the 2PC in low-activity events.

The azimuthal structure of these long-range correlations is quantified using the Fourier coefficients v_2 – v_5 as a function of p_T . The v_n values increase with p_T to 3–4 GeV and then decrease for higher p_T , but remain positive in the measured p_T range. The overall magnitude of $v_n(p_T)$ is observed to decrease with n . The magnitudes of v_n also increase with both $N_{\text{ch}}^{\text{rec}}$ and E_T^{Pb} . The v_2 values seem to saturate at large $N_{\text{ch}}^{\text{rec}}$ or E_T^{Pb} values, while the v_3 values show a linear increase over the measured $N_{\text{ch}}^{\text{rec}}$ or E_T^{Pb} range. The first-order harmonic v_1 is also extracted from the 2PC. The $v_1(p_T)$ function is observed to change sign at $p_T \approx 1.5$ –2.0 GeV and to increase to about 0.1 at $p_T > 4$ GeV.

The extracted $v_2(p_T)$, $v_3(p_T)$ and $v_4(p_T)$ are compared to the v_n coefficients in Pb+Pb collisions at $\sqrt{s_{NN}} = 2.76$ TeV with similar $N_{\text{ch}}^{\text{rec}}$. After applying a scale factor of $K = 1.25$ that accounts for the difference of mean p_T in the two collision systems as suggested in Ref. [55], the shape of the $v_n(p_T/K)$ distribution in Pb+Pb collision is found to be similar to the shape of $v_n(p_T)$ distribution in p +Pb collisions. This suggests that the long-range ridge correlations in high-multiplicity p +Pb collisions and peripheral Pb+Pb collisions are driven by similar dynamics.

ACKNOWLEDGEMENTS

We thank CERN for the very successful operation of the LHC, as well as the support staff from our institutions without whom ATLAS could not be operated efficiently.

We acknowledge the support of ANPCyT, Argentina; YerPhI, Armenia; ARC, Australia; BMWF and FWF, Austria; ANAS, Azerbaijan; SSTC, Belarus; CNPq and FAPESP, Brazil; NSERC, NRC and CFI, Canada; CERN; CONICYT, Chile; CAS, MOST and NSFC, China; COLCIENCIAS, Colombia; MSMT CR, MPO CR and VSC CR, Czech Republic; DNRF, DNSRC and Lundbeck Foundation, Denmark; EPLANET, ERC and NSRF, European Union; IN2P3-CNRS, CEA-DSM/IRFU, France; GNSF, Georgia; BMBF, DFG, HGF, MPG and AvH Foundation, Germany; GSRT and NSRF, Greece; ISF, MINERVA, GIF, I-CORE and Benoziyo Center, Israel; INFN, Italy; MEXT and JSPS, Japan; CNRST, Morocco; FOM and NWO, Netherlands; BRF and RCN, Norway; MNiSW and NCN, Poland; GRICES and FCT, Portugal; MNE/IFA, Romania; MES of Russia and ROSATOM, Russian Federation; JINR; MSTB, Serbia; MSSR, Slovakia; ARRS and MIZŠ, Slovenia; DST/NRF, South Africa; MINECO, Spain; SRC and Wallenberg Foundation, Sweden; SER, SNSF and Cantons of Bern and Geneva, Switzerland; NSC, Taiwan; TAEK, Turkey; STFC, the Royal Society and Leverhulme Trust, United Kingdom; DOE and NSF, United States of America.

The crucial computing support from all WLCG partners is acknowledged gratefully, in particular from CERN and the ATLAS Tier-1 facilities at TRIUMF (Canada), NDGF (Denmark, Norway, Sweden), CC-IN2P3 (France), KIT/GridKA (Germany), INFN-CNAF (Italy), NL-T1 (Netherlands), PIC (Spain), ASGC (Taiwan), RAL (UK) and

BNL (USA) and in the Tier-2 facilities worldwide.

-
- [1] STAR Collaboration, K. Ackermann et al., *Phys. Rev. Lett.* **86** (2001) 402.
 - [2] ALICE Collaboration, K. Aamodt et al., *Phys. Rev. Lett.* **107** (2011) 032301.
 - [3] J. Jia, *J. Phys. G* **31** (2005) S521.
 - [4] PHENIX Collaboration, A. Adare et al., *Phys. Rev. C* **78** (2008) 014901.
 - [5] PHOBOS Collaboration, B. Alver et al., *Phys. Rev. Lett.* **104** (2010) 062301.
 - [6] STAR Collaboration, M. Aggarwal et al., *Phys. Rev. C* **82** (2010) 024912.
 - [7] ALICE Collaboration, K. Aamodt et al., *Phys. Lett. B* **708** (2012) 249.
 - [8] CMS Collaboration, *Eur. Phys. J. C* **72** (2012) 2012.
 - [9] ATLAS Collaboration, *Phys. Rev. C* **86** (2012) 014907.
 - [10] ATLAS Collaboration, *JHEP* **11** (2013) 183.
 - [11] CMS Collaboration, *Phys. Rev. C* **89** (2014) 044906.
 - [12] STAR Collaboration, L. Adamczyk et al., *Phys. Rev. C* **88** (2013) 014904.
 - [13] PHENIX Collaboration, A. Adare et al., *Phys. Rev. Lett.* **107** (2011) 252301.
 - [14] B. Alver and G. Roland, *Phys. Rev. C* **81** (2010) 054905.
 - [15] M. Luzum and J. Y. Ollitrault, *Nucl. Phys. A* **904** (2013) 377c.
 - [16] D. Teaney and L. Yan, *Phys. Rev. C* **83** (2011) 064904.
 - [17] C. Gale, S. Jeon, B. Schenke, P. Tribedy, and R. Venugopalan, *Phys. Rev. Lett.* **110** (2013) 012302.
 - [18] H. Niemi, G. Denicol, H. Holopainen, and P. Huovinen, *Phys. Rev. C* **87** (2013) 054901.
 - [19] Z. Qiu and U. Heinz, *Phys. Lett. B* **717** (2012) 261.
 - [20] D. Teaney and L. Yan, *Phys. Rev. C* **90** (2014) 024902.
 - [21] CMS Collaboration, *JHEP* **09** (2010) 091.
 - [22] CMS Collaboration, *Phys. Lett. B* **718** (2013) 795.
 - [23] ALICE Collaboration, B. Abelev et al., *Phys. Lett. B* **719** (2013) 29.
 - [24] ATLAS Collaboration, *Phys. Rev. Lett.* **110** (2013) 182302.
 - [25] PHENIX Collaboration, A. Adare et al., *Phys. Rev. Lett.* **111** (2013) 212301.
 - [26] ALICE Collaboration, B. B. Abelev et al., *Phys. Lett. B* **726** (2013) 164.
 - [27] ATLAS Collaboration, *Phys. Lett. B* **725** (2013) 60.
 - [28] CMS Collaboration, *Phys. Lett. B* **724** (2013) 213.
 - [29] P. Bozek, *Phys. Rev. C* **85** (2012) 014911.
 - [30] E. Shuryak and I. Zahed, *Phys. Rev. C* **88** (2013) 044915.
 - [31] P. Bozek and W. Broniowski, *Phys. Rev. C* **88** (2013) 014903.
 - [32] G. Y. Qin and B. Muller, *Phys. Rev. C* **89** (2014) 044902.
 - [33] K. Dusling and R. Venugopalan, *Phys. Rev. D* **87** (2013) 051502.
 - [34] K. Dusling and R. Venugopalan, *Phys. Rev. D* **87** (2013) 054014.
 - [35] Y. V. Kovchegov and D. E. Wertepny, *Nucl. Phys. A* **906** (2013) 50.
 - [36] L. McLerran, M. Praszalowicz, and B. Schenke, *Nucl. Phys. A* **916** (2013) 210.
 - [37] K. Dusling and R. Venugopalan, *Phys. Rev. D* **87** (2013) 094034.
 - [38] A. Bzdak, B. Schenke, P. Tribedy, and R. Venugopalan, *Phys. Rev. C* **87** (2013) 064906.
 - [39] ATLAS Collaboration, *JINST* **3** (2008) S08003.
 - [40] ATLAS Collaboration, *Eur. Phys. J. C* **72** (2012) 1849.
 - [41] ATLAS Collaboration, ATLAS-CONF-2013-104. <http://cds.cern.ch/record/1624013>.
 - [42] ATLAS Collaboration, *New J. Phys.* **13** (2011) 053033.
 - [43] X. Wang and M. Gyulassy, *Phys. Rev. D* **44** (1991) 3501.
 - [44] GEANT4 Collaboration, S. Agostinelli et al., *Nucl. Instrum. Meth. A* **506** (2003) 250.
 - [45] ATLAS Collaboration, *Eur. Phys. J. C* **70** (2010) 823.
 - [46] N. Ajitanand et al., *Phys. Rev. C* **72** (2005) 011902.
 - [47] PHENIX Collaboration, K. Adcox et al., *Phys. Rev. Lett.* **89** (2002) 212301.
 - [48] F. G. Gardim, F. Grassi, M. Luzum, and J.-Y. Ollitrault, *Phys. Rev. C* **87** (2013) 031901.
 - [49] U. Heinz, Z. Qiu, and C. Shen, *Phys. Rev. C* **87** (2013) 034913.
 - [50] I. Kozlov, M. Luzum, G. Denicol, S. Jeon, and C. Gale, [arXiv:1405.3976 \[nucl-th\]](https://arxiv.org/abs/1405.3976).
 - [51] E. Retinskaya, M. Luzum, and J. Y. Ollitrault, *Phys. Rev. Lett.* **108** (2012) 252302.
 - [52] N. Borghini, P. M. Dinh, and J. Y. Ollitrault, *Phys. Rev. C* **62** (2000) 034902.
 - [53] N. Borghini, P. Dinh, J. Y. Ollitrault, A. M. Poskanzer, and S. Voloshin, *Phys. Rev. C* **66** (2002) 014901.
 - [54] M. Luzum, C. Gombeaud, and J. Y. Ollitrault, *Phys. Rev. C* **81** (2010) 054910.
 - [55] G. Basar and D. Teaney, [arXiv:1312.6770 \[nucl-th\]](https://arxiv.org/abs/1312.6770).

The ATLAS Collaboration

G. Aad⁸⁴, B. Abbott¹¹², J. Abdallah¹⁵², S. Abdel Khalek¹¹⁶, O. Abdinov¹¹, R. Aben¹⁰⁶, B. Abi¹¹³, M. Abolins⁸⁹, O.S. AbouZeid¹⁵⁹, H. Abramowicz¹⁵⁴, H. Abreu¹⁵³, R. Abreu³⁰, Y. Abulaiti^{147a,147b}, B.S. Acharya^{165a,165b,a}, L. Adamczyk^{38a}, D.L. Adams²⁵, J. Adelman¹⁷⁷, S. Adomeit⁹⁹, T. Adye¹³⁰, T. Agatonovic-Jovin^{13a}, J.A. Aguilar-Saavedra^{125a,125f}, M. Agustoni¹⁷, S.P. Ahlen²², F. Ahmadov^{64,b}, G. Aielli^{134a,134b}, H. Akerstedt^{147a,147b}, T.P.A. Åkesson⁸⁰, G. Akimoto¹⁵⁶, A.V. Akimov⁹⁵, G.L. Alberghi^{20a,20b}, J. Albert¹⁷⁰, S. Albrand⁵⁵, M.J. Alconada Verzini⁷⁰, M. Aleksa³⁰, I.N. Aleksandrov⁶⁴, C. Alexa^{26a}, G. Alexander¹⁵⁴, G. Alexandre⁴⁹, T. Alexopoulos¹⁰, M. Alhroob^{165a,165c}, G. Alimonti^{90a}, L. Alio⁸⁴, J. Alison³¹, B.M.M. Allbrooke¹⁸, L.J. Allison⁷¹, P.P. Allport⁷³, J. Almond⁸³, A. Aloisio^{103a,103b}, A. Alonso³⁶, F. Alonso⁷⁰, C. Alpigiani⁷⁵, A. Altheimer³⁵, B. Alvarez Gonzalez⁸⁹, M.G. Alviggi^{103a,103b}, K. Amako⁶⁵, Y. Amaral Coutinho^{24a}, C. Amelung²³, D. Amidei⁸⁸, S.P. Amor Dos Santos^{125a,125c}, A. Amorim^{125a,125b}, S. Amoroso⁴⁸, N. Amram¹⁵⁴, G. Amundsen²³, C. Anastopoulos¹⁴⁰, L.S. Ancu⁴⁹, N. Andari³⁰, T. Andeen³⁵, C.F. Anders^{58b}, G. Anders³⁰, K.J. Anderson³¹, A. Andreazza^{90a,90b}, V. Andrei^{58a}, X.S. Anduaga⁷⁰, S. Angelidakis⁹, I. Angelozzi¹⁰⁶, P. Anger⁴⁴, A. Angerami³⁵, F. Anghinolfi³⁰, A.V. Anisenkov^{108,c}, N. Anjos^{125a}, A. Annovi⁴⁷, A. Antonaki⁹, M. Antonelli⁴⁷, A. Antonov⁹⁷, J. Antos^{145b}, F. Anulli^{133a}, M. Aoki⁶⁵, L. Aperio Bella¹⁸, R. Apolle^{119,d}, G. Arabidze⁸⁹, I. Aracena¹⁴⁴, Y. Arai⁶⁵, J.P. Araque^{125a}, A.T.H. Arce⁴⁵, J-F. Arguin⁹⁴, S. Argyropoulos⁴², M. Arik^{19a}, A.J. Armbruster³⁰, O. Arnaez³⁰, V. Arnal⁸¹, H. Arnold⁴⁸, M. Arratia²⁸, O. Arslan²¹, A. Artamonov⁹⁶, G. Artoni²³, S. Asai¹⁵⁶, N. Asbah⁴², A. Ashkenazi¹⁵⁴, B. Åsman^{147a,147b}, L. Asquith⁶, K. Assamagan²⁵, R. Astalos^{145a}, M. Atkinson¹⁶⁶, N.B. Atlay¹⁴², B. Auerbach⁶, K. Augsten¹²⁷, M. Aourseu^{146b}, G. Avolio³⁰, G. Azuelos^{94,e}, Y. Azuma¹⁵⁶, M.A. Baak³⁰, A.E. Baas^{58a}, C. Bacci^{135a,135b}, H. Bachacou¹³⁷, K. Bachas¹⁵⁵, M. Backes³⁰, M. Backhaus³⁰, J. Backus Mayes¹⁴⁴, E. Badescu^{26a}, P. Bagiacchi^{133a,133b}, P. Bagnaia^{133a,133b}, Y. Bai^{33a}, T. Bain³⁵, J.T. Baines¹³⁰, O.K. Baker¹⁷⁷, P. Balek¹²⁸, F. Balli¹³⁷, E. Banas³⁹, Sw. Banerjee¹⁷⁴, A.A.E. Bannoura¹⁷⁶, V. Bansal¹⁷⁰, H.S. Bansil¹⁸, L. Barak¹⁷³, S.P. Baranov⁹⁵, E.L. Barberio⁸⁷, D. Barberis^{50a,50b}, M. Barbero⁸⁴, T. Barillari¹⁰⁰, M. Barisonzi¹⁷⁶, T. Barklow¹⁴⁴, N. Barlow²⁸, B.M. Barnett¹³⁰, R.M. Barnett¹⁵, Z. Barnovska⁵, A. Baroncelli^{135a}, G. Barone⁴⁹, A.J. Barr¹¹⁹, F. Barreiro⁸¹, J. Barreiro Guimarães da Costa⁵⁷, R. Bartoldus¹⁴⁴, A.E. Barton⁷¹, P. Bartos^{145a}, V. Bartsch¹⁵⁰, A. Bassalat¹¹⁶, A. Basye¹⁶⁶, R.L. Bates⁵³, J.R. Batley²⁸, M. Battaglia¹³⁸, M. Battistin³⁰, F. Bauer¹³⁷, H.S. Bawa^{144,f}, M.D. Beattie⁷¹, T. Beau⁷⁹, P.H. Beauchemin¹⁶², R. Beccherle^{123a,123b}, P. Bechtel²¹, H.P. Beck¹⁷, K. Becker¹⁷⁶, S. Becker⁹⁹, M. Beckingham¹⁷¹, C. Becot¹¹⁶, A.J. Beddall^{19c}, A. Beddall^{19c}, S. Bedikian¹⁷⁷, V.A. Bednyakov⁶⁴, C.P. Bee¹⁴⁹, L.J. Beemster¹⁰⁶, T.A. Beermann¹⁷⁶, M. Begel²⁵, K. Behr¹¹⁹, C. Belanger-Champagne⁸⁶, P.J. Bell⁴⁹, W.H. Bell⁴⁹, G. Bella¹⁵⁴, L. Bellagamba^{20a}, A. Bellerive²⁹, M. Bellomo⁸⁵, K. Belotskiy⁹⁷, O. Beltramello³⁰, O. Benary¹⁵⁴, D. Bencheikroun^{136a}, K. Bendtz^{147a,147b}, N. Benekos¹⁶⁶, Y. Benhamou¹⁵⁴, E. Benhar Nocchioli⁴⁹, J.A. Benitez Garcia^{160b}, D.P. Benjamin⁴⁵, J.R. Bensinger²³, K. Benslama¹³¹, S. Bentvelsen¹⁰⁶, D. Berge¹⁰⁶, E. Bergeaas Kuutmann¹⁶, N. Berger⁵, F. Berghaus¹⁷⁰, J. Beringer¹⁵, C. Bernard²², P. Bernat⁷⁷, C. Bernius⁷⁸, F.U. Bernlochner¹⁷⁰, T. Berry⁷⁶, P. Berta¹²⁸, C. Bertella⁸⁴, G. Bertoli^{147a,147b}, F. Bertolucci^{123a,123b}, C. Bertsche¹¹², D. Bertsche¹¹², M.I. Besana^{90a}, G.J. Besjes¹⁰⁵, O. Bessidskaia^{147a,147b}, M. Bessner⁴², N. Besson¹³⁷, C. Betancourt⁴⁸, S. Bethke¹⁰⁰, W. Bhimji⁴⁶, R.M. Bianchi¹²⁴, L. Bianchini²³, M. Bianco³⁰, O. Biebel⁹⁹, S.P. Bieniek⁷⁷, K. Bierwagen⁵⁴, J. Biesiada¹⁵, M. Biglietti^{135a}, J. Bilbao De Mendizabal⁴⁹, H. Bilokon⁴⁷, M. Bindi⁵⁴, S. Binet¹¹⁶, A. Bingul^{19c}, C. Bini^{133a,133b}, C.W. Black¹⁵¹, J.E. Black¹⁴⁴, K.M. Black²², D. Blackburn¹³⁹, R.E. Blair⁶, J.-B. Blanchard¹³⁷, T. Blazek^{145a}, I. Bloch⁴², C. Blocker²³, W. Blum^{82,*}, U. Blumenschein⁵⁴, G.J. Bobbink¹⁰⁶, V.S. Bobrovnikov^{108,c}, S.S. Bocchetta⁸⁰, A. Bocci⁴⁵, C. Bock⁹⁹, C.R. Boddy¹¹⁹, M. Boehler⁴⁸, T.T. Boek¹⁷⁶, J.A. Bogaerts³⁰, A.G. Bogdanchikov¹⁰⁸, A. Bogouch^{91,*}, C. Bohm^{147a}, J. Bohm¹²⁶, V. Boisvert⁷⁶, T. Bold^{38a}, V. Boldea^{26a}, A.S. Boldyrev⁹⁸, M. Bomben⁷⁹, M. Bona⁷⁵, M. Boonekamp¹³⁷, A. Borisov¹²⁹, G. Borissov⁷¹, M. Borri⁸³, S. Borroni⁴², J. Bortfeldt⁹⁹, V. Bortolotto^{135a,135b}, K. Bos¹⁰⁶, D. Boscherini^{20a}, M. Bosman¹², H. Boterenbrood¹⁰⁶, J. Boudreau¹²⁴, J. Bouffard², E.V. Bouhova-Thacker⁷¹, D. Boumediene³⁴, C. Bourdarios¹¹⁶, N. Bousson¹¹³, S. Boutouil^{136d}, A. Boveia³¹, J. Boyd³⁰, I.R. Boyko⁶⁴, J. Bracinik¹⁸, A. Brandt⁸, G. Brandt¹⁵, O. Brandt^{58a}, U. Bratzler¹⁵⁷, B. Brau⁸⁵, J.E. Brau¹¹⁵, H.M. Braun^{176,*}, S.F. Brazzale^{165a,165c}, B. Brelief¹⁵⁹, K. Brendlinger¹²¹, A.J. Brennan⁸⁷, R. Brenner¹⁶⁷, S. Bressler¹⁷³, K. Bristow^{146c}, T.M. Bristow⁴⁶, D. Britton⁵³, F.M. Brochu²⁸, I. Brock²¹, R. Brock⁸⁹, C. Bromberg⁸⁹, J. Bronner¹⁰⁰, G. Brooijmans³⁵, T. Brooks⁷⁶, W.K. Brooks^{32b}, J. Brosamer¹⁵, E. Brost¹¹⁵, J. Brown⁵⁵, P.A. Bruckman de Renstrom³⁹, D. Bruncko^{145b}, R. Bruneliere⁴⁸, S. Brunet⁶⁰, A. Bruni^{20a}, G. Bruni^{20a}, M. Bruschi^{20a}, L. Bryngemark⁸⁰, T. Buanes¹⁴, Q. Buat¹⁴³, F. Bucci⁴⁹, P. Buchholz¹⁴², R.M. Buckingham¹¹⁹, A.G. Buckley⁵³, S.I. Buda^{26a}, I.A. Budagov⁶⁴, F. Buehrer⁴⁸, L. Bugge¹¹⁸, M.K. Bugge¹¹⁸, O. Bulekov⁹⁷, A.C. Bundock⁷³, H. Burckhart³⁰, S. Burdin⁷³, B. Burghgrave¹⁰⁷, S. Burke¹³⁰, I. Burmeister⁴³, E. Busato³⁴, D. Büscher⁴⁸, V. Büscher⁸², P. Bussey⁵³, C.P. Buszello¹⁶⁷, B. Butler⁵⁷, J.M. Butler²², A.I. Butt³, C.M. Buttar⁵³, J.M. Butterworth⁷⁷, P. Butti¹⁰⁶, W. Buttinger²⁸, A. Buzatu⁵³, M. Byszewski¹⁰, S. Cabrera Urbán¹⁶⁸, D. Caforio^{20a,20b}, O. Cakir^{4a}, P. Calafiura¹⁵, A. Calandri¹³⁷, G. Calderini⁷⁹, P. Calfayan⁹⁹, R. Calkins¹⁰⁷, L.P. Caloba^{24a}, D. Calvet³⁴, S. Calvet³⁴, R. Camacho Toro⁴⁹, S. Camarda⁴², D. Cameron¹¹⁸, L.M. Caminada¹⁵,

R. Caminal Armadans¹², S. Campana³⁰, M. Campanelli⁷⁷, A. Campoverde¹⁴⁹, V. Canale^{103a,103b}, A. Canepa^{160a}, M. Cano Bret⁷⁵, J. Cantero⁸¹, R. Cantrill^{125a}, T. Cao⁴⁰, M.D.M. Capeans Garrido³⁰, I. Caprini^{26a}, M. Caprini^{26a}, M. Capua^{37a,37b}, R. Caputo⁸², R. Cardarelli^{134a}, T. Carli³⁰, G. Carlino^{103a}, L. Carminati^{90a,90b}, S. Caron¹⁰⁵, E. Carquin^{32a}, G.D. Carrillo-Montoya^{146c}, J.R. Carter²⁸, J. Carvalho^{125a,125c}, D. Casadei⁷⁷, M.P. Casado¹², M. Casolino¹², E. Castaneda-Miranda^{146b}, A. Castelli¹⁰⁶, V. Castillo Gimenez¹⁶⁸, N.F. Castro^{125a}, P. Catastini⁵⁷, A. Catinaccio³⁰, J.R. Catmore¹¹⁸, A. Cattai³⁰, G. Cattani^{134a,134b}, J. Caudron⁸², S. Caughron⁸⁹, V. Cavaliere¹⁶⁶, D. Cavalli^{90a}, M. Cavalli-Sforza¹², V. Cavasinni^{123a,123b}, F. Ceradini^{135a,135b}, B.C. Cerio⁴⁵, K. Cerny¹²⁸, A.S. Cerqueira^{24b}, A. Cerri¹⁵⁰, L. Cerrito⁷⁵, F. Cerutti¹⁵, M. Cerv³⁰, A. Cervelli¹⁷, S.A. Cetin^{19b}, A. Chafaq^{136a}, D. Chakraborty¹⁰⁷, I. Chalupkova¹²⁸, P. Chang¹⁶⁶, B. Chapleau⁸⁶, J.D. Chapman²⁸, D. Charfeddine¹¹⁶, D.G. Charlton¹⁸, C.C. Chau¹⁵⁹, C.A. Chavez Barajas¹⁵⁰, S. Cheatham⁸⁶, A. Chegwidan⁸⁹, S. Chekanov⁶, S.V. Chekulaev^{160a}, G.A. Chelkov^{64.g}, M.A. Chelstowska⁸⁸, C. Chen⁶³, H. Chen²⁵, K. Chen¹⁴⁹, L. Chen^{33d,h}, S. Chen^{33c}, X. Chen^{146c}, Y. Chen⁶⁶, Y. Chen³⁵, H.C. Cheng⁸⁸, Y. Cheng³¹, A. Cheplakov⁶⁴, R. Cherkaoui El Moursli^{136e}, V. Chernyatin^{25,*}, E. Cheu⁷, L. Chevalier¹³⁷, V. Chiarella⁴⁷, G. Chiefari^{103a,103b}, J.T. Childers⁶, A. Chilingarov⁷¹, G. Chiodini^{72a}, A.S. Chisholm¹⁸, R.T. Chislett⁷⁷, A. Chitan^{26a}, M.V. Chizhov⁶⁴, S. Chouridou⁹, B.K.B. Chow⁹⁹, D. Chromek-Burckhart³⁰, M.L. Chu¹⁵², J. Chudoba¹²⁶, J.J. Chwastowski³⁹, L. Chytka¹¹⁴, G. Ciapetti^{133a,133b}, A.K. Ciftci^{4a}, R. Ciftci^{4a}, D. Cinca⁵³, V. Cindro⁷⁴, A. Ciocio¹⁵, P. Cirkovic^{13b}, Z.H. Citron¹⁷³, M. Citterio^{90a}, M. Ciubancan^{26a}, A. Clark⁴⁹, P.J. Clark⁴⁶, R.N. Clarke¹⁵, W. Cleland¹²⁴, J.C. Clemens⁸⁴, C. Clement^{147a,147b}, Y. Coadou⁸⁴, M. Cobal^{165a,165c}, A. Coccaro¹³⁹, J. Cochran⁶³, L. Coffey²³, J.G. Cogan¹⁴⁴, J. Coggeshall¹⁶⁶, B. Cole³⁵, S. Cole¹⁰⁷, A.P. Colijn¹⁰⁶, J. Collot⁵⁵, T. Colombo^{58c}, G. Colon⁸⁵, G. Compostella¹⁰⁰, P. Conde Muiño^{125a,125b}, E. Coniavitis⁴⁸, M.C. Conidi¹², S.H. Connell^{146b}, I.A. Connelly⁷⁶, S.M. Consonni^{90a,90b}, V. Consorti⁴⁸, S. Constantinescu^{26a}, C. Conta^{120a,120b}, G. Conti⁵⁷, F. Conventi^{103a,i}, M. Cooke¹⁵, B.D. Cooper⁷⁷, A.M. Cooper-Sarkar¹¹⁹, N.J. Cooper-Smith⁷⁶, K. Copic¹⁵, T. Cornelissen¹⁷⁶, M. Corradi^{20a}, F. Corriveau^{86,j}, A. Corso-Radu¹⁶⁴, A. Cortes-Gonzalez¹², G. Cortiana¹⁰⁰, G. Costa^{90a}, M.J. Costa¹⁶⁸, D. Costanzo¹⁴⁰, D. Côté⁸, G. Cottin²⁸, G. Cowan⁷⁶, B.E. Cox⁸³, K. Cranmer¹⁰⁹, G. Cree²⁹, S. Crépe-Renaudin⁵⁵, F. Crescioli⁷⁹, W.A. Cribbs^{147a,147b}, M. Crispin Ortuzar¹¹⁹, M. Cristinziani²¹, V. Croft¹⁰⁵, G. Crosetti^{37a,37b}, C.-M. Cuciuc^{26a}, T. Cuhadar Donszelmann¹⁴⁰, J. Cummings¹⁷⁷, M. Curatolo⁴⁷, C. Cuthbert¹⁵¹, H. Czirr¹⁴², P. Czodrowski³, Z. Czyczula¹⁷⁷, S. D'Auria⁵³, M. D'Onofrio⁷³, M.J. Da Cunha Sargedas De Sousa^{125a,125b}, C. Da Via⁸³, W. Dabrowski^{38a}, A. Dafinca¹¹⁹, T. Dai⁸⁸, O. Dale¹⁴, F. Dallaire⁹⁴, C. Dallapiccola⁸⁵, M. Dam³⁶, A.C. Daniells¹⁸, M. Dano Hoffmann¹³⁷, V. Dao⁴⁸, G. Darbo^{50a}, S. Darmora⁸, J.A. Dassoulas⁴², A. Dattagupta⁶⁰, W. Davey²¹, C. David¹⁷⁰, T. Davidek¹²⁸, E. Davies^{119,d}, M. Davies¹⁵⁴, O. Davignon⁷⁹, A.R. Davison⁷⁷, P. Davison⁷⁷, Y. Davygora^{58a}, E. Dawe¹⁴³, I. Dawson¹⁴⁰, R.K. Daya-Ishmukhametova⁸⁵, K. De⁸, R. de Asmundis^{103a}, S. De Castro^{20a,20b}, S. De Cecco⁷⁹, N. De Groot¹⁰⁵, P. de Jong¹⁰⁶, H. De la Torre⁸¹, F. De Lorenzi⁶³, L. De Nooij¹⁰⁶, D. De Pedis^{133a}, A. De Salvo^{133a}, U. De Sanctis^{165a,165b}, A. De Santo¹⁵⁰, J.B. De Vivie De Regie¹¹⁶, W.J. Dearnaley⁷¹, R. Debbe²⁵, C. Debenedetti¹³⁸, B. Dechenaux⁵⁵, D.V. Dedovich⁶⁴, I. Deigaard¹⁰⁶, J. Del Peso⁸¹, T. Del Prete^{123a,123b}, F. Deliot¹³⁷, C.M. Delitzsch⁴⁹, M. Deliyergiyev⁷⁴, A. Dell'Acqua³⁰, L. Dell'Asta²², M. Dell'Orso^{123a,123b}, M. Della Pietra^{103a,i}, D. della Volpe⁴⁹, M. Delmastro⁵, P.A. Delsart⁵⁵, C. Deluca¹⁰⁶, S. Demers¹⁷⁷, M. Demichev⁶⁴, A. Demilly⁷⁹, S.P. Denisov¹²⁹, D. Derendarz³⁹, J.E. Derkaoui^{136d}, F. Derue⁷⁹, P. Dervan⁷³, K. Desch²¹, C. Deterre⁴², P.O. Deviveiros¹⁰⁶, A. Dewhurst¹³⁰, S. Dhaliwal¹⁰⁶, A. Di Ciaccio^{134a,134b}, L. Di Ciaccio⁵, A. Di Domenico^{133a,133b}, C. Di Donato^{103a,103b}, A. Di Girolamo³⁰, B. Di Girolamo³⁰, A. Di Mattia¹⁵³, B. Di Micco^{135a,135b}, R. Di Nardo⁴⁷, A. Di Simone⁴⁸, R. Di Sipio^{20a,20b}, D. Di Valentino²⁹, F.A. Dias⁴⁶, M.A. Diaz^{32a}, E.B. Diehl⁸⁸, J. Dietrich⁴², T.A. Dietzsch^{58a}, S. Diglio⁸⁴, A. Dimitrievska^{13a}, J. Dingfelder²¹, C. Dionisi^{133a,133b}, P. Dita^{26a}, S. Dita^{26a}, F. Dittus³⁰, F. Djama⁸⁴, T. Djobava^{51b}, M.A.B. do Vale^{24c}, A. Do Valle Wemans^{125a,125g}, T.K.O. Doan⁵, D. Dobos³⁰, C. Doglioni⁴⁹, T. Doherty⁵³, T. Dohmae¹⁵⁶, J. Dolejsi¹²⁸, Z. Dolezal¹²⁸, B.A. Dolgoshein^{97,*}, M. Donadelli^{24d}, S. Donati^{123a,123b}, P. Dondero^{120a,120b}, J. Donini³⁴, J. Dopke¹³⁰, A. Doria^{103a}, M.T. Dova⁷⁰, A.T. Doyle⁵³, M. Dris¹⁰, J. Dubbert⁸⁸, S. Dube¹⁵, E. Dubreuil³⁴, E. Duchovni¹⁷³, G. Duckeck⁹⁹, O.A. Ducu^{26a}, D. Duda¹⁷⁶, A. Dudarev³⁰, F. Dudziak⁶³, L. Dufflot¹¹⁶, L. Duguid⁷⁶, M. Dührssen³⁰, M. Dunford^{58a}, H. Duran Yildiz^{4a}, M. Düren⁵², A. Durglishvili^{51b}, M. Dwuznik^{38a}, M. Dyndal^{38a}, J. Ebke⁹⁹, W. Edson², N.C. Edwards⁴⁶, W. Ehrenfeld²¹, T. Eifert¹⁴⁴, G. Eigen¹⁴, K. Einsweiler¹⁵, T. Ekelof¹⁶⁷, M. El Kacimi^{136c}, M. Ellert¹⁶⁷, S. Elles⁵, F. Ellinghaus⁸², N. Ellis³⁰, J. Elmsheuser⁹⁹, M. Elsing³⁰, D. Emelianov¹³⁰, Y. Enari¹⁵⁶, O.C. Endner⁸², M. Endo¹¹⁷, R. Engelmann¹⁴⁹, J. Erdmann¹⁷⁷, A. Ereditato¹⁷, D. Eriksson^{147a}, G. Ernis¹⁷⁶, J. Ernst²⁵, M. Ernst²⁵, J. Ernwein¹³⁷, D. Errede¹⁶⁶, S. Errede¹⁶⁶, E. Ertel⁸², M. Escalier¹¹⁶, H. Esch⁴³, C. Escobar¹²⁴, B. Esposito⁴⁷, A.I. Etienvre¹³⁷, E. Etzion¹⁵⁴, H. Evans⁶⁰, A. Ezhilov¹²², L. Fabbri^{20a,20b}, G. Facini³¹, R.M. Fakhruddinov¹²⁹, S. Falciano^{133a}, R.J. Falla⁷⁷, J. Faltova¹²⁸, Y. Fang^{33a}, M. Fanti^{90a,90b}, A. Farbin⁸, A. Farilla^{135a}, T. Farooque¹², S. Farrell¹⁵, S.M. Farrington¹⁷¹, P. Farthouat³⁰, F. Fassi^{136e}, P. Fassnacht³⁰, D. Fassouliotis⁹, A. Favareto^{50a,50b}, L. Fayard¹¹⁶, P. Federic^{145a}, O.L. Fedin^{122,k}, W. Fedorko¹⁶⁹, M. Fehling-Kaschek⁴⁸, S. Feigl³⁰, L. Feligioni⁸⁴, C. Feng^{33d}, E.J. Feng⁶, H. Feng⁸⁸, A.B. Fenyuk¹²⁹, S. Fernandez Perez³⁰, S. Ferrag⁵³, J. Ferrando⁵³, A. Ferrari¹⁶⁷, P. Ferrari¹⁰⁶, R. Ferrari^{120a}, D.E. Ferreira de Lima⁵³,

A. Ferrer¹⁶⁸, D. Ferrere⁴⁹, C. Ferretti⁸⁸, A. Ferretto Parodi^{50a,50b}, M. Fiascaris³¹, F. Fiedler⁸², A. Filipčić⁷⁴,
 M. Filipuzzi⁴², F. Filthaut¹⁰⁵, M. Fincke-Keeler¹⁷⁰, K.D. Finelli¹⁵¹, M.C.N. Fiolhais^{125a,125c}, L. Fiorini¹⁶⁸,
 A. Firan⁴⁰, A. Fischer², J. Fischer¹⁷⁶, W.C. Fisher⁸⁹, E.A. Fitzgerald²³, M. Flechl⁴⁸, I. Fleck¹⁴², P. Fleischmann⁸⁸,
 S. Fleischmann¹⁷⁶, G.T. Fletcher¹⁴⁰, G. Fletcher⁷⁵, T. Flick¹⁷⁶, A. Floderus⁸⁰, L.R. Flores Castillo^{174,l},
 A.C. Florez Bustos^{160b}, M.J. Flowerdew¹⁰⁰, A. Formica¹³⁷, A. Forti⁸³, D. Fortin^{160a}, D. Fournier¹¹⁶, H. Fox⁷¹,
 S. Fracchia¹², P. Francavilla⁷⁹, M. Franchini^{20a,20b}, S. Franchino³⁰, D. Francis³⁰, L. Franconi¹¹⁸, M. Franklin⁵⁷,
 S. Franz⁶¹, M. Fraternali^{120a,120b}, S.T. French²⁸, C. Friedrich⁴², F. Friedrich⁴⁴, D. Froidevaux³⁰, J.A. Frost²⁸,
 C. Fukunaga¹⁵⁷, E. Fullana Torregrosa⁸², B.G. Fulsom¹⁴⁴, J. Fuster¹⁶⁸, C. Gabaldon⁵⁵, O. Gabizon¹⁷³,
 A. Gabrielli^{20a,20b}, A. Gabrielli^{133a,133b}, S. Gadatsch¹⁰⁶, S. Gadomski⁴⁹, G. Gagliardi^{50a,50b}, P. Gagnon⁶⁰,
 C. Galea¹⁰⁵, B. Galhardo^{125a,125c}, E.J. Gallas¹¹⁹, V. Gallo¹⁷, B.J. Gallop¹³⁰, P. Gallus¹²⁷, G. Galster³⁶,
 K.K. Gan¹¹⁰, R.P. Gandrajula⁶², J. Gao^{33b,h}, Y.S. Gao^{144,f}, F.M. Garay Walls⁴⁶, F. Garberson¹⁷⁷, C. García¹⁶⁸,
 J.E. García Navarro¹⁶⁸, M. Garcia-Sciveres¹⁵, R.W. Gardner³¹, N. Garelli¹⁴⁴, V. Garonne³⁰, C. Gatti⁴⁷,
 G. Gaudio^{120a}, B. Gaur¹⁴², L. Gauthier⁹⁴, P. Gauzzi^{133a,133b}, I.L. Gavrilenko⁹⁵, C. Gay¹⁶⁹, G. Gaycken²¹,
 E.N. Gazis¹⁰, P. Ge^{33d}, Z. Gecse¹⁶⁹, C.N.P. Gee¹³⁰, D.A.A. Geerts¹⁰⁶, Ch. Geich-Gimbel²¹, K. Gellerstedt^{147a,147b},
 C. Gemme^{50a}, A. Gemmell⁵³, M.H. Genest⁵⁵, S. Gentile^{133a,133b}, M. George⁵⁴, S. George⁷⁶, D. Gerbaudo¹⁶⁴,
 A. Gershon¹⁵⁴, H. Ghazlane^{136b}, N. Ghodbane³⁴, B. Giacobbe^{20a}, S. Giagu^{133a,133b}, V. Giangiobbe¹²,
 P. Giannetti^{123a,123b}, F. Gianotti³⁰, B. Gibbard²⁵, S.M. Gibson⁷⁶, M. Gilchriese¹⁵, T.P.S. Gillam²⁸, D. Gillberg³⁰,
 G. Gilles³⁴, D.M. Gingrich^{3,e}, N. Giokaris⁹, M.P. Giordani^{165a,165c}, R. Giordano^{103a,103b}, F.M. Giorgi^{20a},
 F.M. Giorgi¹⁶, P.F. Giraud¹³⁷, D. Giugni^{90a}, C. Giuliani⁴⁸, M. Giulini^{58b}, B.K. Gjelsten¹¹⁸, S. Gkaitatzis¹⁵⁵,
 I. Gkialas^{155,m}, L.K. Gladilin⁹⁸, C. Glasman⁸¹, J. Glatzer³⁰, P.C.F. Glaysher⁴⁶, A. Glazov⁴², G.L. Glonti⁶⁴,
 M. Goblirsch-Kolb¹⁰⁰, J.R. Goddard⁷⁵, J. Godfrey¹⁴³, J. Godlewski³⁰, C. Goeringer⁸², S. Goldfarb⁸⁸, T. Golling¹⁷⁷,
 D. Golubkov¹²⁹, A. Gomes^{125a,125b,125d}, L.S. Gomez Fajardo⁴², R. Gonçalo^{125a},
 J. Goncalves Pinto Firmino Da Costa¹³⁷, L. Gonella²¹, S. González de la Hoz¹⁶⁸, G. Gonzalez Parra¹²,
 S. Gonzalez-Sevilla⁴⁹, L. Goossens³⁰, P.A. Gorbounov⁹⁶, H.A. Gordon²⁵, I. Gorelov¹⁰⁴, B. Gorini³⁰, E. Gorini^{72a,72b},
 A. Gorišek⁷⁴, E. Gornicki³⁹, A.T. Goshaw⁶, C. Gössling⁴³, M.I. Gostkin⁶⁴, M. Gouighri^{136a}, D. Goujdami^{136c},
 M.P. Goulette⁴⁹, A.G. Goussiou¹³⁹, C. Goy⁵, S. Gozpinar²³, H.M.X. Grabas¹³⁷, L. Graber⁵⁴, I. Grabowska-Bold^{38a},
 P. Grafström^{20a,20b}, K.-J. Grahn⁴², J. Gramling⁴⁹, E. Gramstad¹¹⁸, S. Grancagnolo¹⁶, V. Grassi¹⁴⁹, V. Gratchev¹²²,
 H.M. Gray³⁰, E. Graziani^{135a}, O.G. Grebenyuk¹²², Z.D. Greenwood^{78,n}, K. Gregersen⁷⁷, I.M. Gregor⁴²,
 P. Grenier¹⁴⁴, J. Griffiths⁸, A.A. Grillo¹³⁸, K. Grimm⁷¹, S. Grinstein^{12,o}, Ph. Gris³⁴, Y.V. Grishkevich⁹⁸,
 J.-F. Grivaz¹¹⁶, J.P. Grohs⁴⁴, A. Grohsjean⁴², E. Gross¹⁷³, J. Grosse-Knetter⁵⁴, G.C. Grossi^{134a,134b},
 J. Groth-Jensen¹⁷³, Z.J. Grout¹⁵⁰, L. Guan^{33b}, F. Guescini⁴⁹, D. Guest¹⁷⁷, O. Gueta¹⁵⁴, C. Guicheney³⁴,
 E. Guido^{50a,50b}, T. Guillemin¹¹⁶, S. Guindon², U. Gul⁵³, C. Gumpert⁴⁴, J. Gunther¹²⁷, J. Guo³⁵, S. Gupta¹¹⁹,
 P. Gutierrez¹¹², N.G. Gutierrez Ortiz⁵³, C. Gutsche⁷⁷, N. Guttman¹⁵⁴, C. Guyot¹³⁷, C. Gwenlan¹¹⁹,
 C.B. Gwilliam⁷³, A. Haas¹⁰⁹, C. Haber¹⁵, H.K. Hadavand⁸, N. Haddad^{136e}, P. Haefner²¹, S. Hageböck²¹,
 Z. Hajduk³⁹, H. Hakobyan¹⁷⁸, M. Haleem⁴², D. Hall¹¹⁹, G. Halladjian⁸⁹, K. Hamacher¹⁷⁶, P. Hamal¹¹⁴,
 K. Hamano¹⁷⁰, M. Hamer⁵⁴, A. Hamilton^{146a}, S. Hamilton¹⁶², G.N. Hamity^{146c}, P.G. Hamnett⁴², L. Han^{33b},
 K. Hanagaki¹¹⁷, K. Hanawa¹⁵⁶, M. Hance¹⁵, P. Hanke^{58a}, R. Hanna¹³⁷, J.B. Hansen³⁶, J.D. Hansen³⁶,
 P.H. Hansen³⁶, K. Hara¹⁶¹, A.S. Hard¹⁷⁴, T. Harenberg¹⁷⁶, F. Hariri¹¹⁶, S. Harkusha⁹¹, D. Harper⁸⁸,
 R.D. Harrington⁴⁶, O.M. Harris¹³⁹, P.F. Harrison¹⁷¹, F. Hartjes¹⁰⁶, M. Hasegawa⁶⁶, S. Hasegawa¹⁰²,
 Y. Hasegawa¹⁴¹, A. Hasib¹¹², S. Hassani¹³⁷, S. Haug¹⁷, M. Hauschild³⁰, R. Hauser⁸⁹, M. Havranek¹²⁶,
 C.M. Hawkes¹⁸, R.J. Hawkings³⁰, A.D. Hawkins⁸⁰, T. Hayashi¹⁶¹, D. Hayden⁸⁹, C.P. Hays¹¹⁹, H.S. Hayward⁷³,
 S.J. Haywood¹³⁰, S.J. Head¹⁸, T. Heck⁸², V. Hedberg⁸⁰, L. Heelan⁸, S. Heim¹²¹, T. Heim¹⁷⁶, B. Heinemann¹⁵,
 L. Heinrich¹⁰⁹, J. Hejbal¹²⁶, L. Helary²², C. Heller⁹⁹, M. Heller³⁰, S. Hellman^{147a,147b}, D. Hellmich²¹, C. Helsens³⁰,
 J. Henderson¹¹⁹, R.C.W. Henderson⁷¹, Y. Heng¹⁷⁴, C. Hengler⁴², A. Henrichs¹⁷⁷, A.M. Henriques Correia³⁰,
 S. Henrot-Versille¹¹⁶, C. Hensel⁵⁴, G.H. Herbert¹⁶, Y. Hernández Jiménez¹⁶⁸, R. Herrberg-Schubert¹⁶, G. Hertzen⁴⁸,
 R. Hertzenberger⁹⁹, L. Hervas³⁰, G.G. Hesketh⁷⁷, N.P. Hessey¹⁰⁶, R. Hickling⁷⁵, E. Higón-Rodríguez¹⁶⁸, E. Hill¹⁷⁰,
 J.C. Hill²⁸, K.H. Hiller⁴², S. Hillert²¹, S.J. Hillier¹⁸, I. Hinchliffe¹⁵, E. Hines¹²¹, M. Hirose¹⁵⁸, D. Hirschbuehl¹⁷⁶,
 J. Hobbs¹⁴⁹, N. Hod¹⁰⁶, M.C. Hodgkinson¹⁴⁰, P. Hodgson¹⁴⁰, A. Hoecker³⁰, M.R. Hoferkamp¹⁰⁴, F. Hoenig⁹⁹,
 J. Hoffman⁴⁰, D. Hoffmann⁸⁴, J.I. Hofmann^{58a}, M. Hohlfeld⁸², T.R. Holmes¹⁵, T.M. Hong¹²¹,
 L. Hooft van Huysduynen¹⁰⁹, J.-Y. Hostachy⁵⁵, S. Hou¹⁵², A. Hounmada^{136a}, J. Howard¹¹⁹, J. Howarth⁴²,
 M. Hrabovsky¹¹⁴, I. Hristova¹⁶, J. Hrivnac¹¹⁶, T. Hryn'ova⁵, C. Hsu^{146c}, P.J. Hsu⁸², S.-C. Hsu¹³⁹, D. Hu³⁵,
 X. Hu²⁵, Y. Huang⁴², Z. Hubacek³⁰, F. Hubaut⁸⁴, F. Huegging²¹, T.B. Huffman¹¹⁹, E.W. Hughes³⁵, G. Hughes⁷¹,
 M. Huhtinen³⁰, T.A. Hülsing⁸², M. Hurwitz¹⁵, N. Huseynov^{64,b}, J. Huston⁸⁹, J. Huth⁵⁷, G. Iacobucci⁴⁹,
 G. Iakovidis¹⁰, I. Ibragimov¹⁴², L. Iconomidou-Fayard¹¹⁶, E. Ideal¹⁷⁷, P. Iengo^{103a}, O. Igonkina¹⁰⁶, T. Iizawa¹⁷²,
 Y. Ikegami⁶⁵, K. Ikematsu¹⁴², M. Ikeno⁶⁵, Y. Ilchenko^{31,p}, D. Iliadis¹⁵⁵, N. Ilic¹⁵⁹, Y. Inamaru⁶⁶, T. Ince¹⁰⁰,
 P. Ioannou⁹, M. Iodice^{135a}, K. Iordanidou⁹, V. Ippolito⁵⁷, A. Irls Quiles¹⁶⁸, C. Isaksson¹⁶⁷, M. Ishino⁶⁷,
 M. Ishitsuka¹⁵⁸, R. Ishmukhametov¹¹⁰, C. Issever¹¹⁹, S. Istin^{19a}, J.M. Iturbe Ponce⁸³, R. Iuppa^{134a,134b},
 J. Ivarsson⁸⁰, W. Iwanski³⁹, H. Iwasaki⁶⁵, J.M. Izen⁴¹, V. Izzo^{103a}, B. Jackson¹²¹, M. Jackson⁷³, P. Jackson¹,

M.R. Jaekel³⁰, V. Jain², K. Jakobs⁴⁸, S. Jakobsen³⁰, T. Jakoubek¹²⁶, J. Jakubek¹²⁷, D.O. Jamin¹⁵², D.K. Jana⁷⁸, E. Jansen⁷⁷, H. Jansen³⁰, J. Janssen²¹, M. Janus¹⁷¹, G. Jarlskog⁸⁰, N. Javadov^{64,b}, T. Javurek⁴⁸, L. Jeanty¹⁵, J. Jejelava^{51a,q}, G.-Y. Jeng¹⁵¹, D. Jennens⁸⁷, P. Jenni^{48,r}, J. Jentsch⁴³, C. Jeske¹⁷¹, S. Jézéquel⁵, H. Ji¹⁷⁴, J. Jia¹⁴⁹, Y. Jiang^{33b}, M. Jimenez Belenguer⁴², S. Jin^{33a}, A. Jinaru^{26a}, O. Jinnouchi¹⁵⁸, M.D. Joergensen³⁶, K.E. Johansson^{147a,147b}, P. Johansson¹⁴⁰, K.A. Johns⁷, K. Jon-And^{147a,147b}, G. Jones¹⁷¹, R.W.L. Jones⁷¹, T.J. Jones⁷³, J. Jongmanns^{58a}, P.M. Jorge^{125a,125b}, K.D. Joshi⁸³, J. Jovicevic¹⁴⁸, X. Ju¹⁷⁴, C.A. Jung⁴³, R.M. Jungst³⁰, P. Jussel⁶¹, A. Juste Rozas^{12,o}, M. Kaci¹⁶⁸, A. Kaczmarek³⁹, M. Kado¹¹⁶, H. Kagan¹¹⁰, M. Kagan¹⁴⁴, E. Kajomovitz⁴⁵, C.W. Kalderon¹¹⁹, S. Kama⁴⁰, A. Kamenshchikov¹²⁹, N. Kanaya¹⁵⁶, M. Kaneda³⁰, S. Kaneti²⁸, V.A. Kantserov⁹⁷, J. Kanzaki⁶⁵, B. Kaplan¹⁰⁹, A. Kapliy³¹, D. Kar⁵³, K. Karakostas¹⁰, N. Karastathis¹⁰, M. Karnevskiy⁸², S.N. Karpov⁶⁴, Z.M. Karpova⁶⁴, K. Karthik¹⁰⁹, V. Kartvelishvili⁷¹, A.N. Karyukhin¹²⁹, L. Kashif¹⁷⁴, G. Kasieczka^{58b}, R.D. Kass¹¹⁰, A. Kastanas¹⁴, Y. Kataoka¹⁵⁶, A. Katre⁴⁹, J. Katzy⁴², V. Kaushik⁷, K. Kawagoe⁶⁹, T. Kawamoto¹⁵⁶, G. Kawamura⁵⁴, S. Kazama¹⁵⁶, V.F. Kazanin¹⁰⁸, M.Y. Kazarinov⁶⁴, R. Keeler¹⁷⁰, R. Kehoe⁴⁰, M. Keil⁵⁴, J.S. Keller⁴², J.J. Kempster⁷⁶, H. Keoshkerian⁵, O. Kepka¹²⁶, B.P. Kerševan⁷⁴, S. Kersten¹⁷⁶, K. Kessoku¹⁵⁶, J. Keung¹⁵⁹, F. Khalil-zada¹¹, H. Khandanyan^{147a,147b}, A. Khanov¹¹³, A. Khodinov⁹⁷, A. Khomich^{58a}, T.J. Khoo²⁸, G. Khorauli²¹, A. Khoroshilov¹⁷⁶, V. Khovanskiy⁹⁶, E. Khramov⁶⁴, J. Khubua^{51b}, H.Y. Kim⁸, H. Kim^{147a,147b}, S.H. Kim¹⁶¹, N. Kimura¹⁷², O. Kind¹⁶, B.T. King⁷³, M. King¹⁶⁸, R.S.B. King¹¹⁹, S.B. King¹⁶⁹, J. Kirk¹³⁰, A.E. Kiryunin¹⁰⁰, T. Kishimoto⁶⁶, D. Kisieleska^{38a}, F. Kiss⁴⁸, T. Kittelmann¹²⁴, K. Kiuchi¹⁶¹, E. Kladiva^{145b}, M. Klein⁷³, U. Klein⁷³, K. Kleinknecht⁸², P. Klimek^{147a,147b}, A. Klimentov²⁵, R. Klingenberg⁴³, J.A. Klinger⁸³, T. Klioutchnikova³⁰, P.F. Klok¹⁰⁵, E.-E. Kluge^{58a}, P. Kluit¹⁰⁶, S. Kluth¹⁰⁰, E. Kneringer⁶¹, E.B.F.G. Knoops⁸⁴, A. Knue⁵³, D. Kobayashi¹⁵⁸, T. Kobayashi¹⁵⁶, M. Kobel⁴⁴, M. Kocian¹⁴⁴, P. Kodys¹²⁸, P. Kovesarki²¹, T. Koffas²⁹, E. Koffeman¹⁰⁶, L.A. Kogan¹¹⁹, S. Kohlmann¹⁷⁶, Z. Kohout¹²⁷, T. Kohriki⁶⁵, T. Koi¹⁴⁴, H. Kolanoski¹⁶, I. Koletsou⁵, J. Koll⁸⁹, A.A. Komar^{95,*}, Y. Komori¹⁵⁶, T. Kondo⁶⁵, N. Kondrashova⁴², K. Köneke⁴⁸, A.C. König¹⁰⁵, S. König⁸², T. Kono^{65,s}, R. Konoplich^{109,t}, N. Konstantinidis⁷⁷, R. Kopeliansky¹⁵³, S. Koperny^{38a}, L. Köpke⁸², A.K. Kopp⁴⁸, K. Korcyl³⁹, K. Kordas¹⁵⁵, A. Korn⁷⁷, A.A. Korol^{108,c}, I. Korolkov¹², E.V. Korolkova¹⁴⁰, V.A. Korotkov¹²⁹, O. Kortner¹⁰⁰, S. Kortner¹⁰⁰, V.V. Kostyukhin²¹, V.M. Kotov⁶⁴, A. Kotwal⁴⁵, C. Kourkoumelis⁹, V. Kouskoura¹⁵⁵, A. Koutsman^{160a}, R. Kowalewski¹⁷⁰, T.Z. Kowalski^{38a}, W. Kozanecki¹³⁷, A.S. Kozhin¹²⁹, V. Kral¹²⁷, V.A. Kramarenko⁹⁸, G. Kramberger⁷⁴, D. Krasnopevtsev⁹⁷, M.W. Krasny⁷⁹, A. Krasznahorkay³⁰, J.K. Kraus²¹, A. Kravchenko²⁵, S. Kreiss¹⁰⁹, M. Kretz^{58c}, J. Kretzschmar⁷³, K. Kretzfeldt⁵², P. Krieger¹⁵⁹, K. Kroeninger⁵⁴, H. Kroha¹⁰⁰, J. Kroll¹²¹, J. Kroseberg²¹, J. Krstic^{13a}, U. Kruchonak⁶⁴, H. Krüger²¹, T. Kruker¹⁷, N. Krumnack⁶³, Z.V. Krumshteyn⁶⁴, A. Kruse¹⁷⁴, M.C. Kruse⁴⁵, M. Kruskal²², T. Kubota⁸⁷, S. Kuday^{4a}, S. Kuehn⁴⁸, A. Kugel^{58c}, A. Kuhl¹³⁸, T. Kuhl⁴², V. Kukhtin⁶⁴, Y. Kulchitsky⁹¹, S. Kuleshov^{32b}, M. Kuna^{133a,133b}, J. Kunkle¹²¹, A. Kupco¹²⁶, H. Kurashige⁶⁶, Y.A. Kurochkin⁹¹, R. Kurumida⁶⁶, V. Kus¹²⁶, E.S. Kuwertz¹⁴⁸, M. Kuze¹⁵⁸, J. Kvita¹¹⁴, A. La Rosa⁴⁹, L. La Rotonda^{37a,37b}, C. Lacasta¹⁶⁸, F. Lacava^{133a,133b}, J. Lacey²⁹, H. Lacker¹⁶, D. Lacour⁷⁹, V.R. Lacuesta¹⁶⁸, E. Ladygin⁶⁴, R. Lafaye⁵, B. Laforge⁷⁹, T. Lagouri¹⁷⁷, S. Lai⁴⁸, H. Laier^{58a}, L. Lambourne⁷⁷, S. Lammers⁶⁰, C.L. Lampen⁷, W. Lampl⁷, E. Lançon¹³⁷, U. Landgraf⁴⁸, M.P.J. Landon⁷⁵, V.S. Lang^{58a}, A.J. Lankford¹⁶⁴, F. Lanni²⁵, K. Lantzsck³⁰, S. Laplace⁷⁹, C. Lapoire²¹, J.F. Laporte¹³⁷, T. Lari^{90a}, M. Lassnig³⁰, P. Laurelli⁴⁷, W. Lavrijsen¹⁵, A.T. Law¹³⁸, P. Laycock⁷³, O. Le Dortz⁷⁹, E. Le Guirriec⁸⁴, E. Le Menedeu¹², T. LeCompte⁶, F. Ledroit-Guillon⁵⁵, C.A. Lee¹⁵², H. Lee¹⁰⁶, J.S.H. Lee¹¹⁷, S.C. Lee¹⁵², L. Lee¹⁷⁷, G. Lefebvre⁷⁹, M. Lefebvre¹⁷⁰, F. Legger⁹⁹, C. Leggett¹⁵, A. Lehan⁷³, M. Lehmacher²¹, G. Lehmann Miotto³⁰, X. Lei⁷, W.A. Leight²⁹, A. Leisos¹⁵⁵, A.G. Leister¹⁷⁷, M.A.L. Leite^{24d}, R. Leitner¹²⁸, D. Lellouch¹⁷³, B. Lemmer⁵⁴, K.J.C. Leney⁷⁷, T. Lenz²¹, G. Lenzen¹⁷⁶, B. Lenzi³⁰, R. Leone⁷, S. Leone^{123a,123b}, K. Leonhardt⁴⁴, C. Leonidopoulos⁴⁶, S. Leontsinis¹⁰, C. Leroy⁹⁴, C.G. Lester²⁸, C.M. Lester¹²¹, M. Levchenko¹²², J. Levêque⁵, D. Levin⁸⁸, L.J. Levinson¹⁷³, M. Levy¹⁸, A. Lewis¹¹⁹, G.H. Lewis¹⁰⁹, A.M. Leyko²¹, M. Leyton⁴¹, B. Li^{33b,u}, B. Li⁸⁴, H. Li¹⁴⁹, H.L. Li³¹, L. Li⁴⁵, L. Li^{33e}, S. Li⁴⁵, Y. Li^{33c,v}, Z. Liang¹³⁸, H. Liao³⁴, B. Liberti^{134a}, P. Lichard³⁰, K. Lie¹⁶⁶, J. Liebal²¹, W. Liebig¹⁴, C. Limbach²¹, A. Limosani⁸⁷, S.C. Lin^{152,w}, T.H. Lin⁸², F. Linde¹⁰⁶, B.E. Lindquist¹⁴⁹, J.T. Linnemann⁸⁹, E. Lipeles¹²¹, A. Lipniacka¹⁴, M. Lisovsky⁴², T.M. Liss¹⁶⁶, D. Lissauer²⁵, A. Lister¹⁶⁹, A.M. Litke¹³⁸, B. Liu¹⁵², D. Liu¹⁵², J.B. Liu^{33b}, K. Liu^{33b,x}, L. Liu⁸⁸, M. Liu⁴⁵, M. Liu^{33b}, Y. Liu^{33b}, M. Livan^{120a,120b}, S.S.A. Livermore¹¹⁹, A. Lleres⁵⁵, J. Llorente Merino⁸¹, S.L. Lloyd⁷⁵, F. Lo Sterzo¹⁵², E. Lobodzinska⁴², P. Loch⁷, W.S. Lockman¹³⁸, T. Loddenkoetter²¹, F.K. Loebinger⁸³, A.E. Loevschall-Jensen³⁶, A. Loginov¹⁷⁷, T. Lohse¹⁶, K. Lohwasser⁴², M. Lokajicek¹²⁶, V.P. Lombardo⁵, B.A. Long²², J.D. Long⁸⁸, R.E. Long⁷¹, L. Lopez^{125a}, D. Lopez Mateos⁵⁷, B. Lopez Paredes¹⁴⁰, I. Lopez Paz¹², J. Lorenz⁹⁹, N. Lorenzo Martinez⁶⁰, M. Losada¹⁶³, P. Loscutoff¹⁵, X. Lou⁴¹, A. Lounis¹¹⁶, J. Love⁶, P.A. Love⁷¹, A.J. Lowe^{144,f}, F. Lu^{33a}, N. Lu⁸⁸, H.J. Lubatti¹³⁹, C. Luci^{133a,133b}, A. Lucotte⁵⁵, F. Luehring⁶⁰, W. Lukas⁶¹, L. Luminari^{133a}, O. Lundberg^{147a,147b}, B. Lund-Jensen¹⁴⁸, M. Lungwitz⁸², D. Lynn²⁵, R. Lysak¹²⁶, E. Lytken⁸⁰, H. Ma²⁵, L.L. Ma^{33d}, G. Maccarrone⁴⁷, A. Macchiolo¹⁰⁰, J. Machado Miguens^{125a,125b}, D. Macina³⁰, D. Madaffari⁸⁴, R. Madar⁴⁸, H.J. Maddocks⁷¹, W.F. Mader⁴⁴, A. Madsen¹⁶⁷, M. Maeno⁸, T. Maeno²⁵, E. Magradze⁵⁴, K. Mahboubi⁴⁸, J. Mahlstedt¹⁰⁶, S. Mahmoud⁷³, C. Maiani¹³⁷, C. Maidantchik^{24a}, A.A. Maier¹⁰⁰,

A. Maio^{125a,125b,125d}, S. Majewski¹¹⁵, Y. Makida⁶⁵, N. Makovec¹¹⁶, P. Mal^{137,y}, B. Malaescu⁷⁹, Pa. Malecki³⁹, V.P. Maleev¹²², F. Malek⁵⁵, U. Mallik⁶², D. Malon⁶, C. Malone¹⁴⁴, S. Maltezos¹⁰, V.M. Malyshev¹⁰⁸, S. Malyukov³⁰, J. Mamuzic^{13b}, B. Mandelli³⁰, L. Mandelli^{90a}, I. Mandić⁷⁴, R. Mandrysch⁶², J. Maneira^{125a,125b}, A. Manfredini¹⁰⁰, L. Manhaes de Andrade Filho^{24b}, J.A. Manjarres Ramos^{160b}, A. Mann⁹⁹, P.M. Manning¹³⁸, A. Manousakis-Katsikakis⁹, B. Mansoulié¹³⁷, R. Mantifel⁸⁶, L. Mapelli³⁰, L. March^{146c}, J.F. Marchand²⁹, G. Marchiori⁷⁹, M. Marcisovskiy¹²⁶, C.P. Marino¹⁷⁰, M. Marjanovic^{13a}, C.N. Marques^{125a}, F. Marroquin^{24a}, S.P. Marsden⁸³, Z. Marshall¹⁵, L.F. Marti¹⁷, S. Marti-Garcia¹⁶⁸, B. Martin³⁰, B. Martin⁸⁹, T.A. Martin¹⁷¹, V.J. Martin⁴⁶, B. Martin dit Latour¹⁴, H. Martinez¹³⁷, M. Martinez^{12,o}, S. Martin-Haugh¹³⁰, A.C. Martyniuk⁷⁷, M. Marx¹³⁹, F. Marzano^{133a}, A. Marzin³⁰, L. Masetti⁸², T. Mashimo¹⁵⁶, R. Mashinistov⁹⁵, J. Masik⁸³, A.L. Maslennikov^{108,c}, I. Massa^{20a,20b}, L. Massa^{20a,20b}, N. Massol⁵, P. Mastrandrea¹⁴⁹, A. Mastroberardino^{37a,37b}, T. Masubuchi¹⁵⁶, P. Mättig¹⁷⁶, J. Mattmann⁸², J. Maurer^{26a}, S.J. Maxfield⁷³, D.A. Maximov^{108,c}, R. Mazini¹⁵², L. Mazzaferro^{134a,134b}, G. Mc Goldrick¹⁵⁹, S.P. Mc Kee⁸⁸, A. McCarn⁸⁸, R.L. McCarthy¹⁴⁹, T.G. McCarthy²⁹, N.A. McCubbin¹³⁰, K.W. McFarlane^{56,*}, J.A. Mcfayden⁷⁷, G. Mchedlidze⁵⁴, S.J. McMahon¹³⁰, R.A. McPherson^{170,j}, A. Meade⁸⁵, J. Mechnich¹⁰⁶, M. Medinnis⁴², S. Meehan³¹, S. Mehlhase⁹⁹, A. Mehta⁷³, K. Meier^{58a}, C. Meineck⁹⁹, B. Meirose⁸⁰, C. Melachrinou³¹, B.R. Mellado Garcia^{146c}, F. Meloni¹⁷, A. Mengarelli^{20a,20b}, S. Menke¹⁰⁰, E. Meoni¹⁶², K.M. Mercurio⁵⁷, S. Mergelmeyer²¹, N. Meric¹³⁷, P. Mermod⁴⁹, L. Merola^{103a,103b}, C. Meroni^{90a}, F.S. Merritt³¹, H. Merritt¹¹⁰, A. Messina^{30,z}, J. Metcalfe²⁵, A.S. Mete¹⁶⁴, C. Meyer⁸², C. Meyer¹²¹, J.-P. Meyer¹³⁷, J. Meyer³⁰, R.P. Middleton¹³⁰, S. Migas⁷³, L. Mijović²¹, G. Mikenberg¹⁷³, M. Mikestikova¹²⁶, M. Mikuz⁷⁴, A. Milic³⁰, D.W. Miller³¹, C. Mills⁴⁶, A. Milov¹⁷³, D.A. Milstead^{147a,147b}, D. Milstein¹⁷³, A.A. Minaenko¹²⁹, I.A. Minashvili⁶⁴, A.I. Mincer¹⁰⁹, B. Mindur^{38a}, M. Mineev⁶⁴, Y. Ming¹⁷⁴, L.M. Mir¹², G. Mirabelli^{133a}, T. Mitani¹⁷², J. Mitrevski⁹⁹, V.A. Mitsou¹⁶⁸, S. Mitsui⁶⁵, A. Miucci⁴⁹, P.S. Miyagawa¹⁴⁰, J.U. Mjörnmark⁸⁰, T. Moa^{147a,147b}, K. Mochizuki⁸⁴, S. Mohapatra³⁵, W. Mohr⁴⁸, S. Molander^{147a,147b}, R. Moles-Valls¹⁶⁸, K. Mönig⁴², C. Monini⁵⁵, J. Monk³⁶, E. Monnier⁸⁴, J. Montejo Berlingen¹², F. Monticelli⁷⁰, S. Monzani^{133a,133b}, R.W. Moore³, A. Moraes⁵³, N. Morange⁶², D. Moreno⁸², M. Moreno Llácer⁵⁴, P. Morettini^{50a}, M. Morgenstern⁴⁴, M. Morii⁵⁷, S. Moritz⁸², A.K. Morley¹⁴⁸, G. Mornacchi³⁰, J.D. Morris⁷⁵, L. Morvaj¹⁰², H.G. Moser¹⁰⁰, M. Mosidze^{51b}, J. Moss¹¹⁰, K. Motohashi¹⁵⁸, R. Mount¹⁴⁴, E. Mountricha²⁵, S.V. Mouraviev^{95,*}, E.J.W. Moyse⁸⁵, S. Muanza⁸⁴, R.D. Mudd¹⁸, F. Mueller^{58a}, J. Mueller¹²⁴, K. Mueller²¹, T. Mueller²⁸, T. Mueller⁸², D. Muenstermann⁴⁹, Y. Munwes¹⁵⁴, J.A. Murillo Quijada¹⁸, W.J. Murray^{171,130}, H. Musheghyan⁵⁴, E. Musto¹⁵³, A.G. Myagkov^{129,aa}, M. Myska¹²⁷, O. Nackenhorst⁵⁴, J. Nadal⁵⁴, K. Nagai⁶¹, R. Nagai¹⁵⁸, Y. Nagai⁸⁴, K. Nagano⁶⁵, A. Nagarkar¹¹⁰, Y. Nagasaka⁵⁹, M. Nagel¹⁰⁰, A.M. Nairz³⁰, Y. Nakahama³⁰, K. Nakamura⁶⁵, T. Nakamura¹⁵⁶, I. Nakano¹¹¹, H. Namasivayam⁴¹, G. Nanava²¹, R. Narayan^{58b}, T. Nattermann²¹, T. Naumann⁴², G. Navarro¹⁶³, R. Nayyar⁷, H.A. Neal⁸⁸, P.Yu. Nechaeva⁹⁵, T.J. Neep⁸³, P.D. Nef¹⁴⁴, A. Negri^{120a,120b}, G. Negri³⁰, M. Negrini^{20a}, S. Nektarijevic⁴⁹, A. Nelson¹⁶⁴, T.K. Nelson¹⁴⁴, S. Nemecek¹²⁶, P. Nemethy¹⁰⁹, A.A. Nepomuceno^{24a}, M. Nessi^{30,ab}, M.S. Neubauer¹⁶⁶, M. Neumann¹⁷⁶, R.M. Neves¹⁰⁹, P. Nevski²⁵, P.R. Newman¹⁸, D.H. Nguyen⁶, R.B. Nickerson¹¹⁹, R. Nicolaidou¹³⁷, B. Nicquevert³⁰, J. Nielsen¹³⁸, N. Nikiforou³⁵, A. Nikiforov¹⁶, V. Nikolaenko^{129,aa}, I. Nikolic-Audit⁷⁹, K. Nikolics⁴⁹, K. Nikolopoulos¹⁸, P. Nilsson⁸, Y. Ninomiya¹⁵⁶, A. Nisati^{133a}, R. Nisius¹⁰⁰, T. Nobe¹⁵⁸, L. Nodulman⁶, M. Nomachi¹¹⁷, I. Nomidis²⁹, S. Norberg¹¹², M. Nordberg³⁰, O. Novgorodova⁴⁴, S. Nowak¹⁰⁰, M. Nozaki⁶⁵, L. Nozka¹¹⁴, K. Ntekas¹⁰, G. Nunes Hanninger⁸⁷, T. Nunnemann⁹⁹, E. Nurse⁷⁷, F. Nuti⁸⁷, B.J. O'Brien⁴⁶, F. O'grady⁷, D.C. O'Neil¹⁴³, V. O'Shea⁵³, F.G. Oakham^{29,e}, H. Oberlack¹⁰⁰, T. Obermann²¹, J. Ocariz⁷⁹, A. Ochi⁶⁶, M.I. Ochoa⁷⁷, S. Oda⁶⁹, S. Odaka⁶⁵, H. Ogren⁶⁰, A. Oh⁸³, S.H. Oh⁴⁵, C.C. Ohm¹⁵, H. Ohman¹⁶⁷, W. Okamura¹¹⁷, H. Okawa²⁵, Y. Okumura³¹, T. Okuyama¹⁵⁶, A. Olariu^{26a}, A.G. Olchevski⁶⁴, S.A. Olivares Pino⁴⁶, D. Oliveira Damazio²⁵, E. Oliver Garcia¹⁶⁸, A. Olszewski³⁹, J. Olszowska³⁹, A. Onofre^{125a,125e}, P.U.E. Onyisi^{31,p}, C.J. Oram^{160a}, M.J. Oreglia³¹, Y. Oren¹⁵⁴, D. Orestano^{135a,135b}, N. Orlando^{72a,72b}, C. Oropeza Barrera⁵³, R.S. Orr¹⁵⁹, B. Osculati^{50a,50b}, R. Ospanov¹²¹, G. Otero y Garzon²⁷, H. Otono⁶⁹, M. Ouchrif^{136d}, E.A. Ouellette¹⁷⁰, F. Ould-Saada¹¹⁸, A. Ouraou¹³⁷, K.P. Oussoren¹⁰⁶, Q. Ouyang^{33a}, A. Ovcharova¹⁵, M. Owen⁸³, V.E. Ozcan^{19a}, N. Ozturk⁸, K. Pachal¹¹⁹, A. Pacheco Pages¹², C. Padilla Aranda¹², M. Pagáčová⁴⁸, S. Pagan Griso¹⁵, E. Paganis¹⁴⁰, C. Pahl¹⁰⁰, F. Paige²⁵, P. Pais⁸⁵, K. Pajchel¹¹⁸, G. Palacino^{160b}, S. Palestini³⁰, M. Palka^{38b}, D. Pallin³⁴, A. Palma^{125a,125b}, J.D. Palmer¹⁸, Y.B. Pan¹⁷⁴, E. Panagiotopoulou¹⁰, J.G. Panduro Vazquez⁷⁶, P. Pani¹⁰⁶, N. Panikashvili⁸⁸, S. Panitkin²⁵, D. Pantea^{26a}, L. Paolozzi^{134a,134b}, Th.D. Papadopoulos¹⁰, K. Papageorgiou^{155,m}, A. Paramonov⁶, D. Paredes Hernandez³⁴, M.A. Parker²⁸, F. Parodi^{50a,50b}, J.A. Parsons³⁵, U. Parzefall⁴⁸, E. Pasqualucci^{133a}, S. Passaggio^{50a}, A. Passeri^{135a}, F. Pastore^{135a,135b,*}, Fr. Pastore⁷⁶, G. Pásztor²⁹, S. Pataraja¹⁷⁶, N.D. Patel¹⁵¹, J.R. Pater⁸³, S. Patricelli^{103a,103b}, T. Pauly³⁰, J. Pearce¹⁷⁰, M. Pedersen¹¹⁸, S. Pedraza Lopez¹⁶⁸, R. Pedro^{125a,125b}, S.V. Peleganchuk¹⁰⁸, D. Pelikan¹⁶⁷, H. Peng^{33b}, B. Penning³¹, J. Penwell⁶⁰, D.V. Perepelitsa²⁵, E. Perez Codina^{160a}, M.T. Pérez García-Estañ¹⁶⁸, V. Perez Reale³⁵, L. Perini^{90a,90b}, H. Pernegger³⁰, R. Perrino^{72a}, R. Peschke⁴², V.D. Peshekhonov⁶⁴, K. Peters³⁰, R.F.Y. Peters⁸³, B.A. Petersen³⁰, T.C. Petersen³⁶, E. Petit⁴², A. Petridis^{147a,147b}, C. Petridou¹⁵⁵, E. Petrolo^{133a}, F. Petrucci^{135a,135b}, N.E. Pettersson¹⁵⁸, R. Pezoa^{32b}, P.W. Phillips¹³⁰, G. Piacquadio¹⁴⁴, E. Pianori¹⁷¹, A. Picazio⁴⁹, E. Piccaro⁷⁵,

M. Piccinini^{20a,20b}, R. Piegai²⁷, D.T. Pignotti¹¹⁰, J.E. Pilcher³¹, A.D. Pilkington⁷⁷, J. Pina^{125a,125b,125d},
 M. Pinamonti^{165a,165c,ac}, A. Pinder¹¹⁹, J.L. Pinfeld³, A. Pingel³⁶, B. Pinto^{125a}, S. Pires⁷⁹, M. Pitt¹⁷³,
 C. Pizio^{90a,90b}, L. Plazak^{145a}, M.-A. Pleier²⁵, V. Pleskot¹²⁸, E. Plotnikova⁶⁴, P. Plucinski^{147a,147b}, S. Poddar^{58a},
 F. Podlyski³⁴, R. Poettgen⁸², L. Poggioli¹¹⁶, D. Pohl²¹, M. Pohl⁴⁹, G. Polesello^{120a}, A. Policicchio^{37a,37b},
 R. Polifka¹⁵⁹, A. Polini^{20a}, C.S. Pollard⁴⁵, V. Polychronakos²⁵, K. Pommès³⁰, L. Pontecorvo^{133a}, B.G. Pope⁸⁹,
 G.A. Popeneciu^{26b}, D.S. Popovic^{13a}, A. Poppleton³⁰, X. Portell Bueso¹², S. Pospisil¹²⁷, K. Potamianos¹⁵,
 I.N. Potrap⁶⁴, C.J. Potter¹⁵⁰, C.T. Potter¹¹⁵, G. Poulard³⁰, J. Poveda⁶⁰, V. Pozdnyakov⁶⁴, P. Pralavorio⁸⁴,
 A. Pranko¹⁵, S. Prasad³⁰, R. Pravahan⁸, S. Prell⁶³, D. Price⁸³, J. Price⁷³, L.E. Price⁶, D. Prieur¹²⁴,
 M. Primavera^{72a}, M. Proissl⁴⁶, K. Prokofiev⁴⁷, F. Prokoshin^{32b}, E. Protopapadaki¹³⁷, S. Protopopescu²⁵,
 J. Proudfoot⁶, M. Przybycien^{38a}, H. Przysieszniak⁵, E. Ptacek¹¹⁵, D. Puddu^{135a,135b}, E. Pueschel⁸⁵, D. Pulton¹⁴⁹,
 M. Purohit^{25,ad}, P. Puzo¹¹⁶, J. Qian⁸⁸, G. Qin⁵³, Y. Qin⁸³, A. Quadt⁵⁴, D.R. Quarrie¹⁵, W.B. Quayle^{165a,165b},
 M. Queitsch-Maitland⁸³, D. Quilty⁵³, A. Qureshi^{160b}, V. Radeka²⁵, V. Radescu⁴², S.K. Radhakrishnan¹⁴⁹,
 P. Radloff¹¹⁵, P. Rados⁸⁷, F. Ragusa^{90a,90b}, G. Rahal¹⁷⁹, S. Rajagopalan²⁵, M. Rammensee³⁰, A.S. Randle-Conde⁴⁰,
 C. Rangel-Smith¹⁶⁷, K. Rao¹⁶⁴, F. Rauscher⁹⁹, T.C. Rave⁴⁸, T. Ravenscroft⁵³, M. Raymond³⁰, A.L. Read¹¹⁸,
 N.P. Readioff⁷³, D.M. Rebuffi^{120a,120b}, A. Redelbach¹⁷⁵, G. Redlinger²⁵, R. Reece¹³⁸, K. Reeves⁴¹, L. Rehnisch¹⁶,
 H. Reisin²⁷, M. Relich¹⁶⁴, C. Rembser³⁰, H. Ren^{33a}, Z.L. Ren¹⁵², A. Renaud¹¹⁶, M. Rescigno^{133a}, S. Resconi^{90a},
 O.L. Rezanova^{108,c}, P. Reznicek¹²⁸, R. Rezvani⁹⁴, R. Richter¹⁰⁰, M. Ridel⁷⁹, P. Rieck¹⁶, J. Rieger⁵⁴,
 M. Rijssenbeek¹⁴⁹, A. Rimoldi^{120a,120b}, L. Rinaldi^{20a}, E. Ritsch⁶¹, I. Riu¹², F. Rizatdinova¹¹³, E. Rizvi⁷⁵,
 S.H. Robertson^{86,j}, A. Robichaud-Veronneau⁸⁶, D. Robinson²⁸, J.E.M. Robinson⁸³, A. Robson⁵³, C. Roda^{123a,123b},
 L. Rodrigues³⁰, S. Roe³⁰, O. Röhne¹¹⁸, S. Rolli¹⁶², A. Romaniouk⁹⁷, M. Romano^{20a,20b}, E. Romero Adam¹⁶⁸,
 N. Rompotis¹³⁹, M. Ronzani⁴⁸, L. Roos⁷⁹, E. Ros¹⁶⁸, S. Rosati^{133a}, K. Rosbach⁴⁹, M. Rose⁷⁶, P. Rose¹³⁸,
 P.L. Rosendahl¹⁴, O. Rosenthal¹⁴², V. Rossetti^{147a,147b}, E. Rossi^{103a,103b}, L.P. Rossi^{50a}, R. Rosten¹³⁹, M. Rotaru^{26a},
 I. Roth¹⁷³, J. Rothberg¹³⁹, D. Rousseau¹¹⁶, C.R. Royon¹³⁷, A. Rozanov⁸⁴, Y. Rozen¹⁵³, X. Ruan^{146c}, F. Rubbo¹²,
 I. Rubinskiy⁴², V.I. Rud⁹⁸, C. Rudolph⁴⁴, M.S. Rudolph¹⁵⁹, F. Rühr⁴⁸, A. Ruiz-Martinez³⁰, Z. Rurikova⁴⁸,
 N.A. Rusakovich⁶⁴, A. Ruschke⁹⁹, J.P. Rutherford⁷, N. Ruthmann⁴⁸, Y.F. Ryabov¹²², M. Rybar¹²⁸, G. Rybkin¹¹⁶,
 N.C. Ryder¹¹⁹, A.F. Saavedra¹⁵¹, S. Sacerdoti²⁷, A. Saddique³, I. Sadeh¹⁵⁴, H.F.W. Sadrozinski¹³⁸, R. Sadykov⁶⁴,
 F. Safai Tehrani^{133a}, H. Sakamoto¹⁵⁶, Y. Sakurai¹⁷², G. Salamanna^{135a,135b}, A. Salamon^{134a}, M. Saleem¹¹²,
 D. Salek¹⁰⁶, P.H. Sales De Bruin¹³⁹, D. Salihagic¹⁰⁰, A. Salmikov¹⁴⁴, J. Salt¹⁶⁸, D. Salvatore^{37a,37b}, F. Salvatore¹⁵⁰,
 A. Salvucci¹⁰⁵, A. Salzburger³⁰, D. Sampsonidis¹⁵⁵, A. Sanchez^{103a,103b}, J. Sánchez¹⁶⁸, V. Sanchez Martinez¹⁶⁸,
 H. Sandaker¹⁴, R.L. Sandbach⁷⁵, H.G. Sander⁸², M.P. Sanders⁹⁹, M. Sandhoff¹⁷⁶, T. Sandoval²⁸, C. Sandoval¹⁶³,
 R. Sandstroem¹⁰⁰, D.P.C. Sankey¹³⁰, A. Sansoni⁴⁷, C. Santoni³⁴, R. Santonico^{134a,134b}, H. Santos^{125a},
 I. Santoyo Castillo¹⁵⁰, K. Sapp¹²⁴, A. Saponov⁶⁴, J.G. Saraiva^{125a,125d}, B. Sarrazin²¹, G. Sartisohn¹⁷⁶, O. Sasaki⁶⁵,
 Y. Sasaki¹⁵⁶, G. Sauvage^{5,*}, E. Sauvan⁵, P. Savard^{159,e}, D.O. Savu³⁰, C. Sawyer¹¹⁹, L. Sawyer^{78,n}, D.H. Saxon⁵³,
 J. Saxon¹²¹, C. Sbarra^{20a}, A. Sbrizzi³, T. Scanlon⁷⁷, D.A. Scannicchio¹⁶⁴, M. Scarcella¹⁵¹, V. Scarfone^{37a,37b},
 J. Schaarschmidt¹⁷³, P. Schacht¹⁰⁰, D. Schaefer³⁰, R. Schaefer⁴², S. Schaepe²¹, S. Schaezel^{58b}, U. Schäfer⁸²,
 A.C. Schaffer¹¹⁶, D. Schaile⁹⁹, R.D. Schamberger¹⁴⁹, V. Scharf^{58a}, V.A. Schegelsky¹²², D. Scheirich¹²⁸,
 M. Schernau¹⁶⁴, M.I. Scherzer³⁵, C. Schiavi^{50a,50b}, J. Schieck⁹⁹, C. Schillo⁴⁸, M. Schioppa^{37a,37b}, S. Schlenker³⁰,
 E. Schmidt⁴⁸, K. Schmieden³⁰, C. Schmitt⁸², S. Schmitt^{58b}, B. Schneider¹⁷, Y.J. Schnellbach⁷³, U. Schnoor⁴⁴,
 L. Schoeffel¹³⁷, A. Schoening^{58b}, B.D. Schoenrock⁸⁹, A.L.S. Schorlemmer⁵⁴, M. Schott⁸², D. Schouten^{160a},
 J. Schovancova²⁵, S. Schramm¹⁵⁹, M. Schreyer¹⁷⁵, C. Schroeder⁸², N. Schuh⁸², M.J. Schultens²¹,
 H.-C. Schultz-Coulon^{58a}, H. Schulz¹⁶, M. Schumacher⁴⁸, B.A. Schumm¹³⁸, Ph. Schune¹³⁷, C. Schwanenberger⁸³,
 A. Schwartzman¹⁴⁴, Ph. Schwegler¹⁰⁰, Ph. Schwemling¹³⁷, R. Schwienhorst⁸⁹, J. Schwindling¹³⁷, T. Schwindt²¹,
 M. Schwoerer⁵, F.G. Sciacca¹⁷, E. Scifo¹¹⁶, G. Sciolla²³, W.G. Scott¹³⁰, F. Scuri^{123a,123b}, F. Scutti²¹, J. Searcy⁸⁸,
 G. Sedov⁴², E. Sedykh¹²², S.C. Seidel¹⁰⁴, A. Seiden¹³⁸, F. Seifert¹²⁷, J.M. Seixas^{24a}, G. Sekhniaidze^{103a},
 S.J. Sekula⁴⁰, K.E. Selbach⁴⁶, D.M. Seliverstov^{122,*}, G. Sellers⁷³, N. Semprini-Cesari^{20a,20b}, C. Serfon³⁰, L. Serin¹¹⁶,
 L. Serkin⁵⁴, T. Serre⁸⁴, R. Seuster^{160a}, H. Severini¹¹², T. Sfiligoi⁷⁴, F. Sforza¹⁰⁰, A. Sfyrla³⁰, E. Shabalina⁵⁴,
 M. Shamim¹¹⁵, L.Y. Shan^{33a}, R. Shang¹⁶⁶, J.T. Shank²², M. Shapiro¹⁵, P.B. Shatalov⁹⁶, K. Shaw^{165a,165b},
 C.Y. Shehu¹⁵⁰, P. Sherwood⁷⁷, L. Shi^{152,ae}, S. Shimizu⁶⁶, C.O. Shimmin¹⁶⁴, M. Shimojima¹⁰¹, M. Shiyakova⁶⁴,
 A. Shmeleva⁹⁵, M.J. Shochet³¹, D. Short¹¹⁹, S. Shrestha⁶³, E. Shulga⁹⁷, M.A. Shupe⁷, S. Shushkevich⁴², P. Sicho¹²⁶,
 O. Sidiropoulou¹⁵⁵, D. Sidorov¹¹³, A. Sidoti^{133a}, F. Siegert⁴⁴, Dj. Sijacki^{13a}, J. Silva^{125a,125d}, Y. Silver¹⁵⁴,
 D. Silverstein¹⁴⁴, S.B. Silverstein^{147a}, V. Simak¹²⁷, O. Simard⁵, Lj. Simic^{13a}, S. Simion¹¹⁶, E. Simioni⁸²,
 B. Simmons⁷⁷, R. Simioniello^{90a,90b}, M. Simonyan³⁶, P. Sinervo¹⁵⁹, N.B. Sinev¹¹⁵, V. Sipica¹⁴², G. Siragusa¹⁷⁵,
 A. Sircar⁷⁸, A.N. Sisakyan^{64,*}, S.Yu. Sivoklokov⁹⁸, J. Sjölin^{147a,147b}, T.B. Sjursen¹⁴, H.P. Skottowe⁵⁷,
 K.Yu. Skovpen¹⁰⁸, P. Skubic¹¹², M. Slater¹⁸, T. Slavicek¹²⁷, K. Sliwa¹⁶², V. Smakhtin¹⁷³, B.H. Smart⁴⁶,
 L. Smestad¹⁴, S.Yu. Smirnov⁹⁷, Y. Smirnov⁹⁷, L.N. Smirnova^{98,af}, O. Smirnova⁸⁰, K.M. Smith⁵³, M. Smizanska⁷¹,
 K. Smolek¹²⁷, A.A. Snesarev⁹⁵, G. Snidero⁷⁵, S. Snyder²⁵, R. Sobie^{170,j}, F. Socher⁴⁴, A. Soffer¹⁵⁴, D.A. Soh^{152,ae},
 C.A. Solans³⁰, M. Solar¹²⁷, J. Solc¹²⁷, E.Yu. Soldatov⁹⁷, U. Soldevila¹⁶⁸, A.A. Solodkov¹²⁹, A. Soloshenko⁶⁴,
 O.V. Solovyanov¹²⁹, V. Solovyev¹²², P. Sommer⁴⁸, H.Y. Song^{33b}, N. Soni¹, A. Sood¹⁵, A. Sopczak¹²⁷, B. Sopko¹²⁷,

V. Sopko¹²⁷, V. Sorin¹², M. Sosebee⁸, R. Soualah^{165a,165c}, P. Soueid⁹⁴, A.M. Soukharev^{108,c}, D. South⁴², S. Spagnolo^{72a,72b}, F. Spanò⁷⁶, W.R. Spearman⁵⁷, F. Spettel¹⁰⁰, R. Spighi^{20a}, G. Spigo³⁰, L.A. Spiller⁸⁷, M. Spousta¹²⁸, T. Spreitzer¹⁵⁹, B. Spurlock⁸, R.D. St. Denis^{53,*}, S. Staerz⁴⁴, J. Stahman¹²¹, R. Stamen^{58a}, S. Stamm¹⁶, E. Stanecka³⁹, R.W. Stanek⁶, C. Stanescu^{135a}, M. Stanescu-Bellu⁴², M.M. Stanitzki⁴², S. Stapnes¹¹⁸, E.A. Starchenko¹²⁹, J. Stark⁵⁵, P. Staroba¹²⁶, P. Starovoitov⁴², R. Staszewski³⁹, P. Stavina^{145a,*}, P. Steinberg²⁵, B. Stelzer¹⁴³, H.J. Stelzer³⁰, O. Stelzer-Chilton^{160a}, H. Stenzel⁵², S. Stern¹⁰⁰, G.A. Stewart⁵³, J.A. Stillings²¹, M.C. Stockton⁸⁶, M. Stoebe⁸⁶, G. Stoicea^{26a}, P. Stolte⁵⁴, S. Stonjek¹⁰⁰, A.R. Stradling⁸, A. Straessner⁴⁴, M.E. Stramaglia¹⁷, J. Strandberg¹⁴⁸, S. Strandberg^{147a,147b}, A. Strandlie¹¹⁸, E. Strauss¹⁴⁴, M. Strauss¹¹², P. Striznec^{145b}, R. Ströhmer¹⁷⁵, D.M. Strom¹¹⁵, R. Stroynowski⁴⁰, S.A. Stucci¹⁷, B. Stugu¹⁴, N.A. Styles⁴², D. Su¹⁴⁴, J. Su¹²⁴, R. Subramaniam⁷⁸, A. Succurro¹², Y. Sugaya¹¹⁷, C. Suhr¹⁰⁷, M. Suk¹²⁷, V.V. Sulim⁹⁵, S. Sultansoy^{4c}, T. Sumida⁶⁷, S. Sun⁵⁷, X. Sun^{33a}, J.E. Sundermann⁴⁸, K. Suruliz¹⁴⁰, G. Susinno^{37a,37b}, M.R. Sutton¹⁵⁰, Y. Suzuki⁶⁵, M. Svatos¹²⁶, S. Swedish¹⁶⁹, M. Swiatlowski¹⁴⁴, I. Sykora^{145a}, T. Sykora¹²⁸, D. Ta⁸⁹, C. Taccini^{135a,135b}, K. Tackmann⁴², J. Taenzer¹⁵⁹, A. Taffard¹⁶⁴, R. Tafirout^{160a}, N. Taiblum¹⁵⁴, H. Takai²⁵, R. Takashima⁶⁸, H. Takeda⁶⁶, T. Takeshita¹⁴¹, Y. Takubo⁶⁵, M. Talby⁸⁴, A.A. Talyshev^{108,c}, J.Y.C. Tam¹⁷⁵, K.G. Tan⁸⁷, J. Tanaka¹⁵⁶, R. Tanaka¹¹⁶, S. Tanaka¹³², S. Tanaka⁶⁵, A.J. Tanasijczuk¹⁴³, B.B. Tannenwald¹¹⁰, N. Tannoury²¹, S. Tapprogge⁸², S. Tarem¹⁵³, F. Tarrade²⁹, G.F. Tartarelli^{90a}, P. Tas¹²⁸, M. Tasevsky¹²⁶, T. Tashiro⁶⁷, E. Tassi^{37a,37b}, A. Tavares Delgado^{125a,125b}, Y. Tayalati^{136d}, F.E. Taylor⁹³, G.N. Taylor⁸⁷, W. Taylor^{160b}, F.A. Teischinger³⁰, M. Teixeira Dias Castanheira⁷⁵, P. Teixeira-Dias⁷⁶, K.K. Temming⁴⁸, H. Ten Kate³⁰, P.K. Teng¹⁵², J.J. Teoh¹¹⁷, S. Terada⁶⁵, K. Terashi¹⁵⁶, J. Terron⁸¹, S. Terzo¹⁰⁰, M. Testa⁴⁷, R.J. Teuscher^{159,j}, J. Therhaag²¹, T. Thevenaux-Pelzer³⁴, J.P. Thomas¹⁸, J. Thomas-Wilsker⁷⁶, E.N. Thompson³⁵, P.D. Thompson¹⁸, P.D. Thompson¹⁵⁹, R.J. Thompson⁸³, A.S. Thompson⁵³, L.A. Thomsen³⁶, E. Thomson¹²¹, M. Thomson²⁸, W.M. Thong⁸⁷, R.P. Thun^{88,*}, F. Tian³⁵, M.J. Tibbetts¹⁵, V.O. Tikhomirov^{95,ag}, Yu.A. Tikhonov^{108,c}, S. Timoshenko⁹⁷, E. Tiouchichine⁸⁴, P. Tipton¹⁷⁷, S. Tisserant⁸⁴, T. Todorov⁵, S. Todorova-Nova¹²⁸, B. Toggerson⁷, J. Tojo⁶⁹, S. Tokár^{145a}, K. Tokushuku⁶⁵, K. Tollefson⁸⁹, L. Tomlinson⁸³, M. Tomoto¹⁰², L. Tompkins³¹, K. Toms¹⁰⁴, N.D. Topilin⁶⁴, E. Torrence¹¹⁵, H. Torres¹⁴³, E. Torró Pastor¹⁶⁸, J. Toth^{84,ah}, F. Touchard⁸⁴, D.R. Tovey¹⁴⁰, H.L. Tran¹¹⁶, T. Trefzger¹⁷⁵, L. Tremblet³⁰, A. Tricoli³⁰, I.M. Trigger^{160a}, S. Trincas-Duvoid⁷⁹, M.F. Tripiana¹², W. Trischuk¹⁵⁹, B. Trocme⁵⁵, C. Troncon^{90a}, M. Trotter-McDonald¹⁴³, M. Trovatelli^{135a,135b}, P. True⁸⁹, M. Trzebinski³⁹, A. Trzupek³⁹, C. Tsarouchas³⁰, J.C.L. Tseng¹¹⁹, P.V. Tsiarahadze^{51a}, D. Tsionou¹³⁷, G. Tsipolitis¹⁰, N. Tsirintanis⁹, S. Tsiskaridze¹², V. Tsiskaridze⁴⁸, E.G. Tskhadadze^{51a}, I.I. Tsukerman⁹⁶, V. Tsulaia¹⁵, S. Tsuno⁶⁵, D. Tsybychev¹⁴⁹, A. Tudorache^{26a}, V. Tudorache^{26a}, A.N. Tuna¹²¹, S.A. Tuptuti^{20a,20b}, S. Turchikhin^{98,af}, D. Turecek¹²⁷, I. Turk Cakir^{4d}, R. Turra^{90a,90b}, P.M. Tuts³⁵, A. Tykhonov⁴⁹, M. Tylmad^{147a,147b}, M. Tyndel¹³⁰, K. Uchida²¹, I. Ueda¹⁵⁶, R. Ueno²⁹, M. Ughetto⁸⁴, M. Uglan¹⁴, M. Uhlenbrock²¹, F. Ukegawa¹⁶¹, G. Unal³⁰, A. Undrus²⁵, G. Unel¹⁶⁴, F.C. Ungaro⁴⁸, Y. Unno⁶⁵, C. Unverdorben⁹⁹, D. Urbaniec³⁵, P. Urquijo⁸⁷, G. Usai⁸, A. Usanova⁶¹, L. Vacavant⁸⁴, V. Vacek¹²⁷, B. Vachon⁸⁶, N. Valencic¹⁰⁶, S. Valentinetti^{20a,20b}, A. Valero¹⁶⁸, L. Valery³⁴, S. Valkar¹²⁸, E. Valladolid Gallego¹⁶⁸, S. Vallecorsa⁴⁹, J.A. Valls Ferrer¹⁶⁸, W. Van Den Wollenberg¹⁰⁶, P.C. Van Der Deijl¹⁰⁶, R. van der Geer¹⁰⁶, H. van der Graaf¹⁰⁶, R. Van Der Leeuw¹⁰⁶, D. van der Ster³⁰, N. van Eldik³⁰, P. van Gemmeren⁶, J. Van Nieuwkoop¹⁴³, I. van Vulpen¹⁰⁶, M.C. van Woerden³⁰, M. Vanadia^{133a,133b}, W. Vandelli³⁰, R. Vanguri¹²¹, A. Vaniachine⁶, P. Vankov⁴², F. Vannucci⁷⁹, G. Vardanyan¹⁷⁸, R. Vari^{133a}, E.W. Varnes⁷, T. Varol⁸⁵, D. Varouchas⁷⁹, A. Vartapetian⁸, K.E. Varvell¹⁵¹, F. Vazeille³⁴, T. Vazquez Schroeder⁵⁴, J. Veatch⁷, F. Veloso^{125a,125c}, S. Veneziano^{133a}, A. Ventura^{72a,72b}, D. Ventura⁸⁵, M. Venturi¹⁷⁰, N. Venturi¹⁵⁹, A. Venturini²³, V. Vercesi^{120a}, M. Verducci^{133a,133b}, W. Verkerke¹⁰⁶, J.C. Vermeulen¹⁰⁶, A. Vest⁴⁴, M.C. Vetterli^{143,e}, O. Viazlo⁸⁰, I. Vichou¹⁶⁶, T. Vickey^{146c,ai}, O.E. Vickey Boeriu^{146c}, G.H.A. Viehhauser¹¹⁹, S. Viel¹⁶⁹, R. Vigne³⁰, M. Villa^{20a,20b}, M. Villaplana Perez^{90a,90b}, E. Vilucchi⁴⁷, M.G. Vincker²⁹, V.B. Vinogradov⁶⁴, J. Virzi¹⁵, I. Vivarelli¹⁵⁰, F. Vives Vaque³, S. Vlachos¹⁰, D. Vladoiu⁹⁹, M. Vlasak¹²⁷, A. Vogel²¹, M. Vogel^{32a}, P. Vokac¹²⁷, G. Volpi^{123a,123b}, M. Volpi⁸⁷, H. von der Schmitt¹⁰⁰, H. von Radziewski⁴⁸, E. von Toerne²¹, V. Vorobel¹²⁸, K. Vorobev⁹⁷, M. Vos¹⁶⁸, R. Voss³⁰, J.H. Vosseveld⁷³, N. Vranjes¹³⁷, M. Vranjes Milosavljevic¹⁰⁶, V. Vrba¹²⁶, M. Vreeswijk¹⁰⁶, T. Vu Anh⁴⁸, R. Vuillermet³⁰, I. Vukotic³¹, Z. Vykydal¹²⁷, P. Wagner²¹, W. Wagner¹⁷⁶, H. Wahlberg⁷⁰, S. Wahrenmund⁴⁴, J. Wakabayashi¹⁰², J. Walder⁷¹, R. Walker⁹⁹, W. Walkowiak¹⁴², R. Wall¹⁷⁷, P. Waller⁷³, B. Walsh¹⁷⁷, C. Wang^{152,aj}, C. Wang⁴⁵, F. Wang¹⁷⁴, H. Wang¹⁵, H. Wang⁴⁰, J. Wang⁴², J. Wang^{33a}, K. Wang⁸⁶, R. Wang¹⁰⁴, S.M. Wang¹⁵², T. Wang²¹, X. Wang¹⁷⁷, C. Wanotayaroj¹¹⁵, A. Warburton⁸⁶, C.P. Ward²⁸, D.R. Wardrope⁷⁷, M. Warsinsky⁴⁸, A. Washbrook⁴⁶, C. Wasicki⁴², P.M. Watkins¹⁸, A.T. Watson¹⁸, I.J. Watson¹⁵¹, M.F. Watson¹⁸, G. Watts¹³⁹, S. Watts⁸³, B.M. Waugh⁷⁷, S. Webb⁸³, M.S. Weber¹⁷, S.W. Weber¹⁷⁵, J.S. Webster³¹, A.R. Weidberg¹¹⁹, P. Weigell¹⁰⁰, B. Weinert⁶⁰, J. Weingarten⁵⁴, C. Weiser⁴⁸, H. Weits¹⁰⁶, P.S. Wells³⁰, T. Wenaus²⁵, D. Wendland¹⁶, Z. Weng^{152,ae}, T. Wengler³⁰, S. Wenig³⁰, N. Wermes²¹, M. Werner⁴⁸, P. Werner³⁰, M. Wessels^{58a}, J. Wetter¹⁶², K. Whalen²⁹, A. White⁸, M.J. White¹, R. White^{32b}, S. White^{123a,123b}, D. Whiteson¹⁶⁴, D. Wicke¹⁷⁶, F.J. Wickens¹³⁰, W. Wiedenmann¹⁷⁴, M. Wielers¹³⁰, P. Wienemann²¹, C. Wiglesworth³⁶, L.A.M. Wiik-Fuchs²¹, P.A. Wijeratne⁷⁷,

A. Wildauer¹⁰⁰, M.A. Wildt^{42,ak}, H.G. Wilkens³⁰, J.Z. Will⁹⁹, H.H. Williams¹²¹, S. Williams²⁸, C. Willis⁸⁹, S. Willocq⁸⁵, A. Wilson⁸⁸, J.A. Wilson¹⁸, I. Wingerter-Seez⁵, F. Winklmeier¹¹⁵, B.T. Winter²¹, M. Wittgen¹⁴⁴, T. Wittig⁴³, J. Wittkowski⁹⁹, S.J. Wollstadt⁸², M.W. Wolter³⁹, H. Wolters^{125a,125c}, B.K. Wosiek³⁹, J. Wotschack³⁰, M.J. Woudstra⁸³, K.W. Wozniak³⁹, M. Wright⁵³, M. Wu⁵⁵, S.L. Wu¹⁷⁴, X. Wu⁴⁹, Y. Wu⁸⁸, E. Wulf⁶⁵, T.R. Wyatt⁸³, B.M. Wynne⁴⁶, S. Xella³⁶, M. Xiao¹³⁷, D. Xu^{33a}, L. Xu^{33b,al}, B. Yabsley¹⁵¹, S. Yacoob^{146b,am}, R. Yakabe⁶⁶, M. Yamada⁶⁵, H. Yamaguchi¹⁵⁶, Y. Yamaguchi¹¹⁷, A. Yamamoto⁶⁵, K. Yamamoto⁶³, S. Yamamoto¹⁵⁶, T. Yamamura¹⁵⁶, T. Yamanaka¹⁵⁶, K. Yamauchi¹⁰², Y. Yamazaki⁶⁶, Z. Yan²², H. Yang^{33e}, H. Yang¹⁷⁴, U.K. Yang⁸³, Y. Yang¹¹⁰, S. Yanush⁹², L. Yao^{33a}, W.-M. Yao¹⁵, Y. Yasu⁶⁵, E. Yatsenko⁴², K.H. Yau Wong²¹, J. Ye⁴⁰, S. Ye²⁵, I. Yeletskikh⁶⁴, A.L. Yen⁵⁷, E. Yildirim⁴², M. Yilmaz^{4b}, R. Yoosoofmiya¹²⁴, K. Yorita¹⁷², R. Yoshida⁶, K. Yoshihara¹⁵⁶, C. Young¹⁴⁴, C.J.S. Young³⁰, S. Youssef²², D.R. Yu¹⁵, J. Yu⁸, J.M. Yu⁸⁸, J. Yu¹¹³, L. Yuan⁶⁶, A. Yurkewicz¹⁰⁷, I. Yusuff^{28,an}, B. Zabinski³⁹, R. Zaidan⁶², A.M. Zaitsev^{129,aa}, A. Zaman¹⁴⁹, S. Zambito²³, L. Zanello^{133a,133b}, D. Zanzi¹⁰⁰, C. Zeitnitz¹⁷⁶, M. Zeman¹²⁷, A. Zemla^{38a}, K. Zengel²³, O. Zenin¹²⁹, T. Ženiš^{145a}, D. Zerwas¹¹⁶, G. Zevi della Porta⁵⁷, D. Zhang⁸⁸, F. Zhang¹⁷⁴, H. Zhang⁸⁹, J. Zhang⁶, L. Zhang¹⁵², X. Zhang^{33d}, Z. Zhang¹¹⁶, Z. Zhao^{33b}, A. Zhemchugov⁶⁴, J. Zhong¹¹⁹, B. Zhou⁸⁸, L. Zhou³⁵, N. Zhou¹⁶⁴, C.G. Zhu^{33d}, H. Zhu^{33a}, J. Zhu⁸⁸, Y. Zhu^{33b}, X. Zhuang^{33a}, K. Zhukov⁹⁵, A. Zibell¹⁷⁵, D. Zieminska⁶⁰, N.I. Zimine⁶⁴, C. Zimmermann⁸², R. Zimmermann²¹, S. Zimmermann²¹, S. Zimmermann⁴⁸, Z. Zinonos⁵⁴, M. Ziolkowski¹⁴², G. Zoernig¹⁷⁴, A. Zoccolì^{20a,20b}, M. zur Nedden¹⁶, G. Zurzolo^{103a,103b}, V. Zutshi¹⁰⁷, L. Zwalinski³⁰.

¹ Department of Physics, University of Adelaide, Adelaide, Australia

² Physics Department, SUNY Albany, Albany NY, United States of America

³ Department of Physics, University of Alberta, Edmonton AB, Canada

⁴ ^(a) Department of Physics, Ankara University, Ankara; ^(b) Department of Physics, Gazi University, Ankara; ^(c) Division of Physics, TOBB University of Economics and Technology, Ankara; ^(d) Turkish Atomic Energy Authority, Ankara, Turkey

⁵ LAPP, CNRS/IN2P3 and Université de Savoie, Annecy-le-Vieux, France

⁶ High Energy Physics Division, Argonne National Laboratory, Argonne IL, United States of America

⁷ Department of Physics, University of Arizona, Tucson AZ, United States of America

⁸ Department of Physics, The University of Texas at Arlington, Arlington TX, United States of America

⁹ Physics Department, University of Athens, Athens, Greece

¹⁰ Physics Department, National Technical University of Athens, Zografou, Greece

¹¹ Institute of Physics, Azerbaijan Academy of Sciences, Baku, Azerbaijan

¹² Institut de Física d'Altes Energies and Departament de Física de la Universitat Autònoma de Barcelona, Barcelona, Spain

¹³ ^(a) Institute of Physics, University of Belgrade, Belgrade; ^(b) Vinca Institute of Nuclear Sciences, University of Belgrade, Belgrade, Serbia

¹⁴ Department for Physics and Technology, University of Bergen, Bergen, Norway

¹⁵ Physics Division, Lawrence Berkeley National Laboratory and University of California, Berkeley CA, United States of America

¹⁶ Department of Physics, Humboldt University, Berlin, Germany

¹⁷ Albert Einstein Center for Fundamental Physics and Laboratory for High Energy Physics, University of Bern, Bern, Switzerland

¹⁸ School of Physics and Astronomy, University of Birmingham, Birmingham, United Kingdom

¹⁹ ^(a) Department of Physics, Bogazici University, Istanbul; ^(b) Department of Physics, Dogus University, Istanbul;

^(c) Department of Physics Engineering, Gaziantep University, Gaziantep, Turkey

²⁰ ^(a) INFN Sezione di Bologna; ^(b) Dipartimento di Fisica e Astronomia, Università di Bologna, Bologna, Italy

²¹ Physikalisches Institut, University of Bonn, Bonn, Germany

²² Department of Physics, Boston University, Boston MA, United States of America

²³ Department of Physics, Brandeis University, Waltham MA, United States of America

²⁴ ^(a) Universidade Federal do Rio De Janeiro COPPE/EE/IF, Rio de Janeiro; ^(b) Federal University of Juiz de Fora (UFJF), Juiz de Fora; ^(c) Federal University of Sao Joao del Rei (UFSJ), Sao Joao del Rei; ^(d) Instituto de Física, Universidade de Sao Paulo, Sao Paulo, Brazil

²⁵ Physics Department, Brookhaven National Laboratory, Upton NY, United States of America

²⁶ ^(a) National Institute of Physics and Nuclear Engineering, Bucharest; ^(b) National Institute for Research and Development of Isotopic and Molecular Technologies, Physics Department, Cluj Napoca; ^(c) University Politehnica Bucharest, Bucharest; ^(d) West University in Timisoara, Timisoara, Romania

²⁷ Departamento de Física, Universidad de Buenos Aires, Buenos Aires, Argentina

²⁸ Cavendish Laboratory, University of Cambridge, Cambridge, United Kingdom

²⁹ Department of Physics, Carleton University, Ottawa ON, Canada

- ³⁰ CERN, Geneva, Switzerland
- ³¹ Enrico Fermi Institute, University of Chicago, Chicago IL, United States of America
- ³² ^(a) Departamento de Física, Pontificia Universidad Católica de Chile, Santiago; ^(b) Departamento de Física, Universidad Técnica Federico Santa María, Valparaíso, Chile
- ³³ ^(a) Institute of High Energy Physics, Chinese Academy of Sciences, Beijing; ^(b) Department of Modern Physics, University of Science and Technology of China, Anhui; ^(c) Department of Physics, Nanjing University, Jiangsu; ^(d) School of Physics, Shandong University, Shandong; ^(e) Physics Department, Shanghai Jiao Tong University, Shanghai, China
- ³⁴ Laboratoire de Physique Corpusculaire, Clermont Université and Université Blaise Pascal and CNRS/IN2P3, Clermont-Ferrand, France
- ³⁵ Nevis Laboratory, Columbia University, Irvington NY, United States of America
- ³⁶ Niels Bohr Institute, University of Copenhagen, Kobenhavn, Denmark
- ³⁷ ^(a) INFN Gruppo Collegato di Cosenza, Laboratori Nazionali di Frascati; ^(b) Dipartimento di Fisica, Università della Calabria, Rende, Italy
- ³⁸ ^(a) AGH University of Science and Technology, Faculty of Physics and Applied Computer Science, Krakow; ^(b) Marian Smoluchowski Institute of Physics, Jagiellonian University, Krakow, Poland
- ³⁹ The Henryk Niewodniczanski Institute of Nuclear Physics, Polish Academy of Sciences, Krakow, Poland
- ⁴⁰ Physics Department, Southern Methodist University, Dallas TX, United States of America
- ⁴¹ Physics Department, University of Texas at Dallas, Richardson TX, United States of America
- ⁴² DESY, Hamburg and Zeuthen, Germany
- ⁴³ Institut für Experimentelle Physik IV, Technische Universität Dortmund, Dortmund, Germany
- ⁴⁴ Institut für Kern- und Teilchenphysik, Technische Universität Dresden, Dresden, Germany
- ⁴⁵ Department of Physics, Duke University, Durham NC, United States of America
- ⁴⁶ SUPA - School of Physics and Astronomy, University of Edinburgh, Edinburgh, United Kingdom
- ⁴⁷ INFN Laboratori Nazionali di Frascati, Frascati, Italy
- ⁴⁸ Fakultät für Mathematik und Physik, Albert-Ludwigs-Universität, Freiburg, Germany
- ⁴⁹ Section de Physique, Université de Genève, Geneva, Switzerland
- ⁵⁰ ^(a) INFN Sezione di Genova; ^(b) Dipartimento di Fisica, Università di Genova, Genova, Italy
- ⁵¹ ^(a) E. Andronikashvili Institute of Physics, Iv. Javakhishvili Tbilisi State University, Tbilisi; ^(b) High Energy Physics Institute, Tbilisi State University, Tbilisi, Georgia
- ⁵² II Physikalisches Institut, Justus-Liebig-Universität Giessen, Giessen, Germany
- ⁵³ SUPA - School of Physics and Astronomy, University of Glasgow, Glasgow, United Kingdom
- ⁵⁴ II Physikalisches Institut, Georg-August-Universität, Göttingen, Germany
- ⁵⁵ Laboratoire de Physique Subatomique et de Cosmologie, Université Grenoble-Alpes, CNRS/IN2P3, Grenoble, France
- ⁵⁶ Department of Physics, Hampton University, Hampton VA, United States of America
- ⁵⁷ Laboratory for Particle Physics and Cosmology, Harvard University, Cambridge MA, United States of America
- ⁵⁸ ^(a) Kirchhoff-Institut für Physik, Ruprecht-Karls-Universität Heidelberg, Heidelberg; ^(b) Physikalisches Institut, Ruprecht-Karls-Universität Heidelberg, Heidelberg; ^(c) ZITI Institut für technische Informatik, Ruprecht-Karls-Universität Heidelberg, Mannheim, Germany
- ⁵⁹ Faculty of Applied Information Science, Hiroshima Institute of Technology, Hiroshima, Japan
- ⁶⁰ Department of Physics, Indiana University, Bloomington IN, United States of America
- ⁶¹ Institut für Astro- und Teilchenphysik, Leopold-Franzens-Universität, Innsbruck, Austria
- ⁶² University of Iowa, Iowa City IA, United States of America
- ⁶³ Department of Physics and Astronomy, Iowa State University, Ames IA, United States of America
- ⁶⁴ Joint Institute for Nuclear Research, JINR Dubna, Dubna, Russia
- ⁶⁵ KEK, High Energy Accelerator Research Organization, Tsukuba, Japan
- ⁶⁶ Graduate School of Science, Kobe University, Kobe, Japan
- ⁶⁷ Faculty of Science, Kyoto University, Kyoto, Japan
- ⁶⁸ Kyoto University of Education, Kyoto, Japan
- ⁶⁹ Department of Physics, Kyushu University, Fukuoka, Japan
- ⁷⁰ Instituto de Física La Plata, Universidad Nacional de La Plata and CONICET, La Plata, Argentina
- ⁷¹ Physics Department, Lancaster University, Lancaster, United Kingdom
- ⁷² ^(a) INFN Sezione di Lecce; ^(b) Dipartimento di Matematica e Fisica, Università del Salento, Lecce, Italy
- ⁷³ Oliver Lodge Laboratory, University of Liverpool, Liverpool, United Kingdom
- ⁷⁴ Department of Physics, Jožef Stefan Institute and University of Ljubljana, Ljubljana, Slovenia
- ⁷⁵ School of Physics and Astronomy, Queen Mary University of London, London, United Kingdom
- ⁷⁶ Department of Physics, Royal Holloway University of London, Surrey, United Kingdom

- 77 Department of Physics and Astronomy, University College London, London, United Kingdom
- 78 Louisiana Tech University, Ruston LA, United States of America
- 79 Laboratoire de Physique Nucléaire et de Hautes Energies, UPMC and Université Paris-Diderot and CNRS/IN2P3, Paris, France
- 80 Fysiska institutionen, Lunds universitet, Lund, Sweden
- 81 Departamento de Física Teórica C-15, Universidad Autónoma de Madrid, Madrid, Spain
- 82 Institut für Physik, Universität Mainz, Mainz, Germany
- 83 School of Physics and Astronomy, University of Manchester, Manchester, United Kingdom
- 84 CPPM, Aix-Marseille Université and CNRS/IN2P3, Marseille, France
- 85 Department of Physics, University of Massachusetts, Amherst MA, United States of America
- 86 Department of Physics, McGill University, Montreal QC, Canada
- 87 School of Physics, University of Melbourne, Victoria, Australia
- 88 Department of Physics, The University of Michigan, Ann Arbor MI, United States of America
- 89 Department of Physics and Astronomy, Michigan State University, East Lansing MI, United States of America
- 90 ^(a) INFN Sezione di Milano; ^(b) Dipartimento di Fisica, Università di Milano, Milano, Italy
- 91 B.I. Stepanov Institute of Physics, National Academy of Sciences of Belarus, Minsk, Republic of Belarus
- 92 National Scientific and Educational Centre for Particle and High Energy Physics, Minsk, Republic of Belarus
- 93 Department of Physics, Massachusetts Institute of Technology, Cambridge MA, United States of America
- 94 Group of Particle Physics, University of Montreal, Montreal QC, Canada
- 95 P.N. Lebedev Institute of Physics, Academy of Sciences, Moscow, Russia
- 96 Institute for Theoretical and Experimental Physics (ITEP), Moscow, Russia
- 97 Moscow Engineering and Physics Institute (MEPhI), Moscow, Russia
- 98 D.V.Skobeltzyn Institute of Nuclear Physics, M.V.Lomonosov Moscow State University, Moscow, Russia
- 99 Fakultät für Physik, Ludwig-Maximilians-Universität München, München, Germany
- 100 Max-Planck-Institut für Physik (Werner-Heisenberg-Institut), München, Germany
- 101 Nagasaki Institute of Applied Science, Nagasaki, Japan
- 102 Graduate School of Science and Kobayashi-Maskawa Institute, Nagoya University, Nagoya, Japan
- 103 ^(a) INFN Sezione di Napoli; ^(b) Dipartimento di Fisica, Università di Napoli, Napoli, Italy
- 104 Department of Physics and Astronomy, University of New Mexico, Albuquerque NM, United States of America
- 105 Institute for Mathematics, Astrophysics and Particle Physics, Radboud University Nijmegen/Nikhef, Nijmegen, Netherlands
- 106 Nikhef National Institute for Subatomic Physics and University of Amsterdam, Amsterdam, Netherlands
- 107 Department of Physics, Northern Illinois University, DeKalb IL, United States of America
- 108 Budker Institute of Nuclear Physics, SB RAS, Novosibirsk, Russia
- 109 Department of Physics, New York University, New York NY, United States of America
- 110 Ohio State University, Columbus OH, United States of America
- 111 Faculty of Science, Okayama University, Okayama, Japan
- 112 Homer L. Dodge Department of Physics and Astronomy, University of Oklahoma, Norman OK, United States of America
- 113 Department of Physics, Oklahoma State University, Stillwater OK, United States of America
- 114 Palacký University, RCPTM, Olomouc, Czech Republic
- 115 Center for High Energy Physics, University of Oregon, Eugene OR, United States of America
- 116 LAL, Université Paris-Sud and CNRS/IN2P3, Orsay, France
- 117 Graduate School of Science, Osaka University, Osaka, Japan
- 118 Department of Physics, University of Oslo, Oslo, Norway
- 119 Department of Physics, Oxford University, Oxford, United Kingdom
- 120 ^(a) INFN Sezione di Pavia; ^(b) Dipartimento di Fisica, Università di Pavia, Pavia, Italy
- 121 Department of Physics, University of Pennsylvania, Philadelphia PA, United States of America
- 122 Petersburg Nuclear Physics Institute, Gatchina, Russia
- 123 ^(a) INFN Sezione di Pisa; ^(b) Dipartimento di Fisica E. Fermi, Università di Pisa, Pisa, Italy
- 124 Department of Physics and Astronomy, University of Pittsburgh, Pittsburgh PA, United States of America
- 125 ^(a) Laboratório de Instrumentação e Física Experimental de Partículas - LIP, Lisboa; ^(b) Faculdade de Ciências, Universidade de Lisboa, Lisboa; ^(c) Department of Physics, University of Coimbra, Coimbra; ^(d) Centro de Física Nuclear da Universidade de Lisboa, Lisboa; ^(e) Departamento de Física, Universidade do Minho, Braga; ^(f) Departamento de Física Teórica y del Cosmos and CAFPE, Universidad de Granada, Granada (Spain); ^(g) Dep Física and CEFITEC of Faculdade de Ciências e Tecnologia, Universidade Nova de Lisboa, Caparica, Portugal
- 126 Institute of Physics, Academy of Sciences of the Czech Republic, Praha, Czech Republic
- 127 Czech Technical University in Prague, Praha, Czech Republic

- 128 Faculty of Mathematics and Physics, Charles University in Prague, Praha, Czech Republic
- 129 State Research Center Institute for High Energy Physics, Protvino, Russia
- 130 Particle Physics Department, Rutherford Appleton Laboratory, Didcot, United Kingdom
- 131 Physics Department, University of Regina, Regina SK, Canada
- 132 Ritsumeikan University, Kusatsu, Shiga, Japan
- 133 (a) INFN Sezione di Roma; (b) Dipartimento di Fisica, Sapienza Università di Roma, Roma, Italy
- 134 (a) INFN Sezione di Roma Tor Vergata; (b) Dipartimento di Fisica, Università di Roma Tor Vergata, Roma, Italy
- 135 (a) INFN Sezione di Roma Tre; (b) Dipartimento di Matematica e Fisica, Università Roma Tre, Roma, Italy
- 136 (a) Faculté des Sciences Ain Chock, Réseau Universitaire de Physique des Hautes Energies - Université Hassan II, Casablanca; (b) Centre National de l'Énergie des Sciences Techniques Nucleaires, Rabat; (c) Faculté des Sciences Semlalia, Université Cadi Ayyad, LPHEA-Marrakech; (d) Faculté des Sciences, Université Mohamed Premier and LPTPM, Oujda; (e) Faculté des sciences, Université Mohammed V-Agdal, Rabat, Morocco
- 137 DSM/IRFU (Institut de Recherches sur les Lois Fondamentales de l'Univers), CEA Saclay (Commissariat à l'Énergie Atomique et aux Énergies Alternatives), Gif-sur-Yvette, France
- 138 Santa Cruz Institute for Particle Physics, University of California Santa Cruz, Santa Cruz CA, United States of America
- 139 Department of Physics, University of Washington, Seattle WA, United States of America
- 140 Department of Physics and Astronomy, University of Sheffield, Sheffield, United Kingdom
- 141 Department of Physics, Shinshu University, Nagano, Japan
- 142 Fachbereich Physik, Universität Siegen, Siegen, Germany
- 143 Department of Physics, Simon Fraser University, Burnaby BC, Canada
- 144 SLAC National Accelerator Laboratory, Stanford CA, United States of America
- 145 (a) Faculty of Mathematics, Physics & Informatics, Comenius University, Bratislava; (b) Department of Subnuclear Physics, Institute of Experimental Physics of the Slovak Academy of Sciences, Kosice, Slovak Republic
- 146 (a) Department of Physics, University of Cape Town, Cape Town; (b) Department of Physics, University of Johannesburg, Johannesburg; (c) School of Physics, University of the Witwatersrand, Johannesburg, South Africa
- 147 (a) Department of Physics, Stockholm University; (b) The Oskar Klein Centre, Stockholm, Sweden
- 148 Physics Department, Royal Institute of Technology, Stockholm, Sweden
- 149 Departments of Physics & Astronomy and Chemistry, Stony Brook University, Stony Brook NY, United States of America
- 150 Department of Physics and Astronomy, University of Sussex, Brighton, United Kingdom
- 151 School of Physics, University of Sydney, Sydney, Australia
- 152 Institute of Physics, Academia Sinica, Taipei, Taiwan
- 153 Department of Physics, Technion: Israel Institute of Technology, Haifa, Israel
- 154 Raymond and Beverly Sackler School of Physics and Astronomy, Tel Aviv University, Tel Aviv, Israel
- 155 Department of Physics, Aristotle University of Thessaloniki, Thessaloniki, Greece
- 156 International Center for Elementary Particle Physics and Department of Physics, The University of Tokyo, Tokyo, Japan
- 157 Graduate School of Science and Technology, Tokyo Metropolitan University, Tokyo, Japan
- 158 Department of Physics, Tokyo Institute of Technology, Tokyo, Japan
- 159 Department of Physics, University of Toronto, Toronto ON, Canada
- 160 (a) TRIUMF, Vancouver BC; (b) Department of Physics and Astronomy, York University, Toronto ON, Canada
- 161 Faculty of Pure and Applied Sciences, University of Tsukuba, Tsukuba, Japan
- 162 Department of Physics and Astronomy, Tufts University, Medford MA, United States of America
- 163 Centro de Investigaciones, Universidad Antonio Narino, Bogota, Colombia
- 164 Department of Physics and Astronomy, University of California Irvine, Irvine CA, United States of America
- 165 (a) INFN Gruppo Collegato di Udine, Sezione di Trieste, Udine; (b) ICTP, Trieste; (c) Dipartimento di Chimica, Fisica e Ambiente, Università di Udine, Udine, Italy
- 166 Department of Physics, University of Illinois, Urbana IL, United States of America
- 167 Department of Physics and Astronomy, University of Uppsala, Uppsala, Sweden
- 168 Instituto de Física Corpuscular (IFIC) and Departamento de Física Atómica, Molecular y Nuclear and Departamento de Ingeniería Electrónica and Instituto de Microelectrónica de Barcelona (IMB-CNM), University of Valencia and CSIC, Valencia, Spain
- 169 Department of Physics, University of British Columbia, Vancouver BC, Canada
- 170 Department of Physics and Astronomy, University of Victoria, Victoria BC, Canada
- 171 Department of Physics, University of Warwick, Coventry, United Kingdom
- 172 Waseda University, Tokyo, Japan
- 173 Department of Particle Physics, The Weizmann Institute of Science, Rehovot, Israel

- ¹⁷⁴ Department of Physics, University of Wisconsin, Madison WI, United States of America
- ¹⁷⁵ Fakultät für Physik und Astronomie, Julius-Maximilians-Universität, Würzburg, Germany
- ¹⁷⁶ Fachbereich C Physik, Bergische Universität Wuppertal, Wuppertal, Germany
- ¹⁷⁷ Department of Physics, Yale University, New Haven CT, United States of America
- ¹⁷⁸ Yerevan Physics Institute, Yerevan, Armenia
- ¹⁷⁹ Centre de Calcul de l'Institut National de Physique Nucléaire et de Physique des Particules (IN2P3), Villeurbanne, France
- ^a Also at Department of Physics, King's College London, London, United Kingdom
- ^b Also at Institute of Physics, Azerbaijan Academy of Sciences, Baku, Azerbaijan
- ^c Also at Novosibirsk State University, Novosibirsk, Russia
- ^d Also at Particle Physics Department, Rutherford Appleton Laboratory, Didcot, United Kingdom
- ^e Also at TRIUMF, Vancouver BC, Canada
- ^f Also at Department of Physics, California State University, Fresno CA, United States of America
- ^g Also at Tomsk State University, Tomsk, Russia
- ^h Also at CPPM, Aix-Marseille Université and CNRS/IN2P3, Marseille, France
- ⁱ Also at Università di Napoli Parthenope, Napoli, Italy
- ^j Also at Institute of Particle Physics (IPP), Canada
- ^k Also at Department of Physics, St. Petersburg State Polytechnical University, St. Petersburg, Russia
- ^l Also at Chinese University of Hong Kong, China
- ^m Also at Department of Financial and Management Engineering, University of the Aegean, Chios, Greece
- ⁿ Also at Louisiana Tech University, Ruston LA, United States of America
- ^o Also at Institutio Catalana de Recerca i Estudis Avancats, ICREA, Barcelona, Spain
- ^p Also at Department of Physics, The University of Texas at Austin, Austin TX, United States of America
- ^q Also at Institute of Theoretical Physics, Ilia State University, Tbilisi, Georgia
- ^r Also at CERN, Geneva, Switzerland
- ^s Also at Ochadai Academic Production, Ochanomizu University, Tokyo, Japan
- ^t Also at Manhattan College, New York NY, United States of America
- ^u Also at Institute of Physics, Academia Sinica, Taipei, Taiwan
- ^v Also at LAL, Université Paris-Sud and CNRS/IN2P3, Orsay, France
- ^w Also at Academia Sinica Grid Computing, Institute of Physics, Academia Sinica, Taipei, Taiwan
- ^x Also at Laboratoire de Physique Nucléaire et de Hautes Energies, UPMC and Université Paris-Diderot and CNRS/IN2P3, Paris, France
- ^y Also at School of Physical Sciences, National Institute of Science Education and Research, Bhubaneswar, India
- ^z Also at Dipartimento di Fisica, Sapienza Università di Roma, Roma, Italy
- ^{aa} Also at Moscow Institute of Physics and Technology State University, Dolgoprudny, Russia
- ^{ab} Also at Section de Physique, Université de Genève, Geneva, Switzerland
- ^{ac} Also at International School for Advanced Studies (SISSA), Trieste, Italy
- ^{ad} Also at Department of Physics and Astronomy, University of South Carolina, Columbia SC, United States of America
- ^{ae} Also at School of Physics and Engineering, Sun Yat-sen University, Guangzhou, China
- ^{af} Also at Faculty of Physics, M.V.Lomonosov Moscow State University, Moscow, Russia
- ^{ag} Also at Moscow Engineering and Physics Institute (MEPhI), Moscow, Russia
- ^{ah} Also at Institute for Particle and Nuclear Physics, Wigner Research Centre for Physics, Budapest, Hungary
- ^{ai} Also at Department of Physics, Oxford University, Oxford, United Kingdom
- ^{aj} Also at Department of Physics, Nanjing University, Jiangsu, China
- ^{ak} Also at Institut für Experimentalphysik, Universität Hamburg, Hamburg, Germany
- ^{al} Also at Department of Physics, The University of Michigan, Ann Arbor MI, United States of America
- ^{am} Also at Discipline of Physics, University of KwaZulu-Natal, Durban, South Africa
- ^{an} Also at University of Malaya, Department of Physics, Kuala Lumpur, Malaysia
- * Deceased